ANALYTICAL AND EXPERIMENTAL STUDIES OF XLPE AND SILICONE OIL HV CABLE TERMINATIONS

A Thesis Presented to

The Faculty of Graduate Studies

The Department of Electrical Engineering

The University of Manitoba

In Partial Fulfillment of the

Requirements for the Degree

Doctor of Philosophy

by

A. M-S Katahoire

April 1980

Analytical and Experimental Studies of XLPE and Silicone Oil HV Cable Terminations.

by

Abel Mac-Sam Katahoire.

A thesis submitted to the Faculty of Graduate Studies of the University of Manitoba in partial fulfillment of the requirements of the degree of

DOCTOR OF PHILOSOPHY

ABSTRACT

An equation describing the geometry of the stress relief profile of a cable termination in terms of the specified maximum longitudinal electrostatic stress has been developed. A computer-aided design procedure was used. The electrostatic field in the cable termination has been calculated using the finite element method.

For experimental studies models have been used to simulate the Silicone Oil/XLPE interface in the cable termination. Both power frequency and standard impulse voltages were used in the studies. These studies have revealed that the Silicone Oil/XLPE interface has a lower breakdown strength than an equivalent silicone oil gap setting. For the gap spacing investigated (2 mm - 7.5 mm) this breakdown strength, under power frequency voltage is practically independent of the Silicone Oil/XLPE gap length.

Various factors that have been reported to affect the breakdown strength of liquid/solid interfaces have been reviewed. Of these factors, obstruction of the electro-hydrodynamic motion of the liquid caused by the solid spacer at the Silicone Oil/XLPE interface is suggested to be the main influencing factor.

ACKNOWLEDGEMENTS

The author wishes to express his gratitude to his supervisor Prof. E. Kuffel, D. Sc., Dean of Faculty of Engineering; for the invaluable counselling, guidance and encouragement during the course of this work.

Special thanks also go to Dr. M.R. Raghuveer for his suggestions and guidance on the numerical analysis part of this work and for reading the manuscript. Technical consultations with Prof. J.P.C. McMath and technical assistance from G.H. Toole are gratefully acknowledged; together with financial support from the Canadian Commonwealth Scholarship and Fellowship Committee awarded through the author's home (UGANDA) government. Mrs. Paulette Giardino deserves special thanks for her efficient and excellent typing.

And when you break it all down, it always comes to mother E. ADYERI KAIKARA for her continued inspiration and encouragement through her own dedication to work to accomplish right from the author's childhood up to this day.

TABLE OF CONTENTS

LIST OF FIGURES

LIST OF TABLES

CHAPTER I

INTRODUCTION

The rapid industrial growth has resulted in a continuous demand for equipment capable of operating at ever-increasing voltages. The need for the efficient and reliable transmission of large blocks of power has resulted in many complex engineering problems. While overhead power lines are widely used for the bulk transmission of power, underground power cables must be used in densely populated areas for both transmission and distribution purposes.

The design, construction and installation of power cables embraces a very wide range of technical problems and the work of numerous investigators on this subject can be found in many technical publications and journals. The different types of cables presently in use may be divided into the following broad classes depending on type of insulation:

(1) Solid-type cable - up to 69 kV system voltage level.

(2) Gas pressure-type and oil pressure-type.

(3) Pipe-type oil filled or gas filled.

(4) Gas-spacer (mainly sulphur hexaflouride) and vacuum insulated cables.

(5) Cryogenic cable - oil-impregnated paper-insulated conductor cooled with liquid nitrogen.

The second and third types of cables have been used extensively at HV (High Voltage) system level (70 kV-245 kV), whereas the last two types are being used at EHV (Extra-High Voltage 345 kV-765 kV).

Polyethylene and cross-linked polyethylene (XLPE) solid-type cables have successfully been used at medium system voltage levels (15 kV-69 kV) and HV XLPE-insulated cables are also in service (see Chapter IV). Currently, EHV XLPE-insulated compact cables are being developed by various manufacturers in Sweden and the U.S. (General Cable Corporation). With each step in the improvement of cable design resulting in a more compact cable the problem of providing joint and terminal construction as strong and reliable as the cable itself becomes increasingly difficult.

Cable termination, in general terms, is to make external electrical connection to a high-voltage conductor in hermetically sealed enclosure. In this regard, the termination is required to meet the following four fundamental characteristics.

(a) Ability to withstand the electrical stresses associated with normal and emergency conditions of system voltage and the occasional high voltage surges to which it will be subjected.

(b) Ability to carry the maximum rated current of the circuit and the maximum fault current of short duration experienced by the circuit.

(c) Retention of its initial electrical and mechanical characteristics without deterioration during the statutory life

of cable circuit in which it is incorporated.

(d) The termination should be so designed as to be economically utilizable.

It should be appreciated that owing to the combination of materials of different permittivity in a termination, and owing to the many factors influencing its geometry, the distribution of electric stress does not readily lend itself to precise mathematical analysis. The terminations have therefore been developed largely on the basis of test results from which the probable performance of new designs can be predicted [1]. Methods of cable termination construction include tape wrapping, voltage grading (capacitive and resistive), molded terminations and metal cones filled with compound insulation. Both tape-wrapped and molded terminations have been used with polyethylene and XLPE cables with the later predominating at HV (see Chapter IV). It is therefore necessary to study the termination problem for EHV XLPE-insulated cables. However, before that can be done a study of the capacitive graded termination and an analytical equation for the stress-relief profile will be presented since both methods have reportedly been used in terminating some EHV cables.

1.1 The Termination Stress Problem

In a shielded power cable, the electrostatic field is contained within and symmetrically distributed radially between the conductors and shield with the maximum voltage gradient occurring at the conductor surface. No axial field component exists. The

value of the radial voltage gradient at any radial point radius R from the centre of the conductor is given by

$$g = E/(R \log_e(R/R_c)) \qquad (1.1)$$

where g is the radial stress in kV/cm

E is the phase voltage in kV

R_c is the radius of the conductor in cm.

In the process of terminating a cable for the purposes of making external electrical connection to the conductor, the insulation shield is stripped back and ended abruptly on the cable insulation. This results in an asymmetrical concentration of the electrostatic field converging at the stripped shield edge as depicted in Fig. 1.1. A weak point is therefore established at the insulation shield edge owing to the consequent introduction of an axial (longitudinal) component of electric stress along the cable insulation surface resulting from the stripping of the insulation shield. The combination of radial and longitudinal electric stresses at the shield edge results in very high electric stresses and may exceed the inherent maximum dielectric strength of the insulation at this point unless this stress concentration is reduced.

Most solid cable insulation materials have much lower dielectric strength longitudinally than radially owing to the anisotropic nature of sheet insulation. For oil-impregnated paper insulation the ratio of radial to axial electric strength

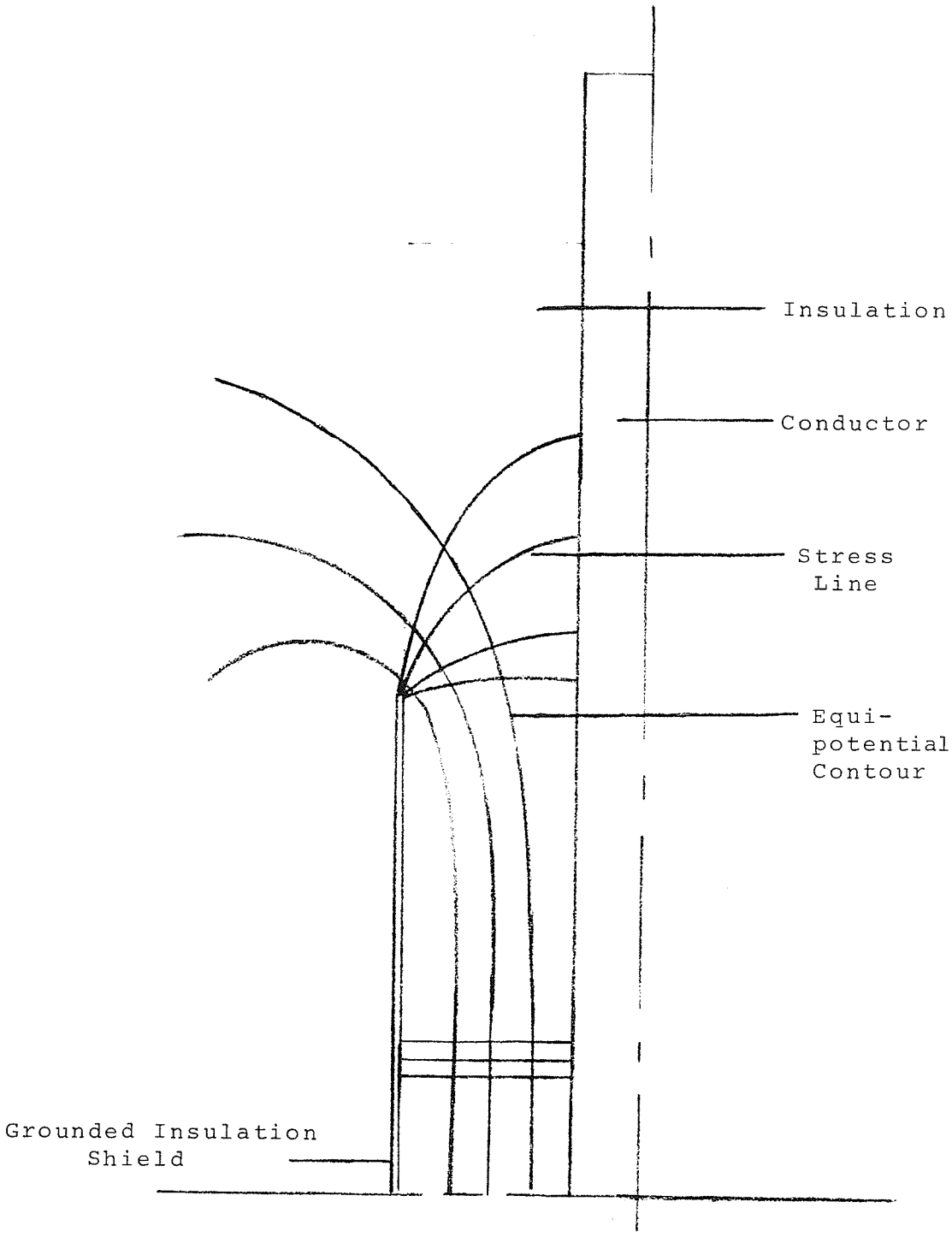

Fig. 1.1: Asymmetrical Stress Distribution at Shield Termination.

is ten to one and a factor of 30 has been recommended for practical designs [2]. Over the years the number of terminations in service has greatly increased but the number of power failures that can be traced to termination defect have not increased in direct proportion thereby indicating an improvement in termination design.

1.2 Capacitive-grading

A possible solution to the high stress concentration problem at the cable sheath termination can be noted from the fact that capacitive or resistive grading elements may be used to attain uniform voltage distribution between the point of sheath termination and at which the cable conductor becomes exposed. Various capacitive-grading devices have been suggested, most of which have been described by Schwaiger [3]. Theoretically the capacities may be arranged to give a uniform gradient, but it is difficult, technologically to make these large enough so as to firmly anchor the potentials which they are supposed to assume without making the design unduly cumbersome. This is due to the effects of small leakage currents and the presence of any slight discharge or corona, which might form at higher voltages [5]. Such disturbances become cumulative in character. Resistive grading has also been used and details to that effect are given in [13] - [16].

A prefabricated condenser cone was first reported by Webb in 1933 [6]. Condenser cone terminations have been used in EHV

systems and therefore merit a more detailed review in this work than do other methods of termination that are principally used at lower voltage levels. The principle of the condenser cone is that of capacitive grading; i.e., a series of concentric metal cylinders is arranged to share the voltage between the conductor and the sheath and the voltage across each cylinder is governed by the values of the interlinking capacitances. The interlinking capacities may be adjusted to give an equal increment of voltage across each pair. It was hoped the resulting stress redistribution would result in a uniform gradient along the dielectric. Two designs are possible, in one the outermost cylinder is connected to the cable core and the innermost to the sheath. The second design is obtained by reversing the connections to the conductor and the sheath. Both these designs are shown in Fig. 1.2.

To determine the values of the capacities required to achieve the ideal conditions it should be observed that three capacities must be considered associated with each cylinder. The main capacitance being that between a given cylinder and the two proximate cylinders. The other two capacitances are to the core and earth, respectively, from the projection of each cylinder beyond its neighbours. In Webb's design the capacitance to earth was considered negligibly small and that to the core was assumed to be equal to the average value for all cylinders. Fig. 1.3 shows the resulting equivalent diagram using the two assumptions.

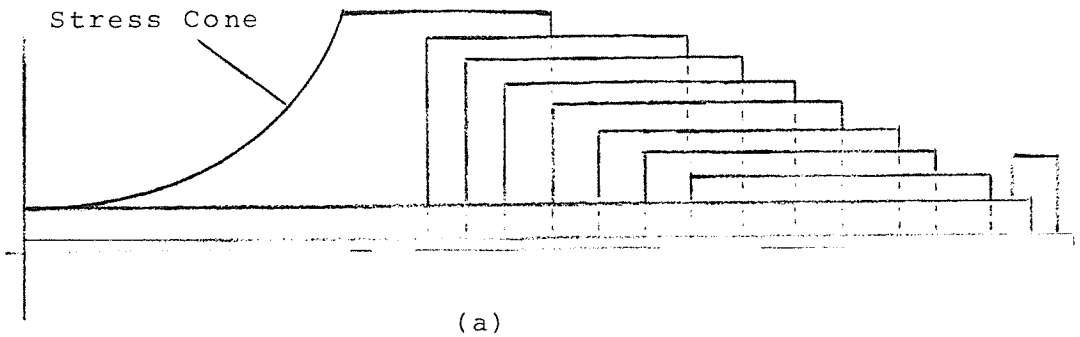

(a)

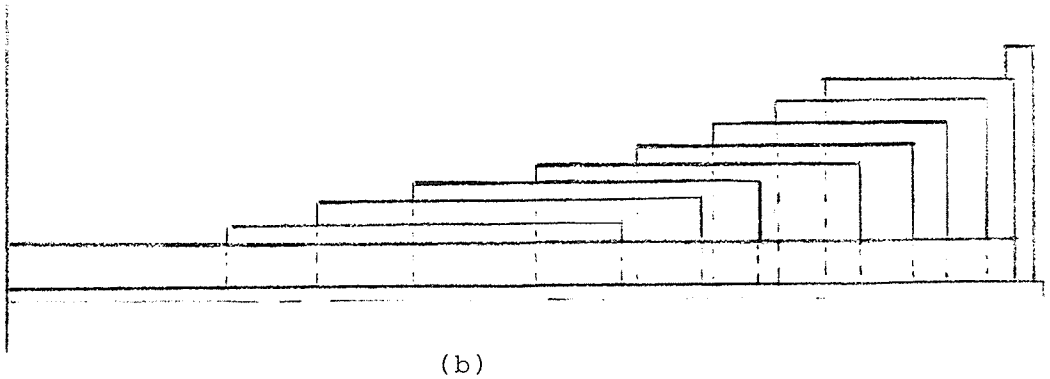

(b)

Fig. 1.2: Condenser Cone Designs.

If V is the voltage drop across each condenser the current-voltage relationship for unit k is given by

$$V = (I + \sum_{m=1}^{k-1} m\, i)\ Z_k \qquad (1.2)$$

where $Z_k = 1/j\omega\, C_k$ for $1 \leq k \leq n$. n is total number of cylinders.

$I = j\omega C_1 V$ as given in Fig. 1.6.

$i = j\omega C_o V$.

Substituting for Z_k, I and i in (1.2) gives

$$C_k = C_1 + \frac{k}{2}\,(k - 1)\, C_0 \ . \qquad (1.3)$$

In practice the term $\frac{k}{2}\,(k - 1)\, C_o$ is only about 30% of C_1 [6] and this therefore justifies the assumption that the capacity to the core of each cylinder can be taken to be equal to a mean value C_o. In designing a cone the dimensions that determine C_n (Fig. 1.3) are initially fixed; the remaining factors are chosen empirically so as to satisfy equation (1.3). For ease of construction it is desirable to use a straight taper on both the inner and outer cones. The total length is mainly determined by the external flashover voltage and the inner cone by the internal flashover clearance. The number of cylinders, n, is a function of the difference between the external diameter and the diameter of the metal former that forms an extension to

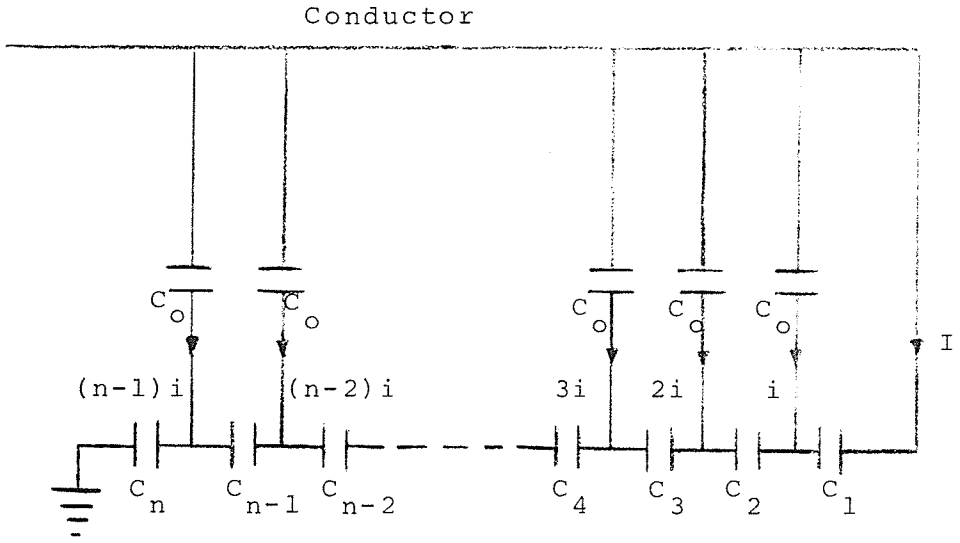

Fig. 1.3: Equivalent Circuit Diagram for a Stress Cone.

It is assumed that all capacitances to core are equal and capacitances to ground are neglected.

C_k are capacitances between cylinders:

$$k = 1, 2, 3, \ldots\ldots n.$$

the sheath in Webb's design. The intermediate metal cylinders take the form of aluminum or tinfoil placed in position during the winding of the dielectric. The dielectric is a continuous spiral, usually, of impregnated paper. A special winding machine being used for the winding operation. The terminal is then dried and vacuum impregnated and then stored under oil.

One problem with a prefabricated condenser cone design as outlined above is the existence of a weak point between the interior cone and the cable. Insulation buildup was thus recommended for higher radial stresses, otherwise a filling compound was used. In any case, the maximum radial gradient was limited to 11 kV/mm [7]. This limitation became very pronounced some fifteen years after Webb's design at which time oil- or gas-filled EHV cables were subjected to radial stresses as high as 20 kV/mm at the lead sheath during normal over-voltage tests.

The addition of extra insulation at the end of the sheath results in an increased diameter of the end; this requires larger hermetic sealed enclosures. Due to the above-mentioned problems of the stress cone as reported by Webb, subsequent designs were made and patents taken out using basically the alternative design, shown in Fig. 1.2(b). The major difference being that instead of designing all the screens on the outside of the cable insulation the conductor is taken directly as the high tension plate of the series of condensers. The outer

condenser plate is jointed to the sheath of the cable by means of a metallization giving a grading of a form calculated according to equation (1.1) in such a way as to maintain the longitudinal component of the electric field below the permissible value. For very compact termination the metal cylinders were made 50 μm thick and the thickness of the dielectric was 1 mm to 2 mm.

The result of the early operational experience gained with the condenser cone was a further refinement and a combined design in which both voltage grading and the axial component of the stress became the design criteria [9] - [11]. Elaborate calculations of such improved designs are given in references [8] and [12]; corona levels are also taken into account. To give the reader an appreciation of such designs, consider the following dimensions and figures: for a 220 kV termination the length of the first screen near the conductor (Fig. 1.3) is about 1000 mm and the length of protrusion between cylinders is taken from experience as 20 mm to 30 mm for a 70 mm diameter, 66 kV cable (150 mm^2) using impregnated paper, the mean longitudinal electric stress was 6 kV/cm along the grading and 3 kV/cm along the cable at flashover rated voltage (usually 3 to 4 times of rated phase voltage).

The principal disadvantage of the prefabricated cones is the time taken in mounting them; however, this is offset by the required labour cost if the insulation were wrapped manually.

Recently, 1977, the Phelps Dodge Cable and Wire Company reported a prefabricated printed circuit capacitive-graded joint for 138 kV which safely passed all the specified test requirements. Such a printed circuit condenser cone termination reduces the above disadvantage. The design objectives for the joint were the usual uniform capacitive voltage grading and a more refined approach for achieving a uniform longitudinal stress by proper selection of the grading elements [13]. By solving incremental voltage and current equations in terms of distributed elements (capacitance) an equation for the longitudinal stress distribution is obtained which is used for the stress relief profile.

1.3 Analytically Calculated Terminal Stress Relief Profiles

As early as the 1920's a patent was taken out in Britain for a terminal stress relief profile that was calculated mathematically [4]. The trumpet-like shape so obtained had to be truncated if the termination was to be of reasonable dimensions.

Another mathematical expression for the stress relief profile has since been proposed. This expression relates the geometry of the profile to the allowable longitudinal stress [17]. Since this expression has been used to calculate the geometry of the stress control profile for a 345 kV paper insulated system, it is worthwhile to review the mathematical details involved.

In Fig. 1.4 a two-dimensional presentation of a three-dimensional axisymmetric problem is shown. Consider a point (r,z) an axial distance dx from the surface of the stress cone and a corresponding radial distance dr. In the axial direction the point (r,z) is a surface that separates two concentric cylinders of radius r and radius r + dr respectively. Considering the two capacities of the two cylinders, the potential difference across the thickness dr is proportional to a ratio of its capacitance and the series combination of the two capacitances, since the stress cone profile is at ground potential. If C_1 and C_2 are the respective capacitances for the first (thickness $r - R_c$) and second layer thickness (thickness dr) the potential difference across dr is given by

$$E_2 = \frac{1/C_2}{1/C_1 + 1/C_2} E \qquad (1.4)$$

where E is the phase voltage,

$$\left.\begin{aligned} \frac{1}{C_1} &\propto 2 \log_e (r/R_c) \\ \frac{1}{C_2} &\propto 2 \log_e (R_s/r) \end{aligned}\right\} \quad \text{(assuming coaxial cylinders)}$$

and $R_s = r + dr$.

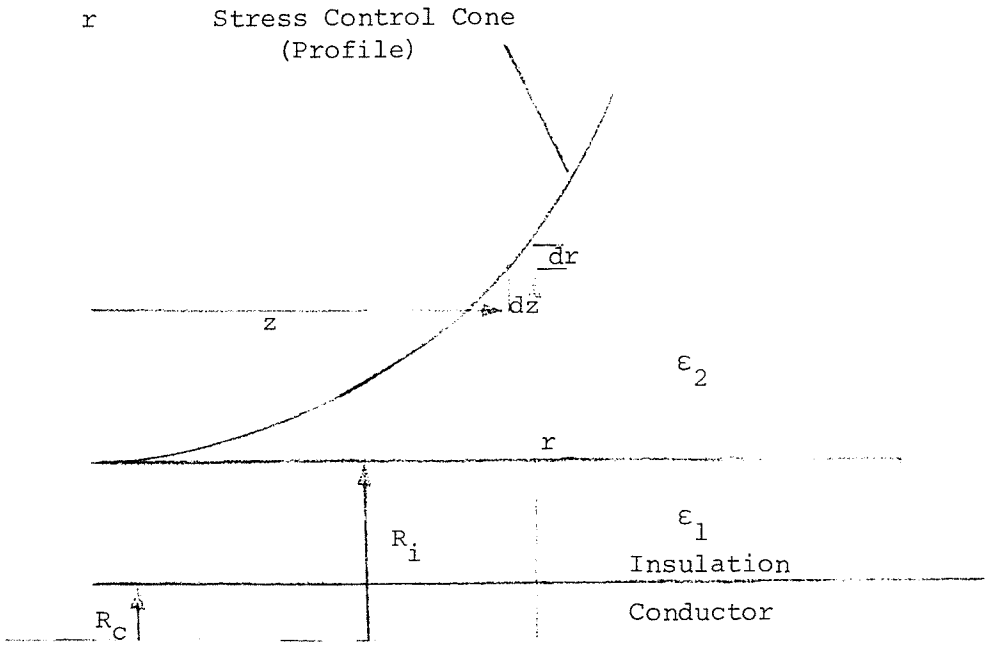

R_c radius of conductor

R_i radius of insulation

$\varepsilon_1, \varepsilon_2$ dielectric constants

Fig. 1.4: Stress Control Cone Analysis.

For dr and dz infinitely small the longtidudinal stress at the stress control cone is given by

$$g = \frac{\partial E_2}{\partial z}$$

or

$$g = \frac{\partial E_2}{\partial R_s} \cdot \frac{\partial R_s}{\partial z} \quad . \tag{1.5}$$

Substitution for E_2 in (1.5) gives:

$$g = \frac{\partial}{\partial R_s} \left(\frac{E \log_e (R_s/r)}{\log_e (R_s/R_c)} \right) \frac{\partial R_s}{\partial z} \quad . \tag{1.6}$$

$$= \frac{E}{R_s} \left(\frac{\log_e (r/R_c)}{(\log_e (R_s/R_c))^2} \right) \frac{\partial R_s}{\partial z} \quad . \tag{1.7}$$

Now if dr and dz are made to tend to zero then $R_s = r$ and (1.7) becomes

$$g = \frac{E}{r} \frac{1}{\log_e (r/R_c)} \frac{\partial r}{\partial z} \quad . \tag{1.8}$$

Integration of (1.8) between the limits,

$$z = \begin{cases} 0 & \text{at point of sheath termination} \\ z & \text{any point along the stress control profile} \end{cases}$$

and

$$r = \begin{cases} R_i & \text{as in Fig. 1.4} \\ r & \text{as for z} \end{cases}$$

gives

$$z = \frac{E}{g} \log_e \left(\frac{\log_e (r/R_c)}{\log_e (R_i/R_c)} \right) . \qquad (1.9)$$

Thus, equation (1.9) gives a certain stress cone contour for a given longitudinal stress. Such a stress is the maximum longitudinal component within the confines of that profile and therefore the maximum value will lie on the profile. For a given case E, R_c, R_i will be specified and a constant longitudinal stress g can be specified from practical limitations of the insulating material. A series of profiles can be drawn as shown in Fig. 1.5, and the maximum diameter of the profile is obtained by a trial and error process as described in reference [18].

In an attempt to reduce installation cost the Rome Cable Company of New Jersey developed an empirical formula for calculating stress control cone profile for 15 kV URD terminations [19]. Insulating tape is wrapped until the profile dimensions are in agreement with the double logarithm empirical formula as given in equation (1.10) using the notation in Fig. 1.4;

$$\log r = \frac{\varepsilon_2/\varepsilon_1 \log_{10} (R_i/R_c)}{E/g_c z - 1.0} + \log_{10} 2R_i \qquad (1.10)$$

where g_c = the maximum gradient at the conductor surface and all other symbols are as given previously for Fig. 1.4.

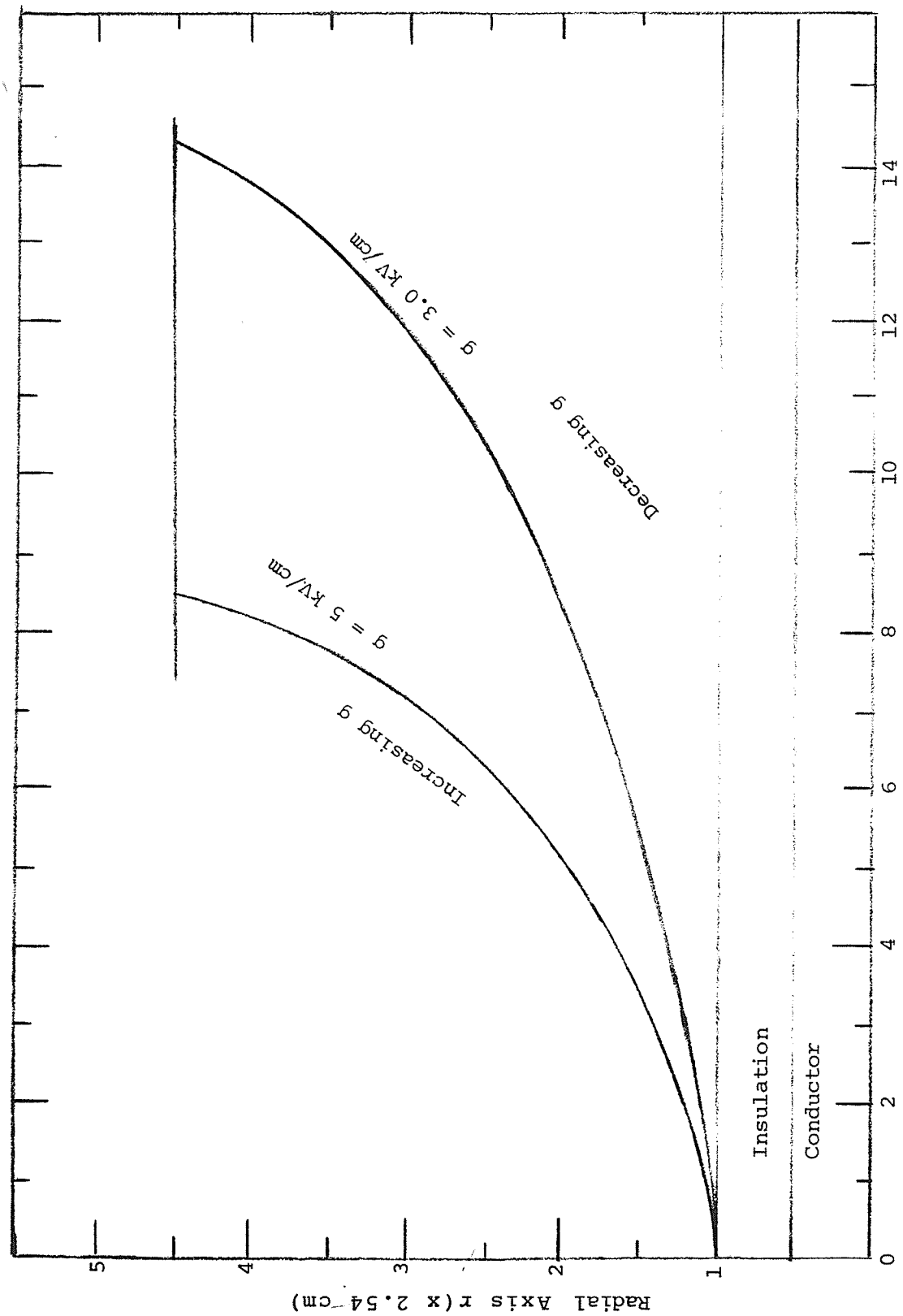

Fig. 1.5: Stress Relief Profiles Using Equation (1.9).

Stress relief profiles obtained using equation (1.10) have been used by various utilities. However, there has been no technical report in the literature about its applicability. It is interesting to note that when geometric dimensions for a 132 kV cable (General Cable Corporation XLPE insulated) are substituted in equation (1.10) absurd profile dimensions result.

1.4 Objective and Format of Dissertation

There exists a need for better cable termination methods as well as for compact EHV cables and compact-terminations. Accordingly one of the objectives of this thesis is to be able to calculate the geometry of the stress relief profile for any specified maximum longitudinal stress; a computer-aided design procedure will be used. In the EHV XLPE termination depicted in Fig. 1.6, an interface between the liquid and the XLPE solid is indicated. To be able to depict contour B both numerical and experimental studies have to be carried out. Therefore the second objective of this thesis is experimental study of the breakdown characteristics of this liquid/XLPE interface in the termination.

It may be pointed out that using XLPE molded termination on an XLPE-insulated cable gives a good design from a thermal point of view. The design of the housing indicated in Fig. 1.6 will not be considered in this work.

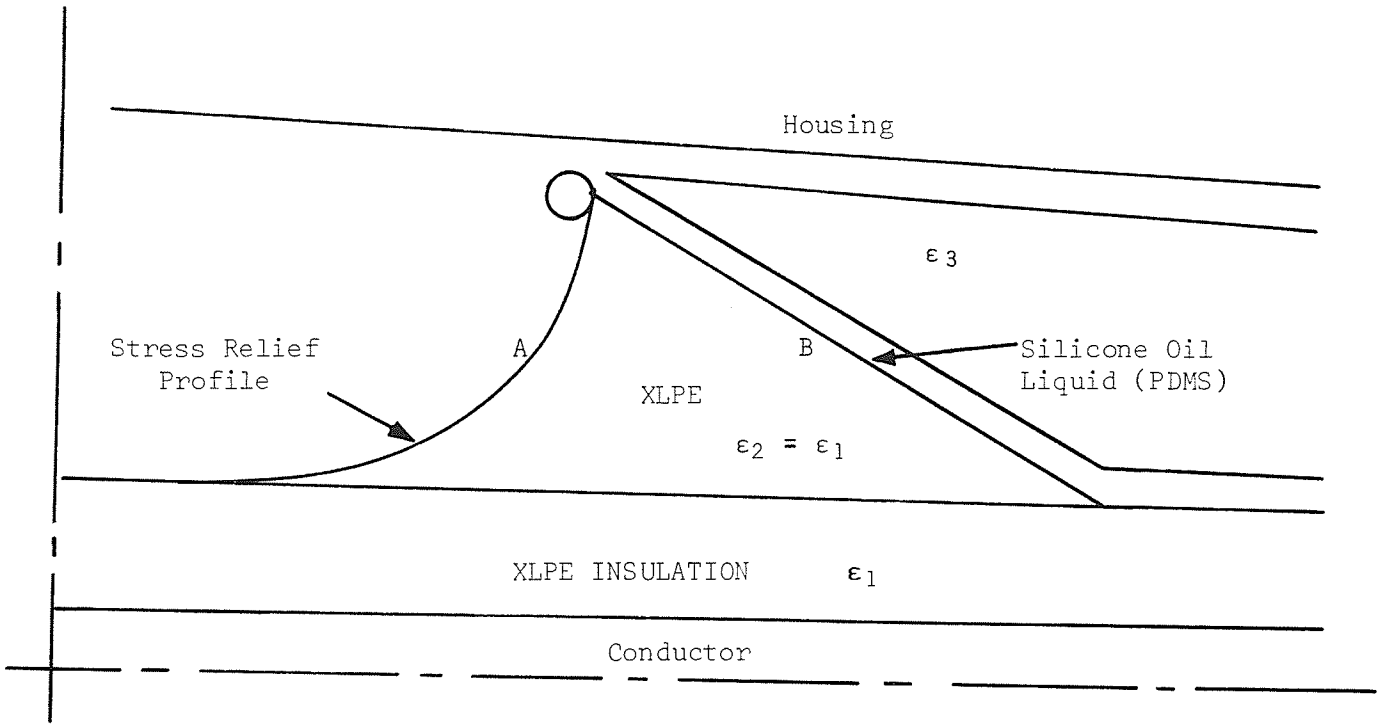

Figure 1.6: Molded XLPE termination for XLPE cable.

In Chapter II, a relatively new method capable of handling unbounded regions is studied in detail with the aim of applying it to solve the electrostatic field of a cable termination. Chapter III deals with cable termination field studies and a stress relief profile equation is proposed from a computer-aided design procedure. As a prelude to the experimental studies of the liquid/XLPE interface given in Chapter VI, the developmental experience and properties of XLPE as well as the dielectric properties of silicon oil are reviewed in Chapter IV; followed by a review of liquid/solid interface breadkown studies in Chapter V. Finally, the salient conclusions of this thesis and suggestions for further work are summarized in Chapter VII.

CHAPTER II

CALCULATION OF THE ELECTROSTATIC FIELD AT THE STRESS RELIEF PROFILE

2.1 Introduction

Transmission voltages have risen rapidly in recent years, and will continue increasing in the future. The high voltage levels pose many difficult problems for the transmission and general equipment designer, especially in connection with insulation. At the same time extensive developments have been made of cable insulation capable of withstanding extremely high radial stresses resulting in very compact EHV (and UHV) power cables rated at thousands of megawatts. An urgent need, therefore, exists for new methods for analysing the electric fields surrounding high voltage conductors, equipment, etc., to provide the system and equipment designers the information relating to stress distribution, corona levels, and so on, for compact and yet reliable designs.

The two fundamental difficulties in determining the electric field near a high voltage device are: (i) the geometry is usually very complicated; and, (ii) part of the space, if not all of it, in which the problem is posed extends outward infinitely far. Consider an underground cable with a termination stress cone as shown in Fig. 2.1: Mathematically, the electrostatic potential function ϕ is determined by solving Laplace's

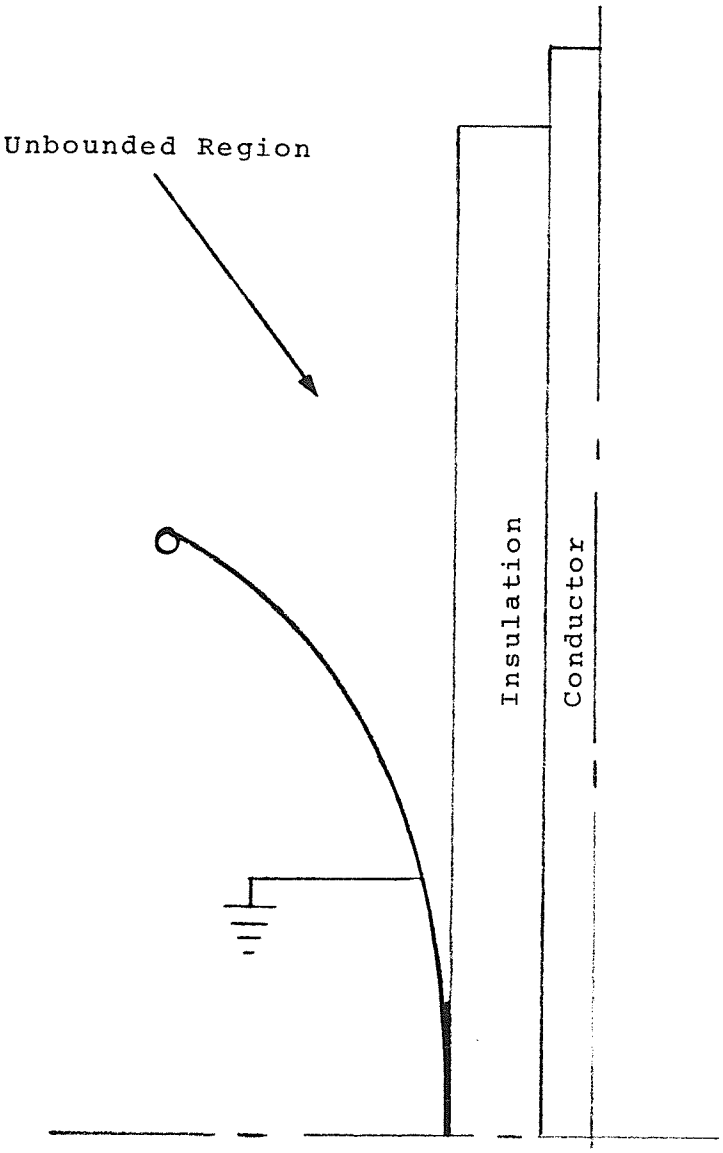

Fig. 2.1: The Infinitely Extending Field of a Cable Termination.

equation (2.1) everywhere outside the conductive portions subject to the restriction that the potential assumes the operating line-neutral voltage at the conductor and ground potential at the grounded sheath and stress relief profile.

$$\nabla^2 \phi = 0 \ . \qquad (2.1)$$

Further, both the potential and the electric flux are continuous at the interface of the dielectric media. The electrostatic field must approach the value zero in a region far from the unbounded portion of the problem. Only purely analytical methods are capable of exactly handling such infinitely extending fields. However, an analytical solution of equation (2.1) is only possible for very simple boundary shapes which are usually of little practical interest to the design engineer [34]; therefore, numerical or analog methods are normally the only practical ones. The latter methods have their own limitations [21] and in the age of very fast computing machines the time involved in setting up a suitable analog, together with inherent measurement inaccuracies have resulted in the former being developed extensively.

A numerical solution of unbounded problems poses certain difficulties. The well known finite-difference approximation methods are successful in treating finite regions, [22] - [26]. With approximations, finite-difference approximations may be used to handle unbounded or exterior problems. Recently, the finite-element method has found increasing application to electric,

magnetic, and electromagnetic-field problems. It has been found to be far superior to the finite-difference method in solving a number of bounded problems. Its use in solving unbounded problems, on the other hand, has suffered restrictions similar to those that limit the finite-difference method. Numerical methods for solving unbounded field problems include:

(1) The Finite-Difference Boundary Relaxation Method [27] - [30]. The main disadvantage of this method stems from the fact that the entries of a large shift matrix have to be calculated and stored; and the usual tedious discretization procedure inherent in the finite difference method when complex geometries and media interfaces are involved.

(2) The Charge Simulation Method [31] - [33]. For complex electrode geometries and media interfaces, this method might suffer from storage restrictions. Furthermore, in order to avoid oscillations of the field function at points on the electrodes more source points would have to be used thus compounding the matrix size problem.

(3) Combined Partial Differential Equation (PDE) and Integral Equation (IE) Formulation. This is a relatively new procedure involving the finite element method for solving the unbounded field problem and one version studied by this author is here below described in detail.

2.2 PDE/IE Formulation

In the finite element method the solution to a field problem governed by, say, equation (2.1) which is a partial differential equation (PDE), is approximated by subdividing the region of interest into elements and representing the solution within each element by a relatively simple function. Such a function is called an interpolation function - a polynomial being the common form of interpolation function. The interpolation polynomial is usually directly substituted into the governing field equation to obtain the nodal value equations. Whereas in the finite difference approach direct solution of the approximating equations subject to specified boundary conditions is sought, in the finite element method a variational formulation is followed. Mathematically, it can be shown by the use of the Euler condition [35] that the problem can be restated identically as the determination of the minimum value of an appropriate functional subject to Dirichlet boundary conditions. The shapes of the elements and their degree of interconnection (number of nodes) are features by which the accuracy of representation can be improved.

For a bounded region the application of the finite element method (PDE formulation) to electrostatic field problems has fully been documented in literature, however, a much greater proliferation exists in literature for application to field problems in mechanics [36] - [40]. A brief review, of the finite element, PDE formulation

for the cable termination is presented. Laplace's equation in cylindrical coordinates is used for the termination problem, assuming it is completely bounded by Dirichlet conditions. Thus equation (2.1) becomes:

$$\nabla^2\phi = \frac{1}{r}\frac{\partial}{\partial r}\left(r\frac{\partial\phi}{\partial r}\right) + \frac{1}{r^2}\frac{\partial^2\phi}{\partial\psi^2} + \frac{\partial^2\phi}{\partial z^2} = 0 \quad . \tag{2.2}$$

Solution of equation (2.2), subject to the corresponding natural boundary conditions can be shown to minimize the functional

$$F(\phi) = \int_\Omega \varepsilon\left[\left(\frac{\partial\phi}{\partial r}\right)^2 + \left(\frac{1}{r}\frac{\partial\phi}{\partial\psi}\right)^2 + \left(\frac{\partial\phi}{\partial z}\right)^2\right] d\Omega \tag{2.3}$$

where Ω is the region of the continuum subdivision - element and

ε is the dielectric constant.

For a rotationally symmetric region, equation (2.3) simplifies to only two derivatives since

$$\frac{\partial\phi}{\partial\psi} = 0$$

$$F(\phi) = \int_\Omega \varepsilon\left[\left(\frac{\partial\phi}{\partial r}\right)^2 + \left(\frac{\partial\phi}{\partial z}\right)^2\right] d\Omega \quad . \tag{2.4}$$

The field in each element is represented by a combination of appropriate polynomial interpolation functions defined on an element basis, and node potentials which are field values at

specific points - corners and sides of the element.

Let

$$\phi = [\alpha]^T \quad [\phi]$$

$$= [\phi]^T \quad [\alpha] \tag{2.5}$$

where

$$\alpha_j = \begin{cases} 1 \text{ at node } j \\ 0 \text{ at any other node} \end{cases}$$

are the interpolation polynomials.

The subscript j refers to specific node positions in the region Ω. For an axisymmetric problem Ω is a volume, thus equation (2.4) becomes for a given element, using vector notation:

$$F(\phi) = [\phi]^T \int_{\Omega} \varepsilon \nabla [\alpha] \cdot \nabla [\alpha]^T [\phi] 2\pi r dr dz \tag{2.6}$$

To carry out the integration of equation (2.6), it is convenient to use numerical integration. In such a case the radial displacement r is expressed in terms of the interpolation polynomials α_j, thus for each element

$$r = \sum_{j=1}^{n} \alpha_i \, r_j \tag{2.7}$$

α_j have the same restrictions as in equation (2.6).

For simple first-order interpolation functions, equation (2.7), when evaluated gives the centroidal value of r for a given element. However, for higher order interpolation functions the integration has to be carried out in terms of area coordinates - a very laborious operation but this need be done only once [38], [41], [42].

Minimizing the functional in equation (2.6) with respect to the field variable ϕ subject to the known Dirichlet boundary conditions, the homogeneous Neumann boundary conditions being satisfied naturally, and summing up for the entire region, a system of linear equations in $[\phi]$ is obtained - equation (2.8)

$$[S] \quad [\phi] \quad = \quad [b]. \qquad (2.8)$$

The right-hand vector [b] results, in this case, from application of the known Dirichlet conditions. For a bounded region Ω equation (2.8) is solved using one of the many methods for solving systems of equations [43], [44]. For an infinitely extending field, so far, integral equation (I.E.) formulations have been used for the modification as will be shown later.

2.2.1 I.E. Formulation

The Integral Equation (I.E.) formulation for solving electrostatic fields was originally derived from the application of classical potential theory [45], [46].

For an interior region R bounded by surface S so as to enclose all sources and media interfaces, the value of the function in the exterior Laplacian region can be given by a mixed double- and single-layer representation provided by Green's formula [46], [48]:

$$\phi(\bar{r}') = \iint_S \left[G(\bar{r}', \bar{r}) \frac{\partial \phi(\bar{r})}{\partial n} - \phi(\bar{r}) \frac{\partial G(\bar{r}', \bar{r})}{\partial n} \right] ds \qquad (2.9)$$

where $G(\bar{r}', \bar{r})$ is the Green's free space function for Laplace's equation (2.1) and is the potential at point $\bar{r}'$ external to R due to unit point source at $\bar{r}$ on surface S [47].

The normal in equation (2.9) is directed into the interior region R.

Since the integral equation formulation describes the field in the exterior region as given by equation (2.9), it can be used in conjunction with a finite element PDE formulation, with the latter used for the solution in the interior region, to solve infinitely extending or unbounded problems. For electrostatic field problems, such combined PDE/IE formulations were first reported by Williams and Cambrell [49] in which an iterative scheme was used for the values of the potential lying on an auxiliary boundary, subject to (2.9) and then used in solving (2.8). Later a direct substitution method for $\phi(\bar{r})$, on an auxiliary boundary in equations (2.8) was reported [50].

The coupling of the PDE formulation and the I.E. formulation is still a subject of research with an effort to develop a more efficient alogrithm and new schemes have been reported [51], [52].

Before presenting the PDE IE - constrained formulation the application of the Integral Equation to fields of simple geometries is studied. The purpose of such numerical experiments will be to learn the behaviour of the normal derivative of the field function ϕ when calculated from an approximation of the field function. For an infinitely extending line charge, say in the z-plane, the field is completely determined in the remaining x- and y- planes. The free space Green's function for such a field is two-dimensional given by

$$G(\bar{r}', \bar{r}) = - \frac{1}{2\pi} \log_e (|\bar{r}' - \bar{r}|) \qquad (2.10)$$

where $\bar{r}'$, is the observation point and $\bar{r}$ the source point. Behaviour at infinity for the field due to an infinitely extending line charge cannot be as easily established as for the three-dimensional case [47]. The appropriate Green's formula for a field due to an infinitely extending line charge is given by

$$\phi(\bar{r}) = \int_{\ell} [G(\bar{r}', \bar{r}) \frac{\partial \phi}{\partial n} (\bar{r}) - \phi(\bar{r}) \frac{\partial G(\bar{r}', \bar{r})}{\partial n}] \, d\ell \qquad (2.11)$$

$d\ell$ is a line segment since the surface enclosing a two-dimensional region is a line contour.

For an infinitely extending charged line with a total charge of $\frac{-1}{(2\pi\varepsilon)}$ C (ε is the dielectric constant of the medium-free space) the value of the electrostatic potential is calculated at a number of points distance $|\bar{r}'|$ from the source, Fig. 2.2. The potential due to this charged line at any distance $|\bar{r}'|$ is logarithmic and is given by:

$$\phi(\bar{r}') = \log_e |\bar{r}'| \qquad (2.12)$$

for a charge of $\frac{-1}{2\pi\varepsilon}$ Coulombs.

Using equation (2.11) $\phi(\bar{r}')$ is calculated at various distances

$$|\bar{r}'| = 0.75,\ 0.7906,\ 0.9014,\ 1.0607\ .$$

The integration contour was initially a circle of radius $|\bar{r}| = 0.625$; this is equivalent to a constant value for $\phi(\bar{r})$ and its normal derivative in equation (2.11). Using Simpson's composite three-point integration formula and single precision arithmetic, a step length of 0.7% of total contour length was found necessary to obtain four figure accuracy. Doubling the step length to 1.4% of the contour length resulted in just one figure accuracy.

The case for varying $\phi(\bar{r})$ and its normal derivative at the integration contour was studied by using a square enclosing the circle used above - Fig. 2.2 Again the same integration

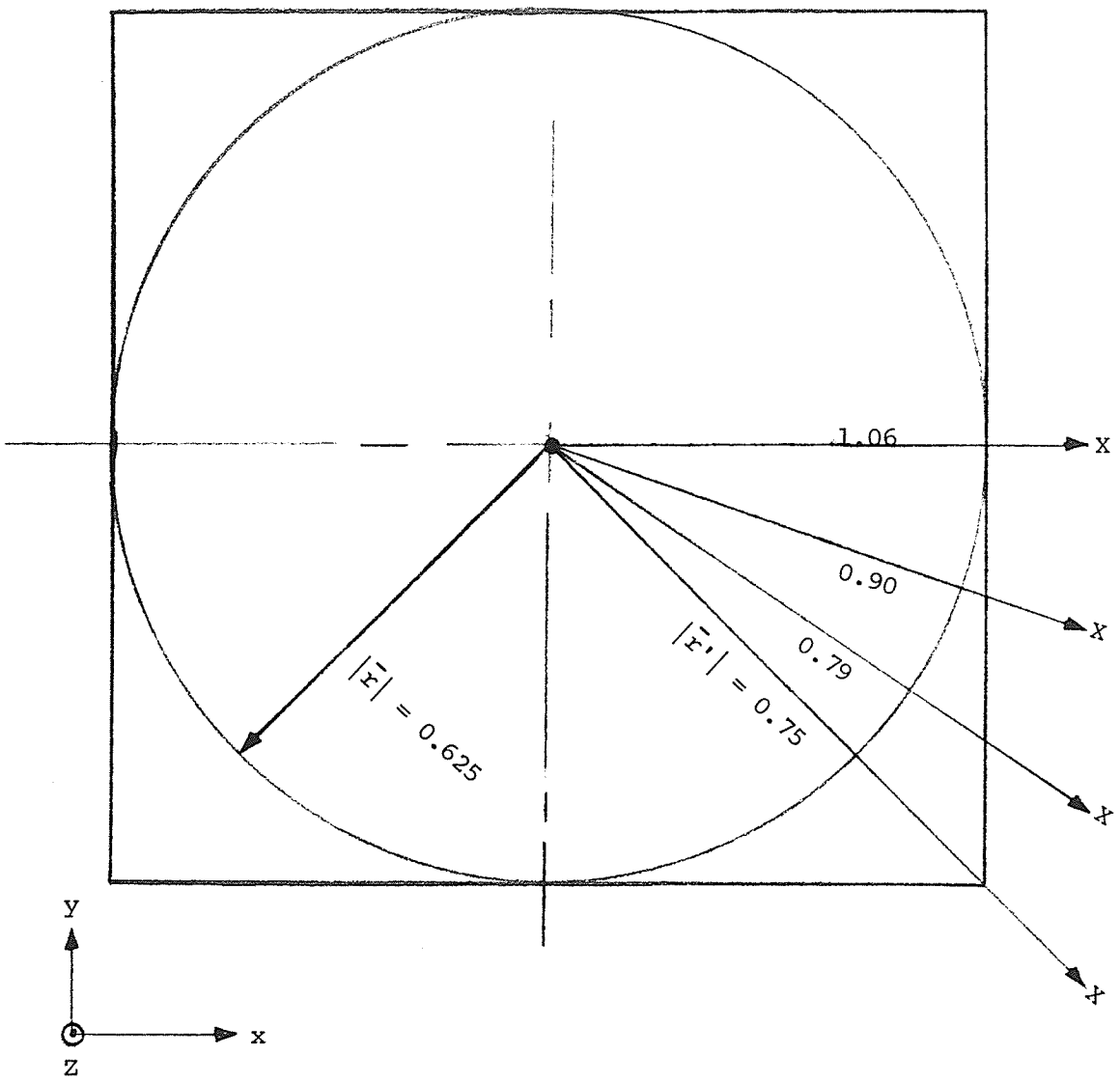

$\lvert\bar{r}'\rvert$	$\phi(\bar{r}') = \log_e \lvert\bar{r}'\rvert$	$\phi^*(\bar{r}')$
0.75	-0.2877	-0.2877
0.7906	-0.2350	-0.2350
0.9014	-0.1038	-0.1038
1.0607	0.05887	0.05889

$\phi^*(\bar{r}')$ obtained from equation (2.24)

Fig. 2.2: Application of the IE to The Field of an Infinitely Extending Charged Line.

procedure was used and four figure accuracy was obtained. The Gauss Quadrature integration scheme was also used.

The next numerical experiment involved a study of the effect of calculating the normal derivative of the potential function from a finite element approximation to the potential function by equation (2.5). Therefore the purpose here is to determine the accuracy of the representation of the normal derivative of the potential function, $\frac{\partial \phi}{\partial n}$, by an approximation of equation (2.13)

$$\frac{\partial \phi}{\partial n} = \Phi^T \frac{\partial \underline{\alpha}}{\partial n} \quad . \tag{2.13}$$

Fig. 2.3 shows an infinitely extending conducting cylinder of radius 0.25 units charged to a potential of 100.0 V. A portion of the region exterior to the cylinder is subdivided into finite elements so as to completely enclose the cylinder as shown in Fig. 2.3. The value of $\phi(\bar{r}')$ at any point distance $|\bar{r}'|$ from the centre of the cylinder can be calculated analytically. With the known values of $\phi(\bar{r})$ and $\frac{\partial \phi(\bar{r})}{\partial n}$ at the node points, using second-order interpolation functions for $\phi(\bar{r})$ in each element, equation (2.11) was used to calculate $\phi(\bar{r}')$. The integration contour was formed by element-side pieces through the vertices; IC_1 in Fig. 2.3. The error between the analytically calculated value of $\phi(\bar{r})$ and that obtained by equation (2.11) was found to be independent of the step length in Simpsons' three-point

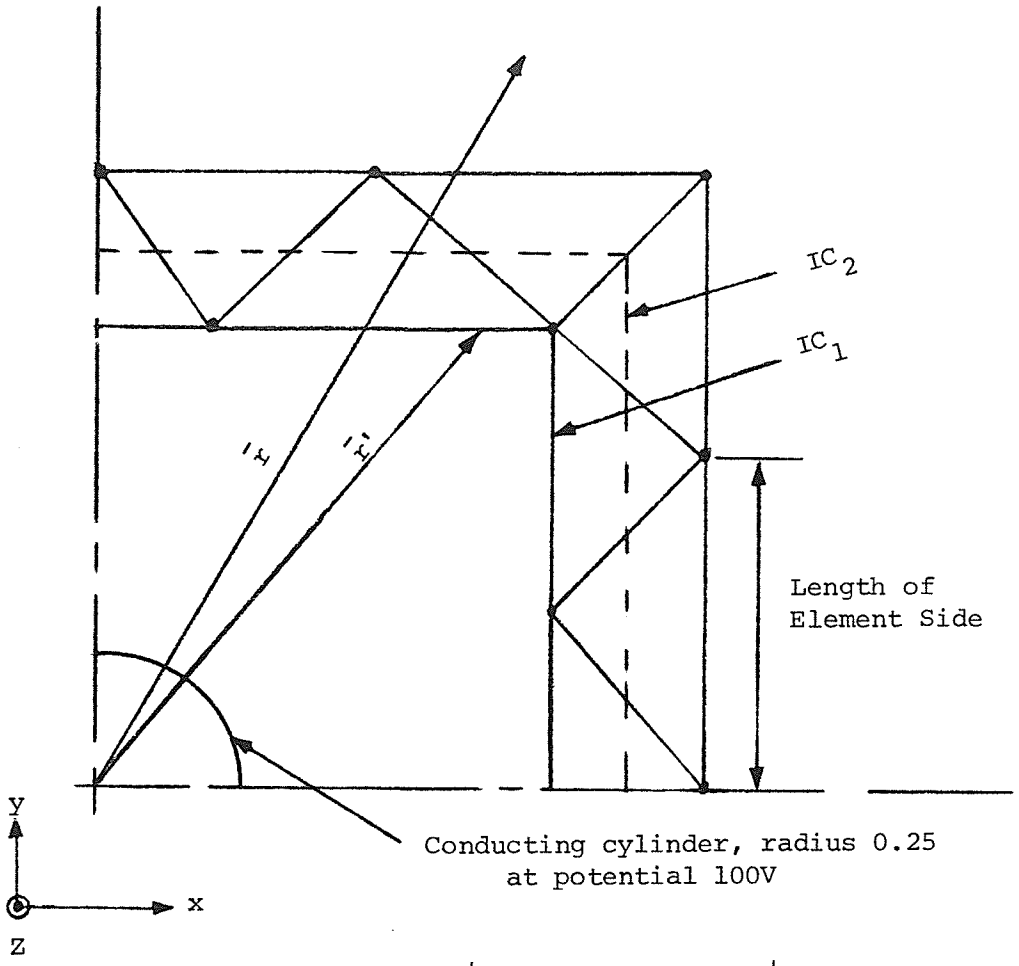

$\lvert\bar{r}'\rvert$	$\phi(\bar{r}')$ Analytical	$\phi^*(\bar{r}')$ (I.E.)
1.0	0.0	-0.1585
1.25	-16.0964	-15.8353
1.5	-29.2481	-28.6850
1.75	-40.3677	-39.5634
2.0	-50.0	-48.9924

IC_1, IC_2 Integration Contours

Fig. 2.3: Application of the I.E. to The Field of an Infinitely Extending Conducting Cylinder.

integration formula or the order of Gaussian Quadrature. The error was 0.36% of the analytical value; in double precision arithmetic agreement was only obtained up to two significant figures. However, when only $\phi(\bar{r})$ was specified (analytical value) at the nodes and the normal derivative being obtained by equation (2.13), even at the nodes the error increased up to 2.0%. The error did not vary significantly with $|\bar{r}' - \bar{r}|$, however, the maximum value of 2.0% occurred at the largest value of $|\bar{r}' - \bar{r}|$ investigated. The error for a lower value was 1.6%. When integration contour IC_2 (as shown in Fig. 2.3) was used, the absolute error changed from 2.0% to 2.9%. Efforts to reduce this error by decreasing the integrating step length or the order of integration did not help. However, when the distance between nodes on IC_1 was halved, the maximum error decreased to 0.38%. Therefore, it can be concluded that approximation of the normal derivative of the potential function by equation (2.13) governs the accuracy obtained using the Integral Equation more than the integration approximation.

From the two-dimensional fields, the next case to be considered is the three-dimensional axisymmetric field. Green's function for a general three-dimensional problem can be stated as:

$$G(\bar{r}', \bar{r}) = \frac{1}{4\pi |\bar{r}' - \bar{r}|} . \qquad (2.14)$$

Now consider a cylindrical surface formed by a series of circular line charges centered at various positions on the z-axis (Fig. 2.4):

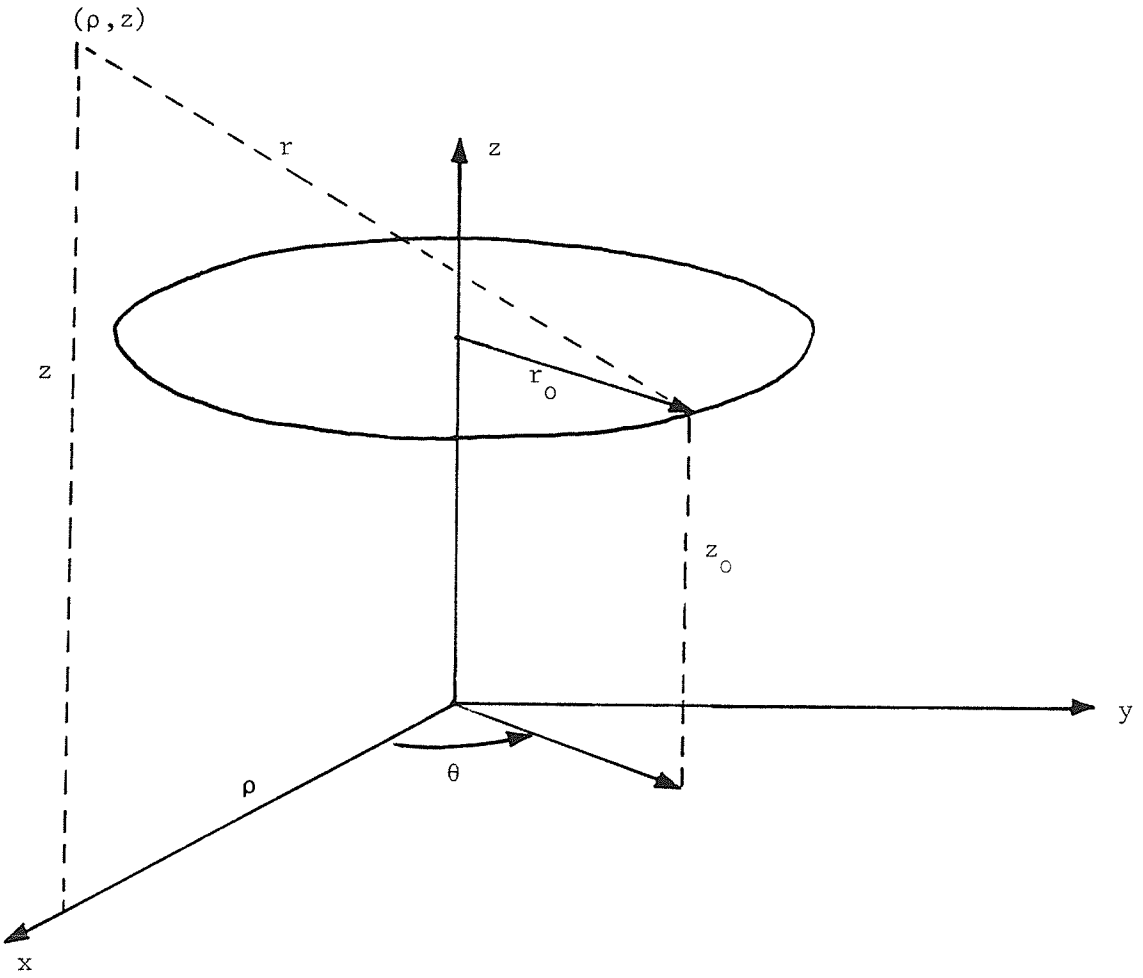

Fig. 2.4: Green's Function for Axisymmetric Field.

For one such circular line charge, the distance between source and observation point is marked as r in Fig. 2.4 and is given by:

$$r = [(\rho - r_o \cos\theta)^2 + (r_o \operatorname{Sin}\theta)^2 + (2 - z_o)^2]^{\frac{1}{2}} \qquad (2.15)$$

for an incremental length of the line. Summing up for the entire line equation (2.14) becomes:

$$G(\bar{r}', \bar{r}) = \int_o^{2\pi} \frac{d\theta}{4\pi[(\rho - r_o \operatorname{Cos}\theta)^2 + (r_o \sin\theta)^2 + (z - z_o)^2]^{\frac{1}{2}}} . \qquad (2.16)$$

Substituting $\theta = \pi - 2\psi$

$$\therefore d\theta = -2d\psi$$

$$\therefore \operatorname{Cos}\theta = -[1 - 2\operatorname{Sin}^2\psi]$$

gives

$$G(\bar{r}', \bar{r}) = \int_{\pi/2}^{\pi/2} \frac{2\, d\psi}{4\pi[\rho^2 + r_o^2 + 2\rho r_o (1 - 2\operatorname{Sin}^2\psi) + (z - z_o)^2]^{\frac{1}{2}}}$$

(2.17)

$$= \frac{1}{\pi[(\rho + r_o)^2 + (z - z_o)^2]^{\frac{1}{2}}} \int_o^{\pi/2} \frac{d\psi}{\left[1 - \frac{4\rho\, r_o \operatorname{Sin}^2\psi}{(\rho + r_o)^2 + (z - z_o)^2}\right]^{\frac{1}{2}}} .$$

(2.18)

The integral in equation (2.18) is a complete elliptic integral of the first kind with modulus

$$[4\rho r_o / [(\rho + r_o)^2 + (z - z_o)^2]]^{\frac{1}{2}} .$$

For a circular line charge the value of the electrostatic potential was calculated using equation (2.9).

2.2.2 The PDE IE-Constrained Formulation

The PDE IE-constrained formulation will now be applied to infinitely extending fields. Consider a surface IC in Fig. 2.5 which divides space into an interior region R_1 and an exterior region R_2, let an auxiliary boundary AB be drawn in R_2 to enclose completely region R_1.

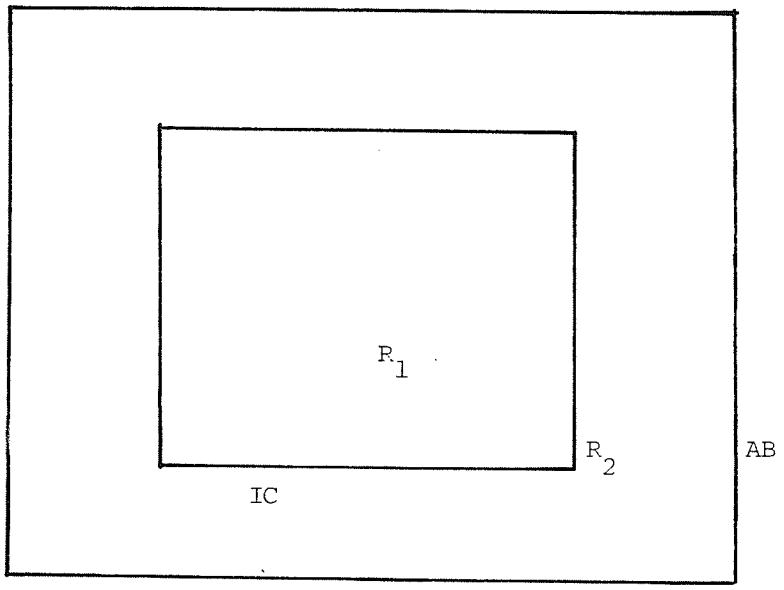

Fig. 2.5: PDE IE-constrained formulation.

IC Integration contour surface

AB Auxiliary boundary

The only restrictions on IC and AB are that IC be drawn to enclose all conductors and media-interfaces and AB should be drawn in a homogeneous region - free space in this case. Application of the PDE formulation to the entire region interior to AB results in equations (2.8). The value of $[\Phi]$ obtained from solving equation (2.8) would, in this case, imply that the auxiliary boundary AB has implicit natural boundary conditions. Such a solution would therefore be in error. However, if the values of the function at points on AB are known from an I.E. formulation, then such values may be used to constrain equations (2.8) to give the proper solution to $[\Phi]$. Since the function is not known at AB, its approximation of equation (2.5) may be used in the Integral Equation (2.9) to give equation (2.19):

$$[\alpha_i]^T [\Phi_B] = [\Phi_{IC}]^T \int_{IC} \int [G(\bar{r}', \bar{r}) \frac{\partial [\alpha]}{\partial n} - [\alpha] \frac{\partial G}{\partial n} (\bar{r}', \bar{r}] \, dS \tag{2.19}$$

IC is the surface integration contour

$[\Phi_{IC}]$ are nodal values of the potential function for elements through which IC passes

$[\Phi_B]$ are values of the function at node points on AB.

If the integral equation is applied at each node on the auxiliary boundary AB then

$$\alpha_i \Phi_B = \Phi_B \quad . \tag{2.20}$$

Since $\alpha_i = 1$ at node points.

If for each node at the auxiliary boundary the value of the potential function is expressed by equations (2.19) and (2.20), then a system of equations in $[\Phi_{IC}]$ may be written for all nodes on AB as

$$[\Phi_B] = [P]\ [\Phi_{IC}] \tag{2.21a}$$

[P] is a rectangular matrix with the number of rows equal to the number of nodes on the auxiliary boundary AB and number of columns equal to the number of nodes on all the elements through which the integration contour IC passes. By interspersing with zeros in matrix [P] the number of columns of [P] may be increased to include all the nodes of the whole system including those on the auxiliary boundary. Thus equation (2.21a) becomes

$$[\Phi_B] = [Q]\ [\Phi] \tag{2.21b}$$

$[\Phi]$ is the unknown potential vector as in equation (2.8). Since vector $[\Phi]$ contains the unknown nodal potential values for the entire system including those on the boundary, equation (2.21b) may further be simplified to

$$[C]\ [\Phi] = [O] \tag{2.21c}$$

where matrix [C] is obtained by subtracting an appropriate rectangular identity matrix from [Q] so as to absorb $[\Phi_B]$ into $[\Phi]$.

Matrix [C] has as many rows as there are nodes on the auxiliary boundary AB and as many columns as there are nodes in the entire region interiorally to and including AB.

Equation (2.21c) may be used to constrain equation (2.8) by using the concept of Lagrange multipliers [53]. Constraining equation (2.8) by the Lagrange multiplier method with constraints of (2.21c) results in an augmented matrix equation:

$$\begin{bmatrix} \underline{S} & \underline{C}^T \\ \underline{C} & \underline{O} \end{bmatrix} = \begin{bmatrix} \underline{\Phi} \\ \underline{\lambda} \end{bmatrix} \quad \begin{bmatrix} \underline{b} \\ \underline{O} \end{bmatrix} \tag{2.22}$$

$\underline{\lambda}$ are the Lagrange multipliers.

Equation (2.22) may be solved directly, but as the augmented matrix is positive semi-definite, therefore, care must be exercised in the choice of an appropriate solution algorithm Alternatively a partitioned solution may be obtained; since [S] is nonsingular, the upper portion may be solved for $[\Phi]$

$$[\Phi] = [S]^{-1} [b] - [S]^{-1} [C]^T [\lambda] \tag{2.23a}$$

and $[\lambda]$ may be obtained from the lower portion of the augmented matrix as

$$[\lambda] = [\underline{C}\ \underline{S}^{-1}\ \underline{C}^T]^{-1} [C] [S]^{-1} [b] \ . \tag{2.23b}$$

Then substituting equation (2.23b) into (2.23a) gives $\underline{\Phi}$ in terms of known quantities:

$$\underline{\Phi} = \underline{S}^{-1}\ \underline{b} - \underline{S}^{-1}\underline{C}^{T}\ [\underline{C}\ \underline{S}^{-1}\underline{C}^{T}]^{-1}\ \underline{C}\ \underline{S}^{-1}\ \underline{b}\ . \qquad (2.23c)$$

To experimentally prove the validity of equation (2.23a), a P.D.E. interior formulation was constrained by analytically calculated values of Φ_B instead of using the Integral Equation. In such a case equation (2.21c) has a non-zero right-hand side containing the known values of $[\Phi_B]$ at nodes on the auxiliary boundary.

$$[C]\ [\Phi] = [g]\ . \qquad (2.24)$$

Matrix [C] has unity entries for each position corresponding to a boundary node, otherwise the entry is zero. Results obtained for an infinitely extending cylinder, similar to that shown in Fig. 2.4, for various positions $\bar{r}'$ from the center of the cylinder for first, second and third order finite element interpolation polynomials are shown in Tables 2.1, 2.2 and 2.3, respectively. The corresponding errors are also included. The order of matrix [S] was 52, 76, 96 for first, second and third order interpolation polynomials for the same problem area.

Equation (2.24) can also be used to generate more constraints, if an element through which the integration contour passes has a node on, say, an electrode in addition to those

Table 2.1: Electrostatic potential at $\bar{r}$ due to an infinitely extending cylinder centered at $|\bar{r}| = 0$ calculated using a PDE constrained formulation - First Order Interpolation Polynomials

$\|\bar{r}\|$	$\phi^*(\bar{r})$ +	$\phi(\bar{r})$ Analytical	Error++ (%)
0.25	100.00	100.00	-
0.3536	77.0591	75.00	2.7
0.5	51.51188	50.00	3.0
0.5590	42.6478	41.9518	1.66
0.7071	25.0684	25.00	0.27
0.75	20.7519	20.7519	0.0
0.79057	16.9518	16.9518	0.0
0.9014	7.489	7.489	0.0
1.0607	- 4.2481	- 4.2481	0.0

+ $\phi^*(\bar{r})$ Calculated from PDE formulation constrained with known values of potential at the boundary.

++ Error = $\frac{\phi^*(\bar{r}) - (\bar{r})}{\phi(\bar{r})} \times 100\%$

Table 2.2: Electrostatic potential at $\bar{r}$ due to an infinitely extending cylinder centered at $|\bar{r}| = 0$ calculated using a PDE constrained formulation - Second Order Interpolation Polynomials

$\|\bar{r}\|$	$\phi^*(\bar{r})$ +	$\phi(\bar{r})$ Analytical	Error++ (%)
0.25	100.00	100.00	-
0.27951	92.0356	91.9518	0.09
0.30177	86.9204	86.42177	0.58
0.35355	76.0513	75.00	1.4
0.51539	48.9520	47.8134	2.4
0.559	42.8502	41.9518	2.1
0.70711	25.1696	25.00	0.68
0.75	20.7519	20.7519	0.0
0.79057	16.9518	16.9518	0.0
0.90139	7.489	7.489	0.0
1.0607	- 4.2481	- 4.2481	0.0

+ $\phi^*(\bar{r})$ Calculated from a PDE formulation constrained by known values of the electrostatic potential at the boundary.

++ $\text{Error} = \dfrac{\phi^*(\bar{r}) - \phi(\bar{r})}{\phi(\bar{r})} \times 100\%$

Table 2.3: Electrostatic potential at $\bar{r}$ due to an infinitely extending cylinder centered at $|\bar{r}| = 0$ calculated using a PDE constrained formulation - Third Order Interpolation Polymials

$(\bar{r})$	$\phi^*(\bar{r})$ +	$\phi(\bar{r})$ Analytical	Error++ (%)
0.25	100.00	100.00	-
0.38627	67.2746	66.7013	0.86
0.41667	63.3161	63.1517	0.26
0.52022	47.0290	47.1403	-0.24
0.5620	41.7247	41.5649	0.38
0.5833	38.7437	38.8804	-0.35
0.6386	32.2632	32.3490	-0.26
0.75	20.7519	20.7519	0.0
0.79045	16.6839	16.9636	-1.6
0.79057	16.9517	16.9517	0.0
0.90139	7.489	7.489	0.0
1.0607	- 4.2481	- 4.2481	0.0

+ $\phi^*(\bar{r})$ Calculated from a PDE formulation constrained by known values of the electrostatic potential at the boundary.

++ Error = $\frac{\phi^*(\bar{r}) - \phi(\bar{r})}{\phi(\bar{r})} \times 100\%$

constraints from equation (2.11). With $[\Phi_B]$ given by equation (2.11), solution of the electrostatic field of the infinitely extending cylinder was obtained, using a PDE IE-constrained formulation with first, second and third order interpolation polynomials. The results together with the error between the analytical solution and that obtained by constraining PDE by IE are given in Tables 2.4 and 2.6. It is seen that the error is significantly high. In an effort to reduce this error the element size was halved and the results obtained are shown in Table 2.7. Second order finite element interpolation polynomials were used.

The effect of the separation distance d between the integration contour IC and the auxiliary boundary AB was investigated for the infinitely extending cylinder case of Fig. 2.6, using third order finite element interpolation polynomials. It was found that the expected symmetry in the solution is lost when d is in the range:

$$0.2 > d > 0.4 .$$

The least average error was obtained for d equal to 0.375. McDonald has reported that the separation, d, has to be at least 0.25 units [54]. The results obtained for various values of this separation are given in Table 2.8 together with the value of $\log_e d$. It can be seen that the variation of the natural logarithmic function is not unusual

Table 2.4: Electrostatic potential at distance $|\bar{r}|$ from the center of an infinitely extending cylinder calculated by a PDE IE-constrained formulation using First Order Interpolation Polynomials

$\lvert\bar{r}\rvert$	$\phi(\bar{r})$ +	$\phi(\bar{r})$ Analytical	Error++ (%)
0.25	100.0000	100.000	-
0.3536	80.6639	75.000	7.5
0.5	56.740	50.000	13.5
0.5590	51.6598	41.9518	23.0
0.7071	30.1431	25.0	20.6
0.75	22.5600	20.7519	8.7
0.79057	19.0760	16.9518	12.6
0.9014	9.103	7.489	21.5
1.0607	- 4.5022	- 4.2481	5.9

\+ $\phi^*(\bar{r})$ Calculated from IE-constrained PDE formulation

++ Error = $\dfrac{\phi(\bar{r})^* - \phi(\bar{r})}{\phi(\bar{r})} \times 100\%$

Table 2.5: Electrostatic potential at distance $|\bar{r}|$ from the center of an infinitely extending cylinder calculated by a PDE IE-constrained formulation using Second Order Interpolation Polynomials

$\lvert\bar{r}\rvert$	$\phi^*(\bar{r})$ +	$\phi(\bar{r})$ Analytical	Error++ (%)
0.25	100.000	100.000	-
0.27951	93.4651	91.9518	1.6
0.30177	88.9949	86.42177	3.0
0.35355	80.0226	75.000	6.0
0.51539	50.2719	47.8134	5.0
0.559	44.7530	41.9518	6.0
0.70711	28.2617	25.000	13.0
0.75	22.8925	20.7519	10.3
0.79057	18.9386	16.9518	11.7
0.90139	8.6644	7.489	15.6
1.0607	- 4.6269	- 4.2481	8.9

+ $\phi^*(\bar{r})$ From IE-constrained PDE formulation

++ $\text{Error} = \dfrac{\phi^*(\bar{r}) - (\bar{r})}{\phi(\bar{r})} \times 100\%$

Table 2.6: Electrostatic potential at distance $|\bar{r}|$ from the center of an infinitely extending cylinder calculated by a PDE IE-constrained formulation using Third Order Interpolation Functions

$\lvert\bar{r}\rvert$	$\phi^*(\bar{r})$ +	$\phi(\bar{r})$ Analytical	Error++ (%)
0.25	100.000	100.000	-
0.38627	68.0683	68.6162	-0.8
0.39667	66.3589	66.7013	-0.5
0.41667	62.1974	63.1517	-1.5
0.52022	48.7826	47.1403	3.5
0.5620	38.5221	41.5649	-7.3
0.5833	35.3382	38.8804	-9.1
0.6386	30.6221	32.3488	-5.3
0.75	23.2172	20.7519	11.9
0.79045	16.6513	16.9636	-1.8
0.79057	19.0422	16.9518	12.0
0.90139	8.4858	7.489	13.0
1.0607	- 4.7419	- 4.2481	11.5

+ $\phi^*(\bar{r})$ From IE-constrained PDE formulation

++ $\text{Error} = \dfrac{\phi^*(\bar{r}) - \phi(\bar{r})}{\phi(\bar{r})} \times 100\%$

Table 2.7: The effect of halving the size of the elements through which IC passes on the results given in Table 2.5

$\lvert\bar{r}\rvert$	$\phi^*(\bar{r})$	$\phi(\bar{r})$ Analytical	Error^{++} (%)
0.25	100.000	100.000	-
0.27951	93.4761	91.5818	1.66
0.30177	89.0081	86.42177	2.99
0.35355	80.04630	75.000	6.73
0.51539	50.3402	47.8134	5.28
0.559	44.8946	41.9518	7.0
0.70711	28.3038	25.000	13.2
0.75	23.31897	20.7519	12.37
0.79057	19.2319	16.9518	13.45
0.90139	8.7669	7.489	17.06
1.0607	- 4.7138	- 4.2481	10.96

+ $\phi^*(\bar{r})$ Calculated from IE-constrained PDE formulation

++ Error $= \dfrac{\phi^*(\bar{r}) - \phi(\bar{r})}{\phi(\bar{r})} \times 100\%$

for d greater than, say, 0.125 and therefore numerical integration of the function can be performed without any difficulty. Therefore, the error arising from different values of d, as tabulated, may be attributed to the inadequate approximation of the normal derivative by equation (2.13) since the change in separation is effected by moving the integration contour IC within an element with the $\bar{r}'$ position remaining unchanged.

When the field distribution in a parallel plate capacitor was calculated using the PDE IE-constrained formulation, it was found necessary to space the auxiliary boundary a distance d of at least 0.25 units away from the Integration Contour in order to obtain a symmetrical solution. The electrostatic field due to a frustum (truncated cone with electrodes at the two plane ends) was also studied using the PDE IE-constrained formulation. The values of the electrostatic potential obtained in this case were found to be in error by visual inspection.

In all the cases studied, it was found that the integration step had a very small effect on the solution - decreasing the integration step ten times resulted in change in the fourth decimal place in the solution. This is similar to what was found when calculating $\phi(\bar{r})$ using equation (2.11) for an infinitely extending line charge. The Fortran Computer Program for implementing the PDE IE-constrained formulation is given in Appendix A.

Table 2.8: Investigation of the effect of d^{++} on the results tabulated in Table 2.6

	Error^{+} for various distances between IC & AB				
$\phi(\bar{r})$ Analytical	d^{++}=0.1825	d=0.25	d=0.3125	d=0.375	d-0.4375
68.6162	15.0	11.7	6.1	-0.7	-6.8
66.7013	14.0	11.0	5.8	-0.5	-7.0
63.1517	13.9	10.7	5.0	-1.5	-8.6
47.1403	26.0	22.0	13.5	3.0	-5.0
41.5649	16.0	7.5	-0.6	-7.0	-9.0
38.8804	16.6	6.9	-2.0	-9.0	-10.0
32.3488	19.0	10.7	1.6	-5.3	
20.7519	25.0	26.0	20.0	11.8	7.0
16.9636	32.5	21.0	8.8	-1.8	3.8
16.9518	28.0	29.0	21.0	12.0	10.0
7.489	38.0	36.0	24.0	13.0	17.8
-4.2481	20.1	24.0	19.0	11.8	23.6
$\log_e(d)$	-2.079	-1.386	-1.163	-0.9808	-0.8207

$^{+}$ $$\text{Error} = \frac{\phi^*(\bar{r}) - \phi(\bar{r})}{\phi(\bar{r})} \times 100\%$$

where $\phi^*(\bar{r})$ is numerically calculated using an I.E. constrained PDE formulation

$^{++}$ d is the separation between the Integration Contour IC and the Auxiliary Boundary AB

2.3 Discussion

Numerical methods for handling the unbounded field problem have been reviwed in this chapter with a comprehensive presentation of the Integral Equation constrained finite element formulation. The numerical experiments performed showed that the normal derivative of the potential function may not be adequately approximated by the product of the normal derivative of the interpolation function and the potential function at the nodes (equation (2.13)). This approximation can be improved by using smaller size elements for elements through which the integration contour IC passes. However, this does not result in a substantial improvement in the solution (Table 2.7) as other factors such as the proximity of the auxiliary boundary contour, (AB) also affect the accuracy of this approximation. It should be mentioned that the error due to the finite element method for a similar, but bounded problem does not exceed 0.4%. Therefore, such large percentage error as tabulated (Table 2.4 - 2.9) could be due to the inadequate approximation to the normal derivatives.

One of the main arguments against using artificial boundaries in the far field of an otherwise unbounded problem (such as homogeneous Dirichlet or Neumann) is the fact that the error thus introduced cannot be estimated. However, this would also be true in any method that uses an approximation to the normal derivative such as the IE constrained PDE formulation when applied to practical geometries such as the cable termination of Fig. 2.2. In one of the early papers on the

PDE/IE constrained formulation [49] it was argued that such a formulation would be efficient in that only the region of interest need be examined. The results reported by the authors for a two-conductor transmission line of square cross-section using their combined PDE/IE formulation are, with minor exceptions, bounded by the results obtained using homogeneous Dirichlet, and homogeneous Neumann in the far field. However, it should be noted that their PDE/IE algorithm is computationally much more efficient [49]. Due to the large error obtained with the algorithm as presented here, the combined PDE/IE formulation will not be used in analysis of the field in a cable termination in the next chapter. After typing the manuscript a publication appeared in which the authors had encountered problems with the PDE IE-constrained formulation method [55] as formulated in reference [50]. Consequently, the authors of [55] developed a different formulation; resulting in satisfactory accuracy.

CHAPTER III

THE STRESS-RELIEF PROFILE EQUATION

3.1 Problem Definition

From the review given in Chapter I it is evident that the EHV cable termination problem has not been satisfactorily solved. The trend towards more compact solid insulation cables has been enhanced by the development of synthetic materials of high dielectric strength. Although such new insulation can withstand high radial stresses, it is still weak longitudinally; hence the need for a properly designed terminal stress-relief profile. With the high stress concentration present in compact EHV cables this need is more so now than before.

The termination problem involves the analytical determination of two contours A and B, shown in Fig. 3.1, such that the longitudinal stress along either contour does not exceed an allowable value. The allowable value can be taken as the maximum radial stress divided by a factor of safety. If contour A is properly designed and the terminal corona shield (Fig. 3.1) placed so as not to influence the field at any point on A, contour B is very easily determined. This assumes that the dielectric constant of the insulation filling the space between A and B is equal to the dielectric constant of the cable insulation. Therefore, in such a case proper design of contour A governs the termination design problem.

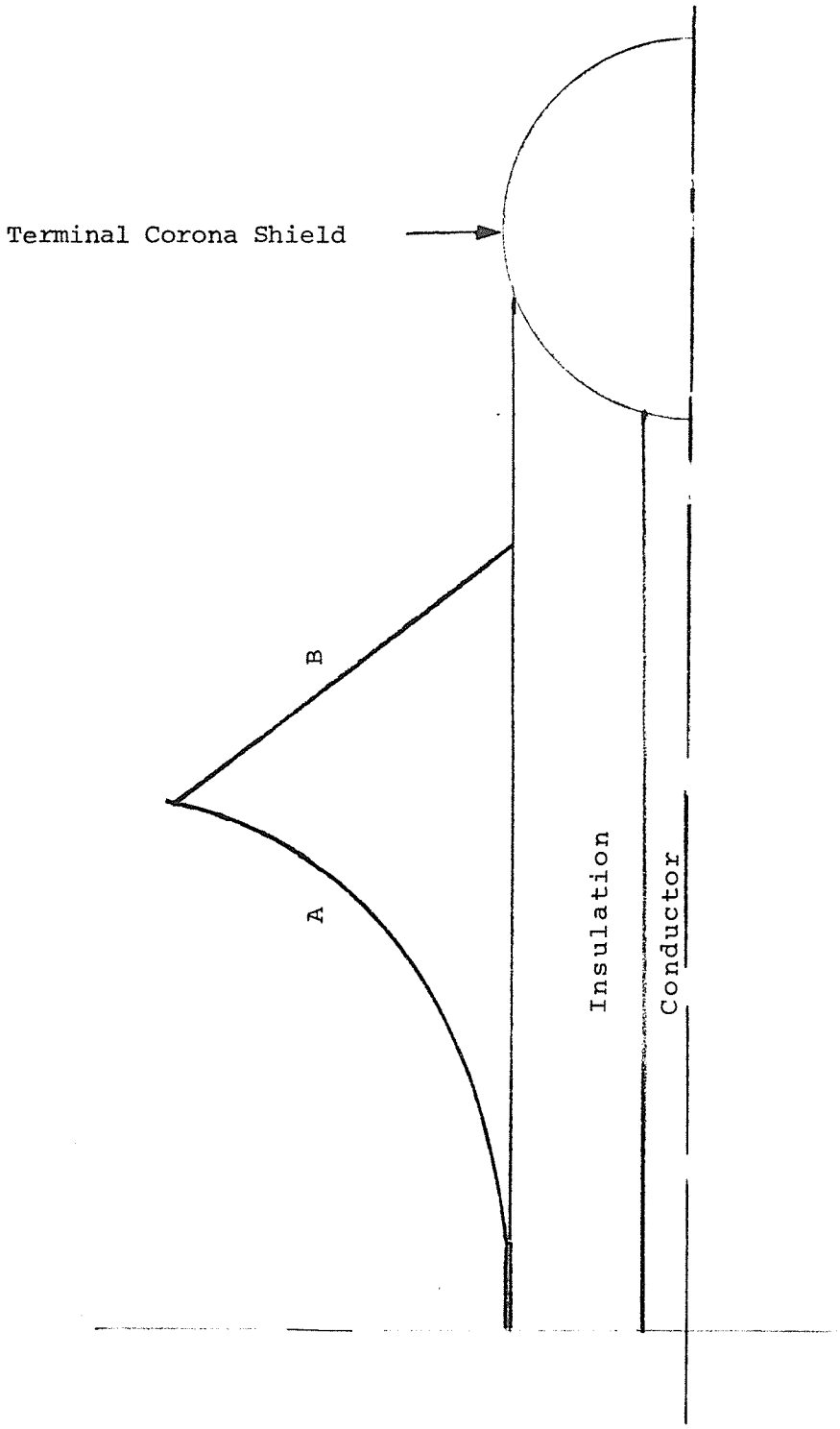

Fig. 3.1: Termination Profile.

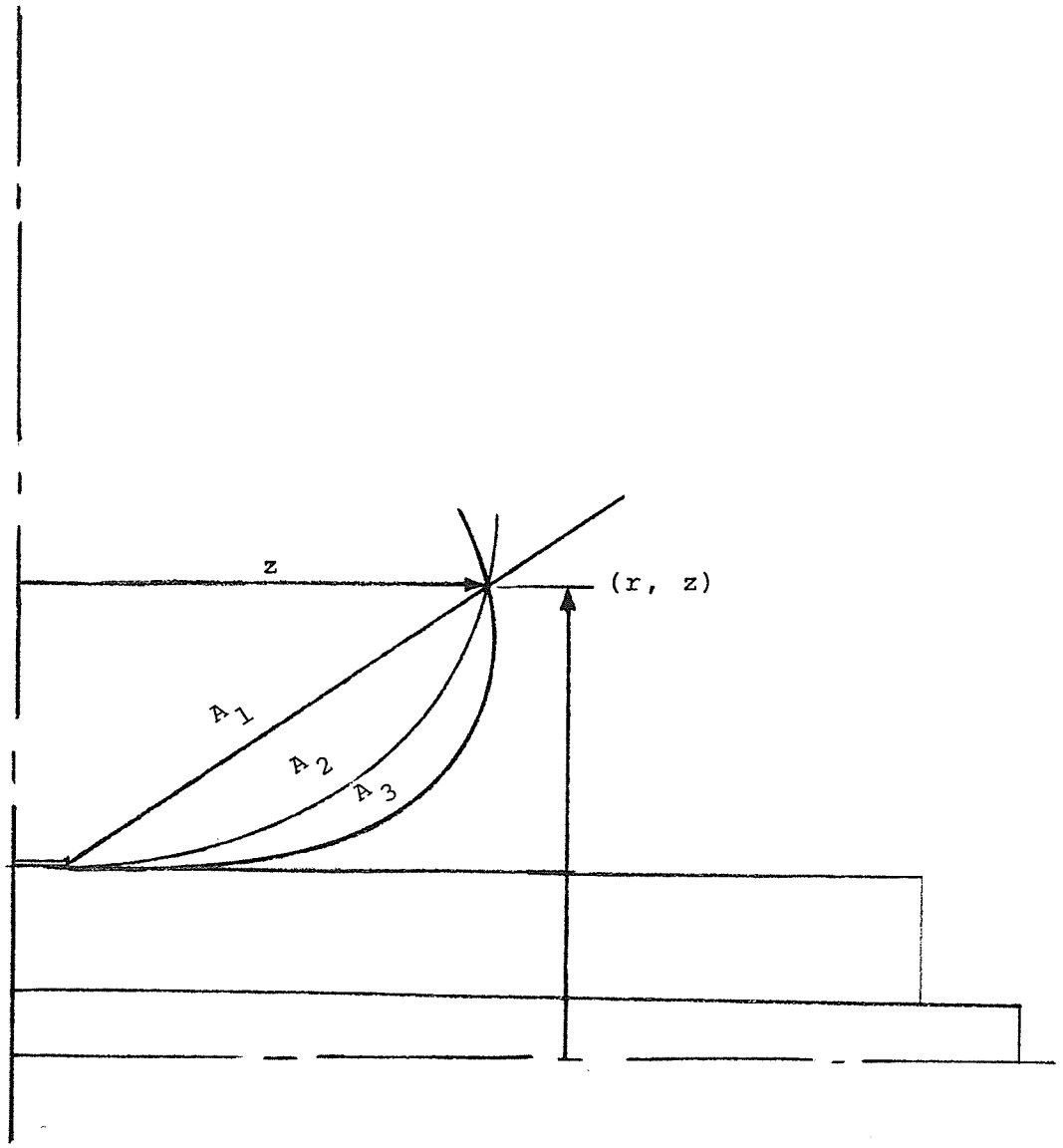

Fig. 3.2: Various Stress Control Profiles.

Since the termination geometry does not lend itself to an analytical solution of the electrostatic field, design of profile A to meet the required stress criterion becomes a difficult task. Therefore calculation of the electrostatic field of the termination is possible only through the use of a digital computer using one of the numerical methods outlined in Chapter II. Even then, only approximate results can be obtained. Without some profile of contour A no such field computation can be possible. Fig. 3.2 shows a point (r, z) in cylindrical coordinates at an axial distance z from the point of termination of the insulation sheath. The radial distance from the centre of the conductor is r. A set of profiles can be drawn through the point of termination of the insulation sheath through (r, z); e.g., A_1, A_2 A_3. For each of these contours the corresponding longitudinal stress along the contour must be found. This is done by a numerical computation of the electrostatic field of the entire geometry using a digital computer.

Thus the computer-aided design of the stress-relief profile involves the following steps:

(1) Choose a suitable stress relief contour such as;

A_1, A_2, A_3 in Fig. 3.2.

(2) Carry out a numerical calculation of the electrostatic longitudinal stress along the contour. This involves solving Laplace's equation in the region bounded by

the high voltage conductor and the stress-relief contour which is at zero electrostatic potential.

(3) If the longitudinal stress at any point exceeds the allowable value, the contour is redefined so as to obtain an improved longitudinal stress distribution. A digital computer calculation of the field is again carried out. This computer-aided design procedure is carried out until the calculated longitudinal stress at any point on the relief contour does not exceed the allowable value. This condition may be defined as the optimal criterion of the problem.

In defining the stress relief contour it is necessary to note that it is economical to minimize the volume of the termination while, at the same time, meeting the optimal stress criterion. The length of the termination is governed by the length of the hermetically sealed enclosure which, in turn, is usually determined by the flashover voltage level of the air-housing interface. Therefore, only the radial dimension can be changed so as to minimize the overall volume of the termination. In the following two sections, a method used in this design for calculating the electrostatic field of a termination is outlined followed by the determination of an equation for stress contour profiles.

3.2 Electrostatic Field Calculation for a Termination

For well defined field problems, both the finite element and finite difference methods have been successfuly used by different researchers. Each method possesses certain merit points over the other and in some cases the choice of one method over the other depends upon the researcher's previous experience. For infinitely extending fields, however, both methods suffer the limitations mentioned in Chapter II.

Approximations have been used with both the finite difference and the finite element methods to bound an otherwise infinitely extending problem [25], [26], [56]. Such approximations involve the introduction of either Dirichlet or natural Neumann conditions in a region sufficiently far from the area of interest. These approximations can be checked by changing the position of the approximated boundary and noting changes, if any, in the value of the field function in the region of interest. However, it is not always possible to bound the otherwise infinitely extending problem.

Close examination of the possible field distribution of the cable termination shown in Fig. 3.1 reveals that, if Dirichlet boundary conditions are used the boundary would have to be imposed very far from the profile in order to avoid distorting the field in the neighbourhood of the stress-relief profile. Therefore, it follows that arbitrary reduction in problem size will result in gross distortion of the field distribution for a cable termination. The natural Neumann

condition (using an approximate flux line), on the other hand appears to be well suited for bounding the infinitely extending field of the cable termination. A flux line can be drawn to join the high voltage conductor and the grounded stress-relief profile. From basic electrostatic theory it is known that a flux line is orthogonal to equipotential contours. Fig. 3.3 shows the construction of an approximate flux line. This is a curve drawn to intersect the two conducting surfaces (electrodes) at right angles.

The approximate flux line technique has been used by various researchers and satisfactory results have been reported [56], [49]. The authors of the paper cited in reference [49] compared the solutions of the field due to two over-head conductors, of square cross-section, obtained using approximate Dirichlet and natural Neumann boundary conditions. The results obtained using their more efficient PDE/IE constrained algarithm are generally bounded by those obtained using the two approximations in the far field. In the case of a cable termination, as shown in Fig. 3.3, the influence of the flux line boundary approximation on the field distribution proximate to the stress-relief contour is monitored by the change in the field function in this latter region as the terminal corona shield is moved in the direction of increasing z. Although this check involves a higher number of system equations being

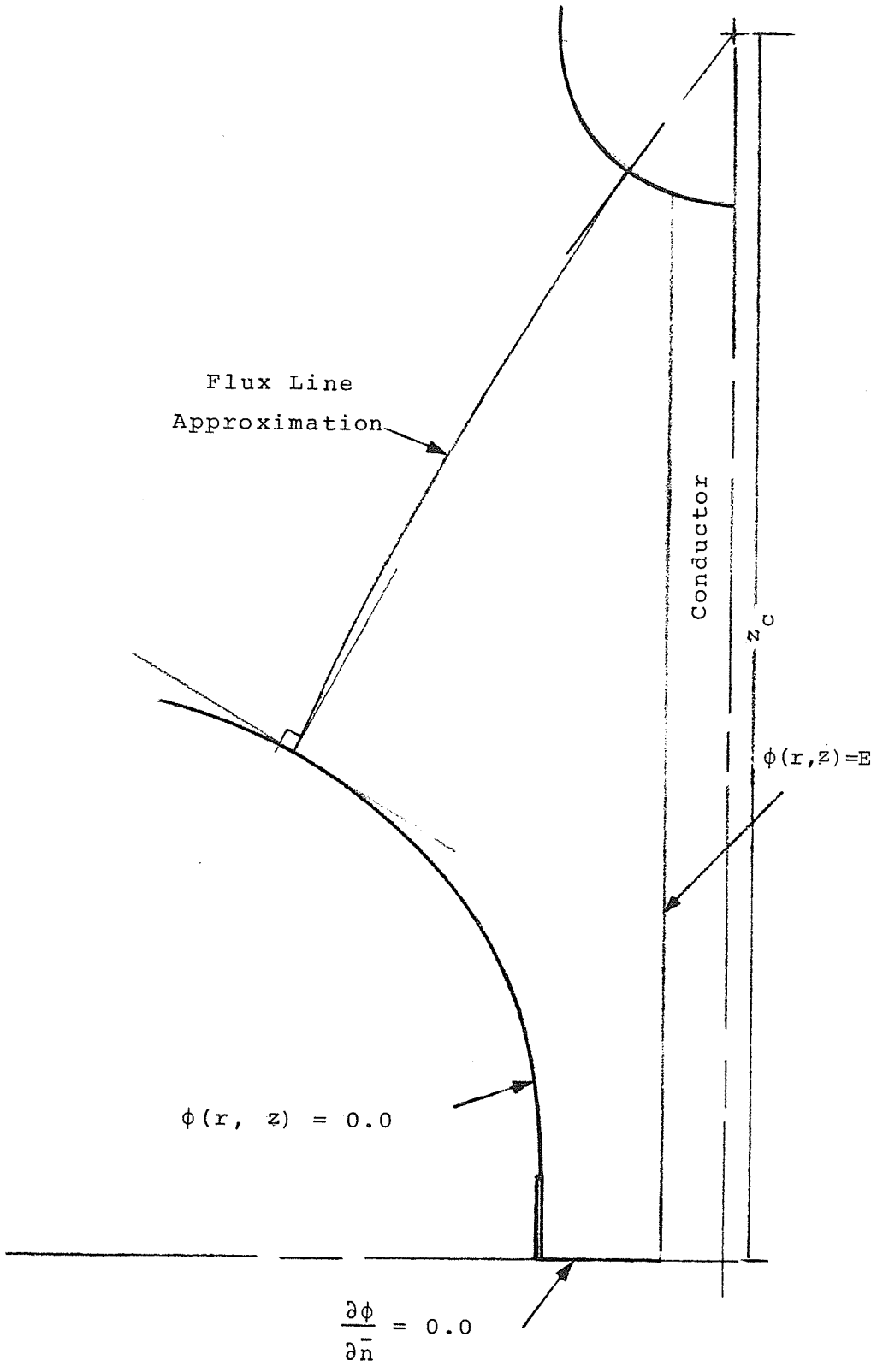

Fig. 3.3: Flux Line Approximation.

solved, larger size elements or grid spacing may be used in the region away from the area of interest where much smaller subdivisions are used.

Fig. 3.4 shows equipotential lines drawn for a stress-relief profile given by the double exponential gradient equation reviewed in Chapter I. This geometry was bounded by using a flux line and a finite element formulation used to arrive at the field solution. The cable geometry used is that for a 132 kV XLPE-insulated cable developed by the General Cable Corporation of New York. The value of the longitudinal component of the electrostatic stress along selected points on the stress-relief profile are tabulated in Table 3.1. The corresponding longitudinal stress distribution along the stress-relief profile for a 365 kV XLPE cable geometry (General Cable Corporation) is also tabulated in Table 3.2 In both cases the maximum allowable longitudinal stress of 5 kV/cm was specified.

It is seen that in one case the maximum longitudinal stress occurs at the point of termination of the insulation sheath - Table 3.1 and 3.2. Furthermore the specified maximum longitudinal stress is not at all attained in one case and only closely in the other. The consequence of such under-stressing is a voluminous termination. The under-stressing may explain why, according to reference [20] in Chapter I, straight line segments are used in actual practice although

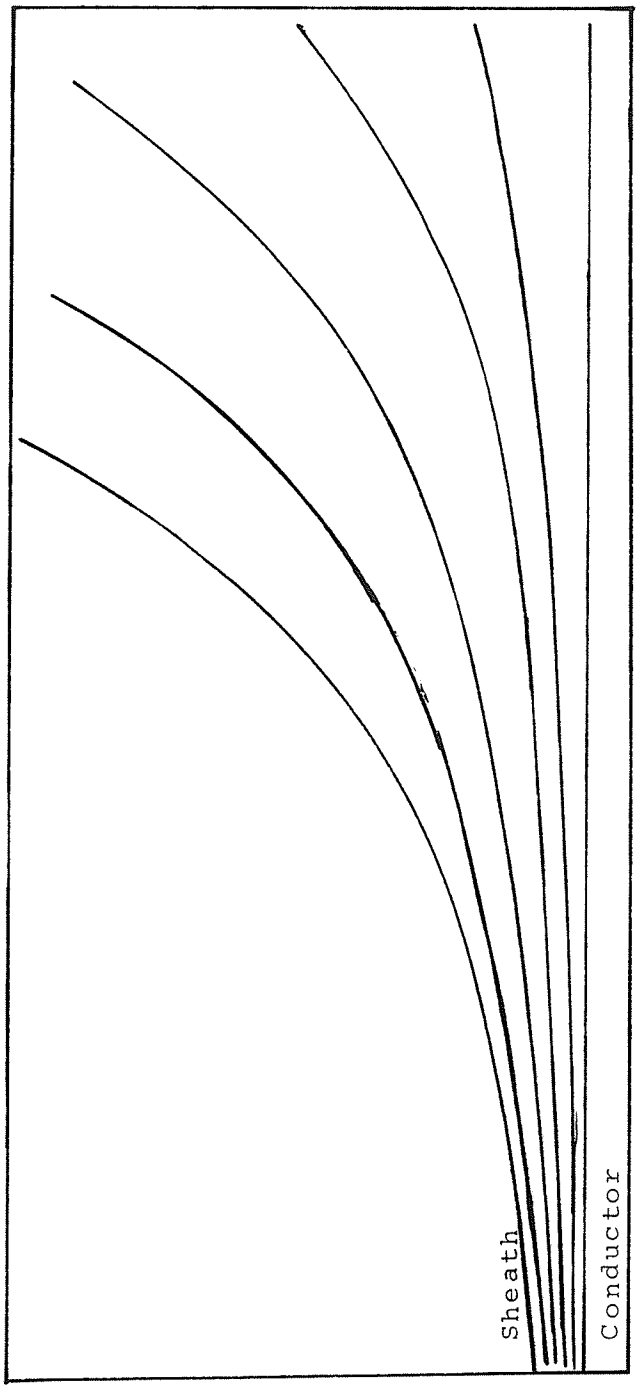

Fig. 3.4: Equipotential Contours for Double Exponential Formula of the Stress Relief Profile.

TABLE 3.1: Longitudinal stress at stress relief profile defined by the double exponential equation

z (x 2.54 cm)	r (x 2.54 cm)	g_m kV/cm
0.0	1.0	6.18
1.0	1.10631	5.44
2.0	1.24208	5.48
3.0	1.41824	5.84
4.0	1.651	5.86
5.0	1.965	5.74
6.0	2.3988	5.53
7.0	3.01479	5.0
7.5	3.42128	4.89
8.0	3.9173	4.61
8.5	4.52821	4.45
9.0	5.28806	4.53
9.125	5.5129	5.04

$$r = e^{f(r_c,\ z,\ g_m,\ E)}$$

$$f\ (r_c,\ z,\ g_m,\ E) = \log_e r_c + e^{z g_m/E} \log_e R/r_c$$

$E = 100$ kV $\qquad R = 2.54$ cm

$r_c = 1.27$ cm $\qquad g_m = 5$ kV/cm

TABLE 3.2: Longitudinal stress at stress relief profile defined as in Table 3.1.

z (x 2.54 cm)	r (x 2.54 cm)	g kV/cm
0.0	1.5	0.0
1.0	1.5	3.6
2.0	1.68049	3.6
3.0	1.78644	3.37
4.0	1.90494	3.27
5.0	2.03789	3.5
6.0	2.18755	3.8
7.0	2.35662	4.0
8.0	2.54829	3.9
9.0	2.76645	4.1
10.0	3.01575	4.0
11.0	3.30186	4.0
12.0	3.63167	4.14
13.0	4.01366	4.27
14.0		4.58

$$r = e^{f(r_c,\ z\, g_m,\ E)}$$

$$f(r_c, z, g_m, E) = \log_e r_c + e^{z\, g_m/E}\ (\log_e R/r_c)$$

$E =$ 200 kV, $r_c = 1.27$, $R = 3.81$ cm, $g_m = 5$ kV/cm

the double exponential geometry is initially used as a guide. These results are not surprising especially in view of the approximation used in deriving the equation for the profile of the stress contour.

3.3 Design Procedure

Having developed the analytical procedure for determining the field distribution on a stress-relief profile the design objectives as outlined in Section 3.3 can now be further examined. In determining the set of allowable curves A_1, A_2, A_3 in Fig. 3.2 it is important to realize two conditions. The first is that a suitable contour would be that whose initial slope (i.e., close to z = 0) is 'small'. This is essential if longitudinal stresses at the point of the insulation sheath termination is to remain within the prescribed limit. Secondly, in order to avoid a voluminous termination, the rate of change of slope with the axial translation z cannot be too 'small'. Thus the suitable stress-relief profile should flare out in an exponential manner with axial distance. Examination of the tabulated curves and surfaces in reference [57] shows that hyperbolic functions can easily be influenced to meet the above two conditions. The parabolic, exponential and power functions all possess different limitations such that it is difficult to influence them to meet the above two conditions. Accordingly, the catenary hyperbolic cosine curve was initially chosen,

$$r = A \cosh (z/A) + K \quad . \qquad (3.1)$$

A and K in equation 3.1 were to be constants only dependent on the maximum radial stress at the conductor and insulation sheath, two factors which determine the cable geometry for a given insulation material. A series of curves given by equation 3.1 can be plotted with A and K as parameters. When this was done for various values of A, inspection of the curves revealed that it is necessary to modify equation 3.1 to the form shown in equation 3.2 and assign A a fractional value in order to meet the conditions imposed on the slope of the profile.

$$r = A (\cosh (z) - 1) + K \quad . \qquad (3.2)$$

With A and K assigned values of 0.25 and unity respectively, a curve drawn using equation 3.2 seemingly satisfied the slope conditions. Having thus defined the stress-relief profile a field solution was then carried out to determine whether the optimal criterion was not being violated. A field solution revealed an unacceptably high longitudinal stress. However, the point of occurrence of the high longitudinal stress was not proximate to the point of termination of the insulation sheath; but at some point in between the two ends of the profile contour. This means that although the initial rise of the curve (equation (3.2) A = 0.25, K = 1) did eliminate the stress concentration at the point of termination of the insulation sheath, the rate of change of the slope with axial translation

was still unacceptably rapid. In order to influence this change the argument of the hyperbolic function in equation (3.2) was modified to

$$\left(\frac{z}{A - z^n}\right) \quad .$$

The index n would be used to influence the hyperbolic function to meet the necessary slope conditions. The resulting equation is given by 3.3

$$r = A \left(\cosh \left(\frac{z}{A - z^n}\right) - 1\right) + K \quad . \qquad (3.3)$$

The value of unity in equation 3.3 is a scale factor such that $r = K$ for $z = 0$.

For fixed values of A and K a series of curves for various values of the index n (equation (3.3)) were examined. The rate of change of the slope with axial translation for each curve was compared to that obtained using equation (3.2) ($A = 0.25$, $K = 1.0$). The curve whose equation had the value of the index n equal to 1.6 gave a satisfactory rate of change of gradient without making the termination voluminous. With the index n determined and K fixed (function of cable geometry) the only variable parameter is A. Thus a family of curves can be obtained by varying A. Fig. 3.5 shows the plot of various stress-relief profiles given by equation (3.3) with A as parameter. The determination of the value of A that does

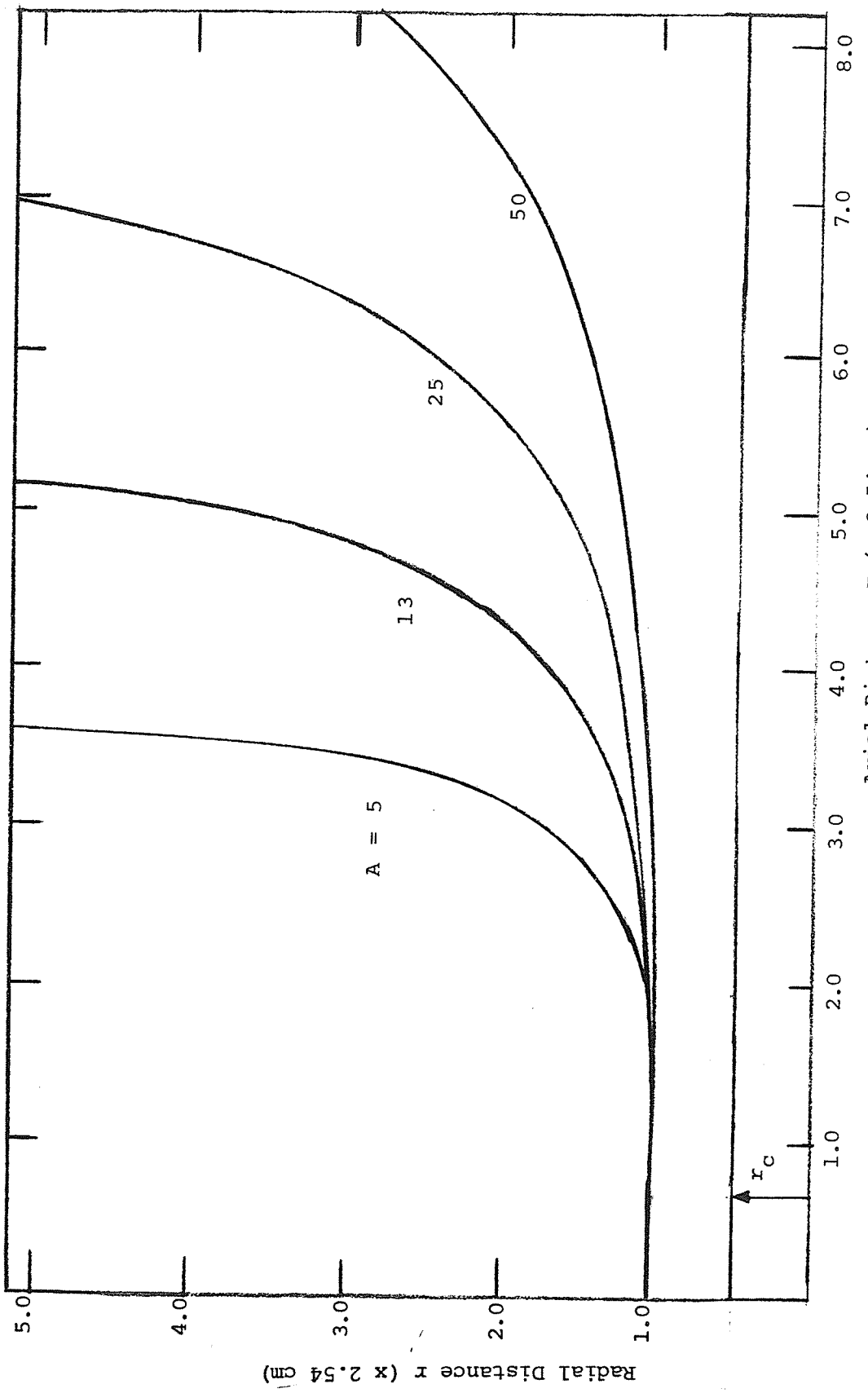

Fig. 3.5: Stress Relief Profiles with A as parameter.

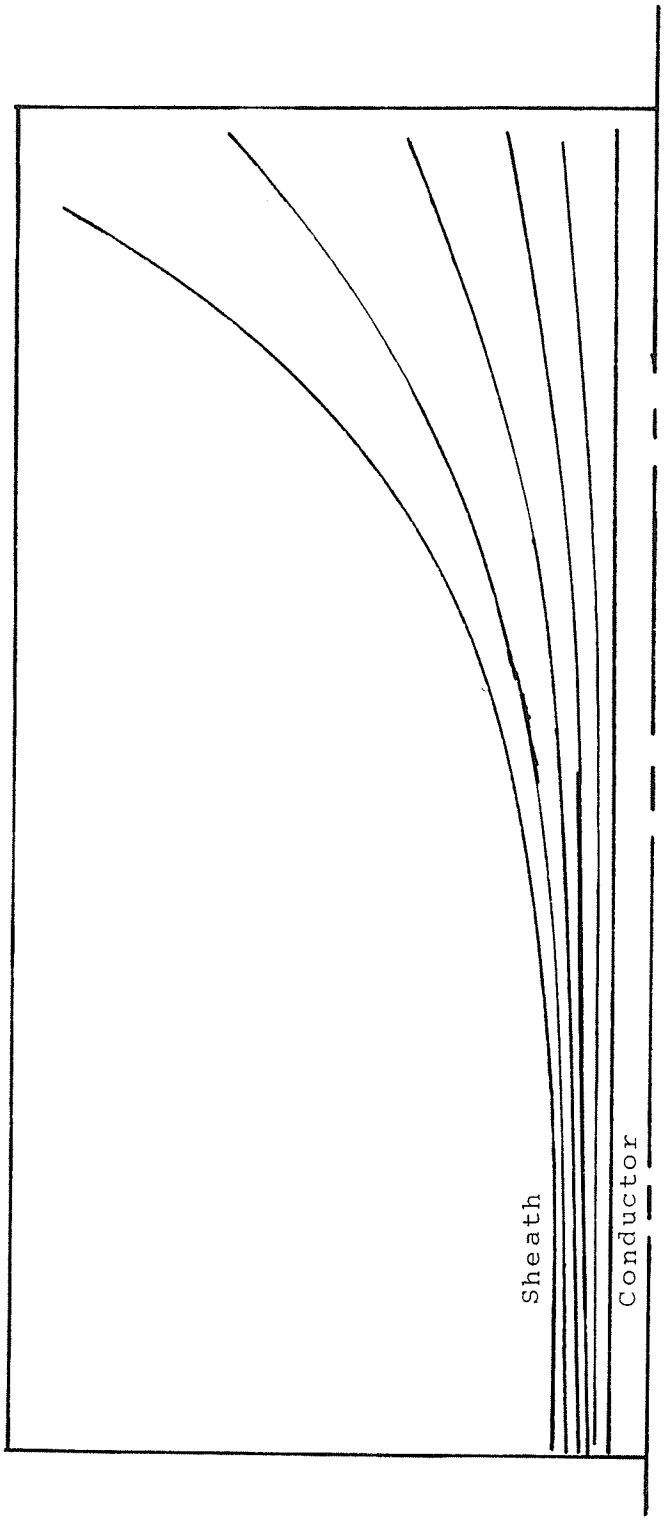

Fig. 3.6: Equipotential Contours for A = 125.

not violate the optimal stress criterion can only be done through numerical experiments. Using the numerical method outlined in Section 3.2 a field analysis was carried out for profiles given by equation 3.3 for different values of A. The longitudinal stress distribution along each profile was then determined. In Table 3.3 to Table 3.10 the longitudinal stress distribution along the stress-relief profiles given by various values of A equal to 13, 17, 21, 25, 29, 50, 75 and 125 is tabulated. For each value of A the coordinates at which the maximum longitudinal stress occurs are underlined in each table. It can be seen that each value of A is associated with a certain value of the maximum longitudinal stress on the stress-relief profile. Therefore the parameter A can be defined as a function of the maximum longitudinal stress. To make sure there was no shifting of maximum stress to the interior region inside the stress-relief profile the longitudinal component of the stress was calculated at all node points in the continuum. Equipotential contours were also drawn and Fig. 3.6 shows one such distribution of equipotential contours.

To determine the relationship between A and the maximum longitudinal stress, say g_m kV/cm, the various values underlined in Table 3.3 - Table 3.10 are plotted against A in Fig. 3.7. Using the least mean square fit an eighth-order polynomial fits the data points. The degree of fit is graphically shown in

TABLE 3.3: Longitudinal stress g at the stress relief profile defined by equation (3.3) - 132 kV cable geometry
A = 13, E = 100 kV

Axial distance z (x 2.54 cm)	Radial distance r (x 2.54 cm)	g kV/cm
0.0	1.0	0.0
1.0	1.0	0.0
1.5	1.0	1.07
2.0	1.01012	3.66
2.5	1.04517	7.16
3.0	1.11916	11.7
3.5	1.26252	15.73
3.75	1.37905	16.81
4.0	1.54448	16.83
4.25	1.78471	16.87
4.5	2.14475	12.13
4.625	2.42643	10.08
4.8125	2.91060	7.91
4.9375	3.37854	6.44
5.0	3.64400	5.82
5.125	4.35619	4.57
5.1875	4.84749	4.10

TABLE 3.4: Longitudinal stress g at the stress relief profile defined by equation (3.3) - 132 kV cable geometry
A = 17, E = 100 kV

Axial distance z (x 2.54 cm)	Radial distance r (x 2.54 cm)	g kV/cm
0.0	1.0	0.0
1.0	1.0	0.0
1.5	1.0	0.81
2.0	1.00765	2.68
2.5	1.03321	4.46
2.75	1.05481	5.76
3.0	1.08409	7.1
3.25	1.12308	8.73
3.5	1.17455	10.31
3.75	1.24239	12.1
4.0	1.33213	13.98
4.25	1.45181	14.77
4.5	1.61346	14.96
4.75	1.8355	13.38
5.0	2.14766	12.45
5.25	2.59934	9.18
5.375	2.90264	8.18
5.5	3.27857	6.7
5.625	3.51472	5.5
5.75	4.35368	4.5

TABLE 3.5: Longitudinal stress q at the stress relief profile defined by equation (3.3) - 132 kV cable geometry
A = 21, E = 100 kV

Axial distance z (x 2.54 cm)	Radial distance r (x 2.54 cm)	9 kV/cm
0.0	1.0	0.0
1.0	1.0	0.0
1.5	1.0	0.64
2.0	1.00614	2.1
2.5	1.02626	3.85
3.0	1.06488	6.0
3.5	1.13022	8.77
4.0	1.23666	10.4
4.25	1.31274	11.67
4.5	1.41033	13.0
4.75	1.53652	13.5
5.0	1.70153	13.3
5.25	1.92039	13.25
5.375	2.068.8	11.1
5.5	2.21598	10.7
5.75	2.62435	8.66
6.0	3.20492	6.4
6.125	3.58940	5.43
6.25	4.06106	4.43
6.375	4.64701	3.4

TABLE 3.6: Longitudinal stress g at the stress relief profile defined by equation (3.3) - 132 kV cable geometry
A = 25, E = 100 kV

Axial distance z (x 2.54 cm)	Radial distance r (z 2.54 cm)	g kV/cm
0.0	1.0	0.0
1.0	1.0	0.0
1.5	1.0	0.54
2.0	1.00313	1.73
2.5	1.0217	3.13
3.0	1.05279	4.75
3.5	1.10367	7.0
4.0	1.18312	8.1
4.25	1.23779	9.3
4.5	1.30578	10.35
4.75	1.39065	11.4
5.0	1.49720	12.0
5.25	1.63203	12.34
5.5	1.80438	11.86
5.75	2.02746	11.0
6.0	2.32069	10.5
6.25	2.71347	8.6
6.375	2.96067	8.0
6.5	3.25194	7.0
6.625	3.59775	6.27
6.75	4.01181	5.24
6.8125	4.26209	4.6

TABLE 3.7: Longitudinal stress g at the stress relief profile defined by equation (3.3) - 132 kV cable geometry
A = 29, E = 100 kV

Axial distance z (x 2.54 cm)	Radial distance r (x 2.54 cm)	g kV/cm
0.0	1.0	0.0
1.0	1.0	0.0
1.5	1.0	0.46
2.0	1.00041	1.47
2.5	1.0185	2.63
3.0	1.04448	3.95
3.5	1.08605	5.45
4.0	1.14906	7.10
4.5	1.24279	8.8
5.0	1.387232	10.0
5.25	1.47662	10.8
5.5	1.59317	11.28
5.75	1.73830	11.73
6.25	2.15274	11.37
6.5	2.45174	9.62
6.75	2.84352	8.78
6.875	3.08568	7.82
7.0	3.36715	7.31
7.1875	3.89030	6.0

TABLE 3. 8 : Longitudinal stress g at the stress relief profile defined by equation (3.3) - 132 kV cable geometry
A = 50, E = 100 kV

Axial distance z (x 2.54 cm)	Radial distance r (x 2.54 cm)	g kV/cm
0.0	1.0	0.0
1.0	1.0	0.13
2.0	1.00253	1.14
3.0	1.02433	2.05
3.75	1.06014	2.68
4.0	1.07494	3.55
4.5	1.11521	4.36
5.0	1.16902	5.5
5.5	1.24036	6.4
6.0	1.33485	7.18
6.5	1.46053	8.1
7.0	1.62924	8.24
7.5	1.85878	8.62
7.75	2.00447	8.83
8.25	2.38218	8.0
8.5	2.62844	7.9
8.75	2.92627	7.5
9.125	3.51419	6.4
9.375	4.01879	5.8
9.625	4.65432	5.2

TABLE 3.9: Longitudinal stress g at the stress relief profile defined by equation (3.3) - 132 kV cable geometry
A = 75, E = 100 kV

Axial distance z (x 2.54 cm)	Radial distance r (x 2.54 cm)	g kV/cm
0.0	1.0	0.0
1.0	1.0	0.24
2.5	1.0	1.14
3.5	1.02896	2.03
4.5	1.07049	3.02
6.0	1.18602	4.12
6.5	1.24507	4.84
7.0	1.31846	5.48
7.5	1.40984	6.0
8.0	1.52405	6.5
8.5	1.66762	6.7
9.5	2.08251	6.9
9.75	2.22346	7.0
10	2.38452	6.8
10.25	2.56929	6.8
10.5	2.78221	6.5
10.75	3.02877	6.11
11.0	3.31587	5.94
11.25	3.65218	5.42
11.5	4.0488	5.2
11.75	4.52013	4.5
12.0	5.08492	4.2
12.125	5.426	4.0

TABLE 3.10: Longitudinal stress g at the stress relief profile defined by equation (3.3) - 132 kV cable geometry A = 125, E = 100 kV

Axial distance z (x 2.54 cm)	Radial distance r (x 2.54 cm)	g kV/cm
0.0	1.0	0.0
1.5	1.0	0.32
3.0	1.01	1.04
4.5	1.03959	1.67
5.5	1.07457	2.21
6.5	1.12488	2.75
7.5	1.19504	3.28
8.5	1.29160	4.07
10.0	1.50809	4.52
10.5	1.60695	4.74
11.0	1.7237	4.93
11.5	1.86220	5.15
12.0	2.02726	5.21
12.5	2.12620	5.3
13.0	2.46399	5.64
13.5	2.75454	5.5
14.0	3.11121	5.2
14.75	3.81519	5.1
15.25	4.44093	5.0
15.625	5.03044	4.6

Fig. 3.8. Very small increments are used in Fig. 3.8 so as to detect any kind of oscillations. The eighth-order polynomial was found to give minimum deviation and therefore negligible oscillation. Close examination of Fig. 3.7 shows that a linear relationship exists between A and maximum longitudinal stress g_m for values of g_m not exceeding 8 kV/cm. This relationship is given by equation (3.4)

$$A = 22.0 \quad (10.5 - g_m) \quad . \tag{3.4}$$

The point on the stress relief profile where the maximum longitudinal stress g_m occurs, for each value of A, is found to have an axial translation from the point of termination of the insulation sheath that increases with the value of A. In fact when A is plotted against the axial distance z_m at which the maximum longitudinal stress g_m occurs a relationship is obtained such that g_m will not occur at points on the stress-relief contour greater than the value of z_m given by equation (3.5)

$$z_m = 1.5 + A/15 \tag{3.5}$$

for $A > 0$

and $z_m > 0$ (i.e., not at point of termination of the insulation sheath).

Investigation of the possibility of a relationship between the maximum longitudinal stress g_m and the geometric

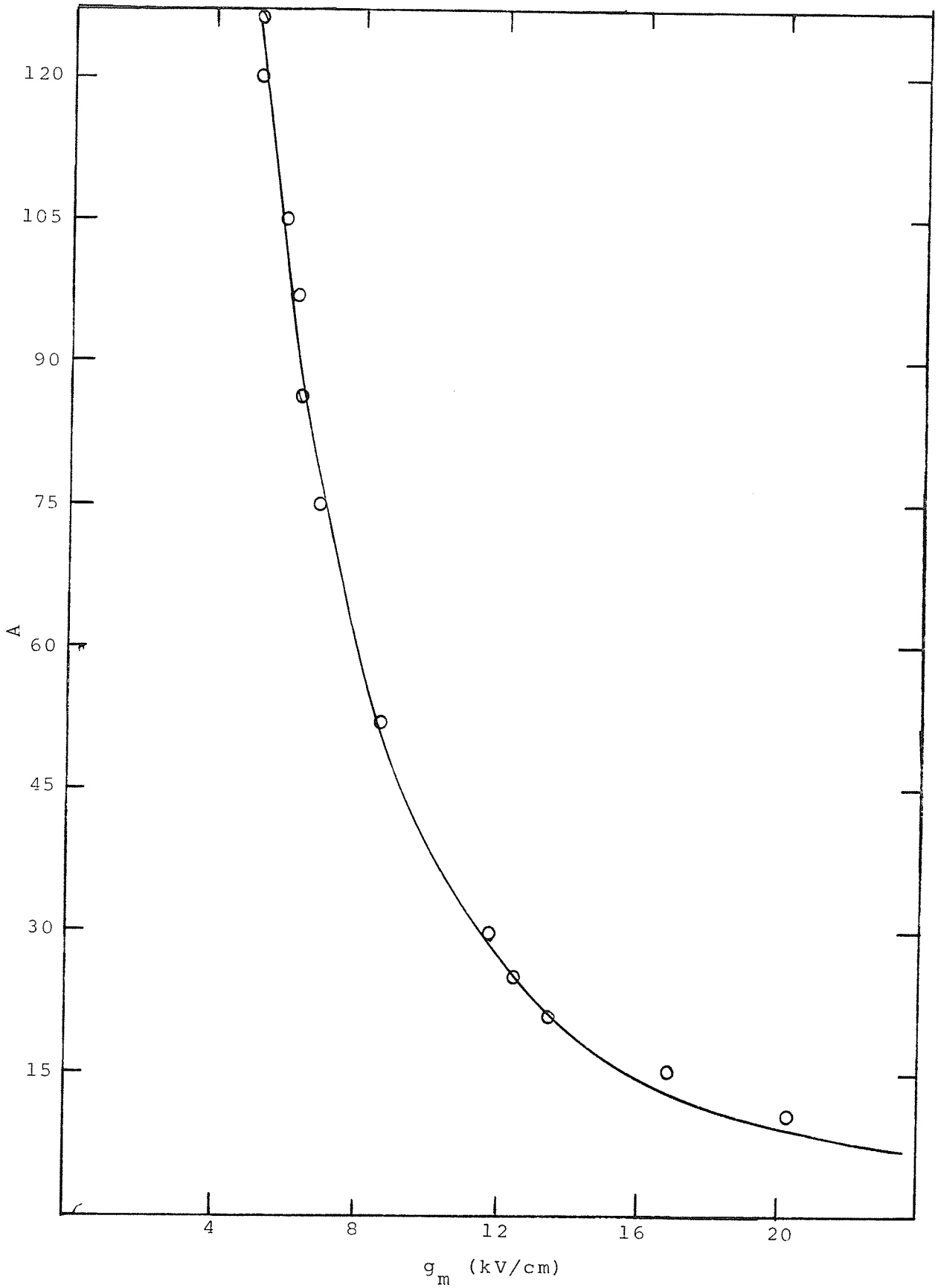

Fig. 3.7: Variation of A with Maximum Longitudinal Stress g_m Obtained from Numerical Experiments.

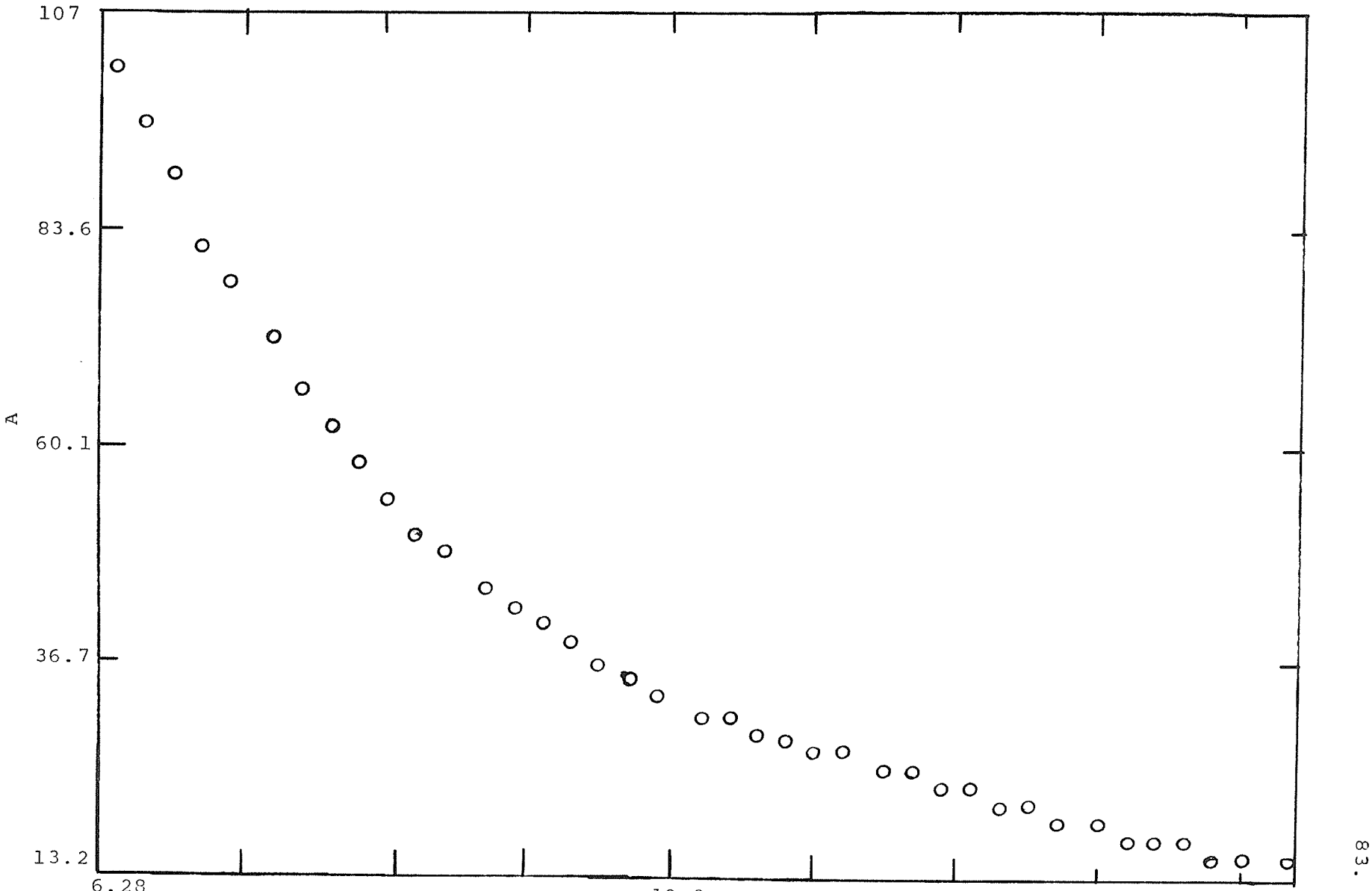

Fig. 3.8: Polynomial Fit of $A = f(g_m)$.

slope of the tangent at the point on the stress-relief contour where g_m occurs showed that the ratio between g_m and the geometric slope was fairly constant for various values of A. This is to be expected since a certain slope/axial translation relationship was one of the conditions an acceptable equation of the stress-relief curve had to satisfy.

Finally the constant K is the radial distance from the centre of the conductor of the insulation sheath and in general is given by:

$$K = (g_s/E) \log_e (R/r_c) \qquad (3.6)$$

g_s = radial stress at insulation sheath, kV/cm

E = phase voltage at conductor, kV

r_c = conductor radius

R = radius of cable.

With all parameters thus defined the equation of the stress control profile is given by:

$$r = 22\,(10.5 - g_m)\left[\cosh\left(\frac{z}{22(10.5 - g_m) - z^{1.6}}\right) - 1\right] + (g_s/E) \log_e (R/r_c) \qquad (3.7(a))$$

for $g_m \leq 8$ kV/cm .

$$r = f(g_m)\left[\cosh\left(\frac{z}{f(g_m) - z^{1.6}}\right) - 1\right] + g_s/E \log_e (R/r_c) \qquad (3.7(b))$$

for $g_m > 8$ kV/cm

where $f(g_m) = \sum_{k=0}^{8} B_k g_m^k$

and

$B_0 = -1401.9006$ $\quad B_5 = 0.2508$

$B_1 = 1121.0388$ $\quad B_6 = -0.8405 \times 10^{-2}$

$B_2 = -326.0093$ $\quad B_7 = 0.1562 \times 10^{-3}$

$B_3 = 49.8616$ $\quad B_8 = -0.1235 \times 10^{-5}$

$B_4 = -4.5139$

3.4 Conclusions

In this chapter an equation for a stress-relief-cone has been presented. This equation was obtained by numerical analysis of the electrostatic field through a computer-aided design. Profiles derived by use of this equation can be used in conjunction with solid dielectric cables with the additional constraint that ε_2 (the dielectric constant of the insulation material in the termination) is equal to or greater than ε_1 - dielectric constant of the cable insulation. The proposed equation may be applied if the maximum allowable longitudinal stress and the cable dimensions are known. In developing the stress cone equation dimensions for a compact

EHV cable were used; i.e., 132 kV, 507 mm^2, 25.4 mm diameter over insulation. To show the general applicability of the stress cone equation, it will be used in Chapter IV to derive a stress control profile for an EHV XLPE cable of higher voltage rating.

The stress cone equation, as presented, can be altered by changing the index n (equation 3.3) from the present value of 1.6 to any desired value. In doing so, the slope of the stress control profile will change; it is thus possible to accommodate not only different cable designs but also cases where the dielectric constant of the termination insulation material is less than that of the cable insulation. Such a design will have to be checked on a digital computer to make sure that the optimal stress criterion is not violated.

CHAPTER IV

PROPERTIES AND DEVELOPMENT OF XLPE AND SILICONE OIL

Research in high voltage cables during the first half of this century has been directed mainly towards improvement of the conventional dielectric consisting of oil-impregnated paper. As a result the maximum operating temperature of oil-impregnated paper insulation has been improved by a factor of two and the maximum operating stress by a factor of six to eight, thus making oil-impregnated paper to be among the best dielectrics presently known in high voltage power cable engineering. However, the inherent properties of cellulose paper limit further improvement of the oil impregnated paper dielectric such that the operating field strength at the surface of the conductor cannot possibly exceed 16 kV/mm [58].

The electric stress at which ionization starts in a cable dielectric can be used as a reliable basis for calculating the maximum operating stress. For oil-impregnated paper discharges start at 40 kV/mm. If a factor of safety of 3 - 4 is allowed for, then the maximum operating stress would be 10 - 12 kV/mm. The operating stress of 16 kV/mm can be attained only if very thin paper of 15 μm thickness is used near the conductor together with high oil pressure - 15 kg/cm^2. The lapping with thin paper, however, without wrinkles and creases is very difficult and the risk of damaging the insulation during bending

and laying of the cable would be greatly enlarged. EHV cables up to 400 kV have been constructed in this way but the limit seems to have been reached.

The unfavourable properties of cellulose paper which prevent further improvement of this oil-impregnated dielectric are indicated below:

a) The high dielectric constant of cellulose ($\varepsilon_r = 5-6$) causes unfavourable stress distribution in the impregnated dielectric since cable oil has a dielectric constant of about two. It also results in relatively high cable capacitance.

b) The porosity of paper favours the originating of conduction channels (trees) leading to break down.

c) Great hygroscopicity results in moisture content amounting up to 20%. This necessitates a long careful drying process. However, the water is partly bound chemically so that complete drying would only be possible if degeneration of the paper is acceptable. Residual water is recognized to be the main cause for the inception of internal discharges and promotes electrolytic conduction in oil-impregnated paper which is initially free from discharges [59].

d) The relatively high loss factor due to polar groups in the cellulose molecules and due to the residual chemically bound water and the sharp increase in the dissipation factor with rising temperature above 80°C for fields greater

than 20 kV/mm result in a risk of thermal instability, thus impeding the application of higher stresses than presently admissible.

e) Degradation of paper occurs at temperatures above 100°C.

f) The lack of transparency makes it difficult to trace the origin of instabilities in cavities that lead to the discharge imitiation.

Therefore, in order to increase the operating stress in high voltage cables it is necessary to change over to other insulating materials. The need for requiring higher operating stresses is a direct consequence of the high energy demands by the growing industries. Many insulating materials for power cables have been developed but in this chapter only cross-linked polyethylene (XLPE) is considered. The properties of XLPE are similar to those of polyethylene and cross-linking is done to achieve improvement in some properties. Therefore development of XLPE is followed through its parent thermal plastic polyethylene.

4.1 Properties and Development of XLPE

The properties of XLPE are similar as those of the parent plastic polyethylene with the exception of a few changes that are a consequence of cross-linking. Therefore, the properties of polyethylene are first discussed followed by modifications that are associated with the cross-linking process.

Polyethylene was first introduced in 1941 at which time ethylene gas was polymerized at 1000 to 2000 atmospheres pressure by the Imperial Chemical Industries [60]. Introduction of organometallic catalyst later resulted in polymerization being carried out at normal pressure. As the chemical structure

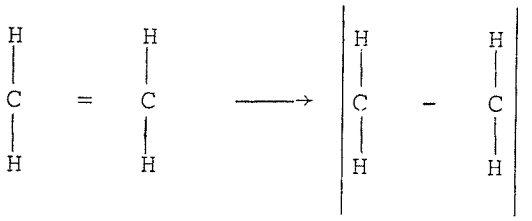

Ethylene (monomer) Polyethylene

indicates, polyethylene is nonpolar in character. The polymer developed especially for dielectric applications to cables has an average molecular weight approximately 18000 to 20000. Like other plastics of higher molecular weight this product is tough, flexible over a wide range of temperatures, transluscent, and normally white in colour. Its structure, as would be expected, results in an unusual resistance to water and chemicals and its nonpolar nature leads to characteristic electrical properties; such as extremely low power factor and low dielectric constant with high resistivity and dielectric strength.

4.1.1 Physical Properties

Depending on the polymerization process the polymer may be produced as low density polyethylene or high density polyethylene. The important characteristic of low density poly-

ethylene is the high "level of branching" [61]. This means that their molecular chains carry numerous lateral branches of variable length and at random disposition. The consequences of this branching are: low density, flexibility at normal ambient temperatures and low melting temperatures; in addition, the degree of crystallinity is low. On the other hand high density polyethylene is more linear in that side branches are less numerous and on the average are shorter. Consequently lateral dimension of the chains is less and the density is higher, intermolecular cohesion is increased reducing the mobility of the chains giving a more rigid product at room temperature and the melting point is raised. The formation of crystalline domains is more probable. Table 4.1 gives the physical properties of both low and high density polyethylene.

Polyethylene is a thermoplastic resin which can be readily molded by injection or by compression; extruded to form sheets, films, fibres, tubes and so on; and extruded on wire and cable. In thin sections it is non rigid, however, in thick specimens, polyethylene is stiff enough to be classified among the more rigid plastics. The degree of rigidity is influenced by molecular weight and also may be varied by the incorporation of auxiliary ingredients. The extrusion of polyethylene involves no special difficulty if suitable equipment is available and reasonable attention is given to quality control[62]. The freshly extruded material, particularly in heavy sections is

TABLE 4.1: Physical properties of polyethylene [60].

Physical Properties	Type of Polyethylene	
	Low Density	High Density
Coefficient of thermal expansion (-40° - $0^{\circ}C$) cm/cm/$^{\circ}C$ x 10^{-5}	10 - 20	10 - 20
Thermal conductivity $20^{\circ}C$ Cal/sec/cm^2/cm/$^{\circ}C$ x 10^{-4}	8	1.9 - 3.3
Water absorption 24 hours %	< 0.05	< 0.02
Hardness R - Rockwell	R10	R30 - R60
Specific gravity	0.91-0.925	0.941-0.965
Mold shrinkage	0.01 - 0.13	0.01 - 0.04
Flamability	slow burning	slow burning
Softening temperature $^{\circ}C$	≃ 100	
Clarity	transparent -opague	transparent -opague
Refractive index ($23^{\circ}C$)	1.52	
Degree of crystallinity	40%-60%	40%-60%

cooled slowly first in hot and then in cold water. This procedure is necessary because of the extremely high coefficient of thermal expansion, otherwise rapid cooling would cause the surface of the coating to become hardened while the centre remains still soft. The decrease in volume during further cooling would result then in the formation of voids in the interior of the mass.

Polyethylene is highly soluble and inert to chemical reagents. At room temperature it is substantially unaffected by concentrated hydrochloric, sulphuric or even hydrofluoric acid, while nitric acid has no visible effect but ultimately does impair the tensile strength and elongation. In 24 hours at 100°C concentrated hydrochloric acid, 50% caustic soda solution, dilute nitric and sulphuric acid have no effect on polyethylene. The only common solvents which will affect polyethylene at room temperature are the chlorinated hydrocarbons, for example carbon tetrachloride and trichloroethylene, and to a lesser extent the aromatic and aliphatic hydrocarbons in general. These solvents at room temperature tend to swell the plastic but do not usually dissolve it [62]. Polyethylene is also reported to be fungus resistant. It is not attacked by salt water and therefore it has been used as insulation on submarine cable and in other applications where contact with salt water has deleterious effects on other materials. Polyethylene burns slowly at 2.5 cm/min.,

however, long time exposure to a flame or an arc is necessary before it ignites. It will continue burning by itself only if the heat produced is sufficient to maintain the molten state. Polyethylene has a very poor weathering ability, it suffers very rapid ultraviolet degradation and is susceptible to stress cracking in certain environments. The rapidity of failure is dependent upon stress and temperature. In all cases there exists an incubation period of several months.

4.1.2 Electrical Properties

Polyethylene in thin samples exhibits high breakdown strength that decreases with thickness. This strength ranges from 1 MV/cm for 10 mm thick samples to 0.25 MV/cm for 100 mm samples. However, the strength is lower for extruded specimens. Polyethylene has a dielectric constant of 2.3 which is independent of temperature and frequency over a very wide range. Due to its nonpolar nature, polyethylene would be expected to have no dielectric loss at all. However, it has a power factor, for the commercially produced polymer, averaging 0.0003. Carefully controlled production conditions have reported a polymer with a power factor of 0.00015. Although polyethylene is essentially nonpolar, it is the small amounts of polar constituents which account for the small but noticeable power factor of the material. The losses are due to rotational displays of polar groups of side chains, polar groups on the chain, or polar bridges cross-linking the long molecules [62], [63]. The power factor, as the

dielectric constant, is fairly constant over a wide range of frequencies and only rises very slightly with increasing temperature. Electrical properties of polyethylene and some other properties required in the application of the polymer as extruded dielectric insulation to high voltage cables are listed in Table 4.2.

In extruded form polyethylene has been used as a high voltage cable dielectric for some time. Underground rural distribution systems have successfully used polyethylene-insulated cables. Application to higher voltages has been slow due to limitations imposed by processing technology resulting in imperfections in the polymer. Longitudinal expansion of cable insulation is usually limited by friction to the amount of expansion of the conductor. For copper conductor this amount is about one tenth of that of polyethylene, therefore, the greater part of volume expansion is taken up by radial expansion which reveals itself by separation of the insulation from the conductor, by pressure against any outer covering, and by the introduction of mechanical stresses. The resultant void between conductor and insulation is liable to be the seat of discharges which, if maintained will lead to failure. Like oil-impregnated paper, polyethylene may fail due to puncture or dendritic discharges [64].

Although imperfections introduced during manufacture such as voids in the extruded dielectric have limited operating

TABLE 4.2: Electrical and other properties of extruded polyethylene for cable insulation.

Dielectric constant (50 Hz - 1000 MHz, 20°C)		2.3
Power factor (50 Hz - 1000 MHz, 20°C)		0.0003-0.0005
Resistivity (20°C)	Ohm - cm	10
Dielectric strength	50 Hz, 23°C	200-250 kV/cm
Specific heat		
20°C - 40°C		0.55 Cal/gm/°C
120°C - 140°C		0.70 Cal/gm/°C
Minimum softening temperature (Vicat)		77°C
Chrystalline melting point		110°C-120°C
Vacuum decomposition temperature		280°C-300°C

stresses to low values, the maximum operating stress has, over the years, increased from about 4 kV/mm to about 15 kV/mm [65], [66], [67]. In Sweden, an extruded polyethylene insulated cable for 240 kV between phases has now been in operation for some time [67]. The change in diameter of polyethylene of 2% due to heating from 20°C to 65°C has made it necessary to use a screen at the conductor adherent to the insulation. Another shortcoming of extruded polyethylene cable is the low short circuit rating due to the low melting temperature of the polyethylene. Attempts have been made to avoid, suppress or at least delay treeing inception so as to attain higher working stress and longer life. Such attempts have resulted in the use of voltage stabilizers [68], [69], use of oil-impregnated polyethylene tapes and compressed gas filled dielectric tapes [66], [70]. Although higher operating stresses have been reported with the lapped polyethylene tape insulation it should be recalled from the physical properties that the polymer swells in oil making it difficult to attain any long time compatibility between the liquid and the solid.

4.1.3 Cross-Linking Polyethylene

The low melting temperature limitation has been minimized by cross-linking polyethylene. Polyethylene is cross-linked as an outcome of the reaction between di-cumyl peroxide

and itself in the presence of heat. The resulting cross-linked polyethylene (XLPE) has improved thermal and some mechanical properties; e.g., decreased plastic flow, increased heat resistance, and improved resistance to solubility in chemicals. In rubber technology this type of reaction is called 'vulcanization', or 'cure' [71]. The chemistry of cross-linking polyethylene by di-cumyl peroxide is briefly summarized in Fig. 4.1. For extruded insulation XLPE cables the short circuit rating has been improved such that a maximum continuous conductor temperature of 90°C is specified. The maximum emergency load conductor temperature is specified at 130°C for 100 hours per year. A maximum short circuit conductor temperature of 250°C is also being used. Thermal conductibility is reported as 0.28 W/m°C at 20°C and 0.18 W/m°C at 90°C [72].

An important development has been the use of semi-conducting cross-linked copolymer in the form of an extruded shield providing an effective integral shield, affording the essential bond between shield and insulation. This extruded shield provides the needed electrostatic shielding since neither polyethylene nor XLPE can tolerate significant corona discharges without serious risk of dielectric failure. Tape shields have performed rather unsatisfactorily and are inferior to extruded shields for EHV applications [73].

EHV extruded XLPE cables are still in the developmental stage; however, such cables will be in general operation in the

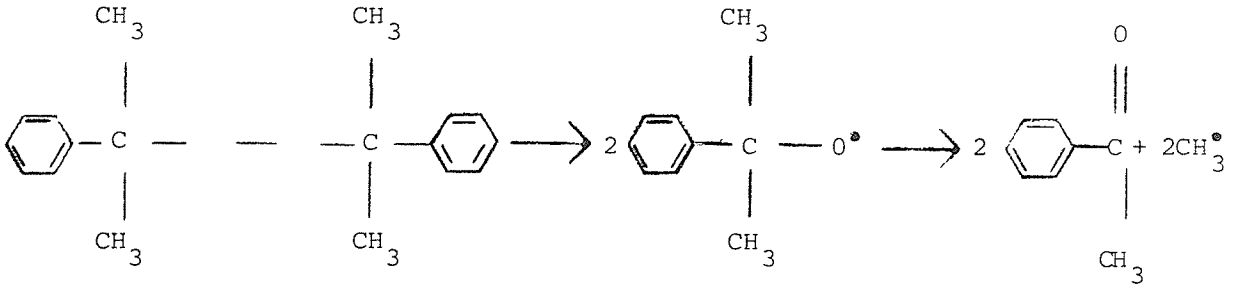

Di-Cumyl Peroxide

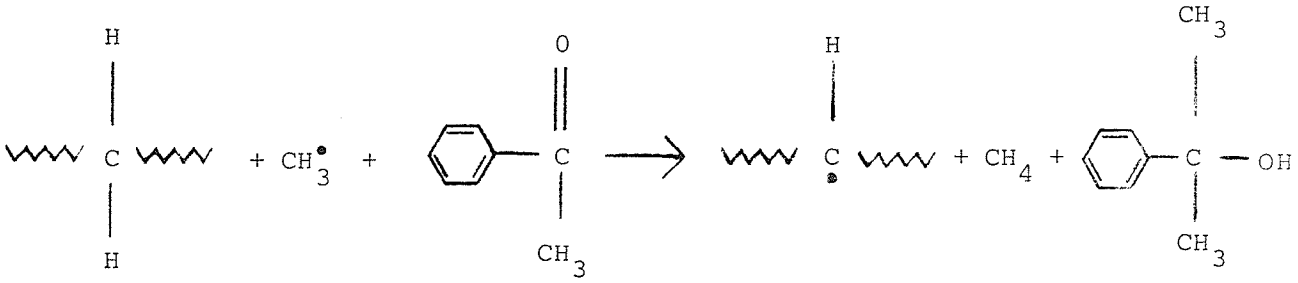

Polyethylene

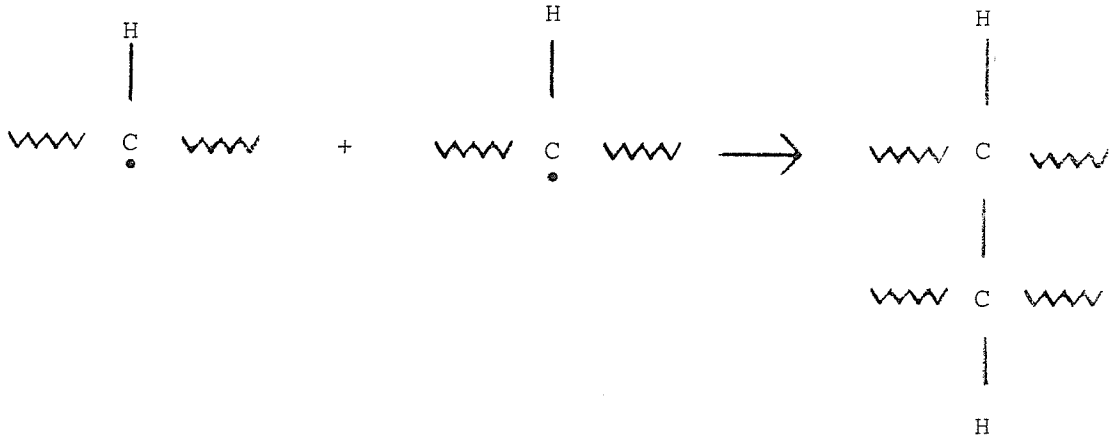

Cross-Linked
Polyethylene

Fig. 4.1: Cross-Linking Polyethylene Using Di-Cumyl Peroxide.

near future due to their successful performance economically and otherwise at lower voltages; for example, the installed cost of a 132 kV XLPE cable as calculated per MVA-mile is significantly lower than that of either oil-filled pipe type or paper cable [67].

Alongside the development of extruded polyethylene and XLPE cables has been that of cable terminations and joints. Molded terminations have been found to perform satisfactorily at lower voltages. At EHV system levels the need for reliable stress profiles as designed and analysed in Chapter III needs no further qualification. A recent idea has been to use molded XLPE terminations in conjunction with XLPE cables. Due to the high coefficient of expansion of XLPE and as a protection against electrostatic discharges use of silicone oil with the molded termination has been suggested. Ordinary cable oil cannot be used for this purpose owing to lack of long-time compatibility with XLPE. Use of silicone oil with a molded XLPE termination introduces a parallel liquid/solid interface. The breakdown characteristics of such interfaces have not yet been reported. Therefore it is necessary to carry out experimental investigations of the silicone oil/XLPE interface. The procedure and results of such a study are presented later.

4.2 Silicone Oil as a Liquid Dielectric

During the search for glass-like polymers at Dow Corning Corporation in 1944, a series of water-white, odourless inert liquid silicones was discovered and became one of the

first families of silicone polymers to reach commercial production. The fluids appear in several different types and are useful as damping and hydraulic fluids, mold release agents, water proofing materials, high temperature lubricants, high vacuum diffusion pump oil, heat transfer medium and liquid dielectrics.

Most silicone fluids are prepared by the hydrolysis of organochlorosilanes:

$$2\ R_3\ Si Cl + n\ R_2\ Si\ Cl_2 + (n+1)\ H_2O$$

organochlorosilanes Water

$$\rightarrow\ R_3\ Si O\ (R_2\ Si O)_n\ Si\ R_3$$

Silicone fluid

$$+\ (2n + 2)\ HCl$$

hydrochloric acid

In the general formula for the organochlorosilanes the R groups may be the same or different and can be selected from practically all known organic radicals. Work with production of silicone fluids has concentrated almost entirely on a methyl radical (i.e., R = CH_3 in the above equation of the chemical reaction) and indeed the generic name 'silicone fluid' is very often used in the discussion of the properties of polydimethyl siloxane (PDMS) [74] whose chemical structure is shown below.

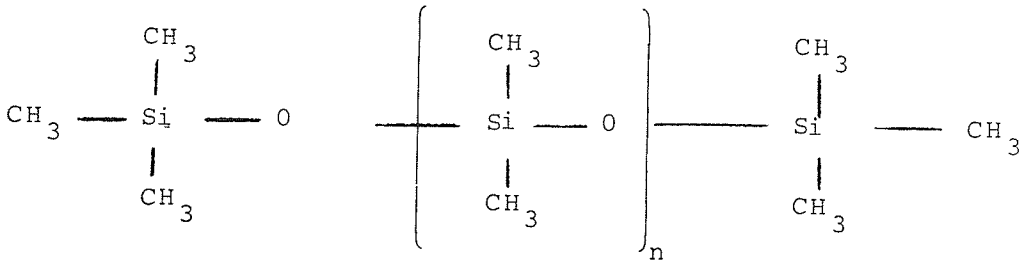

Dow Corning Corporation markets different types of silicone fluids with a variety of applications. Type 200 and Type 500 are the Electrical grades. In this study Type 200 PDMS fluid of 200 cS viscosity was used. The available viscosities range from 0.65 cS to 100 000 centistokes.

4.2.1 Physical Properties

The Electrical grade silicone fluids are characterized by thermal stability and general chemical inertness. They are non-corrosive to metals and non-solvents for rubber, synthetics and other organic plastics. Their flashpoints are considerably higher than petroleum oils of equivalent viscosity. Although they will burn to form silica, carbon dioxide and water, PDMS Electrical grade fluids are considerably more oxidation resistant than most hydrocarbons. Their surface tension is low--about 20 dynes/cm and they readily wet clean dry surfaces of glass and ceramics making them water repellent and maintaining their high surface resistivity--even under moisture condensing conditions.

PDMS Electrical grade fluids are insoluble in water

and are unaffected by aqueous dilute acids or saline solutions. They are soluble to varying extents in most organic solvents including carbon tetrachloride and aromatic napthas but not in lower alcohols and acetone. In general silicone fluids of Electric grade are essentially non-toxic and non-volatile. Table 4.3 gives the physical properties of Dow Corning fluid DC 200.

Temperature variations of viscosity in Electric grade liquid silicones are very low compared with other fluid materials. This is largely because of the very low molecular cohesion of siloxane polymers [75]. Fig. 4.2 shows such variation for PDMS DC 200/200 cS. The temperature coefficient of viscosity for transformer oil is also shown for comparison.

4.2.2 Dielectric Properties

The dielectric constant of the Dow Corning Type 200 PDMS fluids ranges from 2.7 to 2.8 at room temperature depending on viscosity grade (DC 200/0.65 cS to DC 200/12000 cS). The variation of the dielectric constant with frequency and temperature for DC 200/10 cS and DC 200/200 cS is shown in Fig. 4.3(a) and (b). The corresponding variation for transformer oil is given for comparison in the same figure. It should be recognized that the change in dielectric constant with temperature is that which would be expected from the expansion data given in Table 4.3.

The dissipation factor of PDMS DC 200 fluids is very

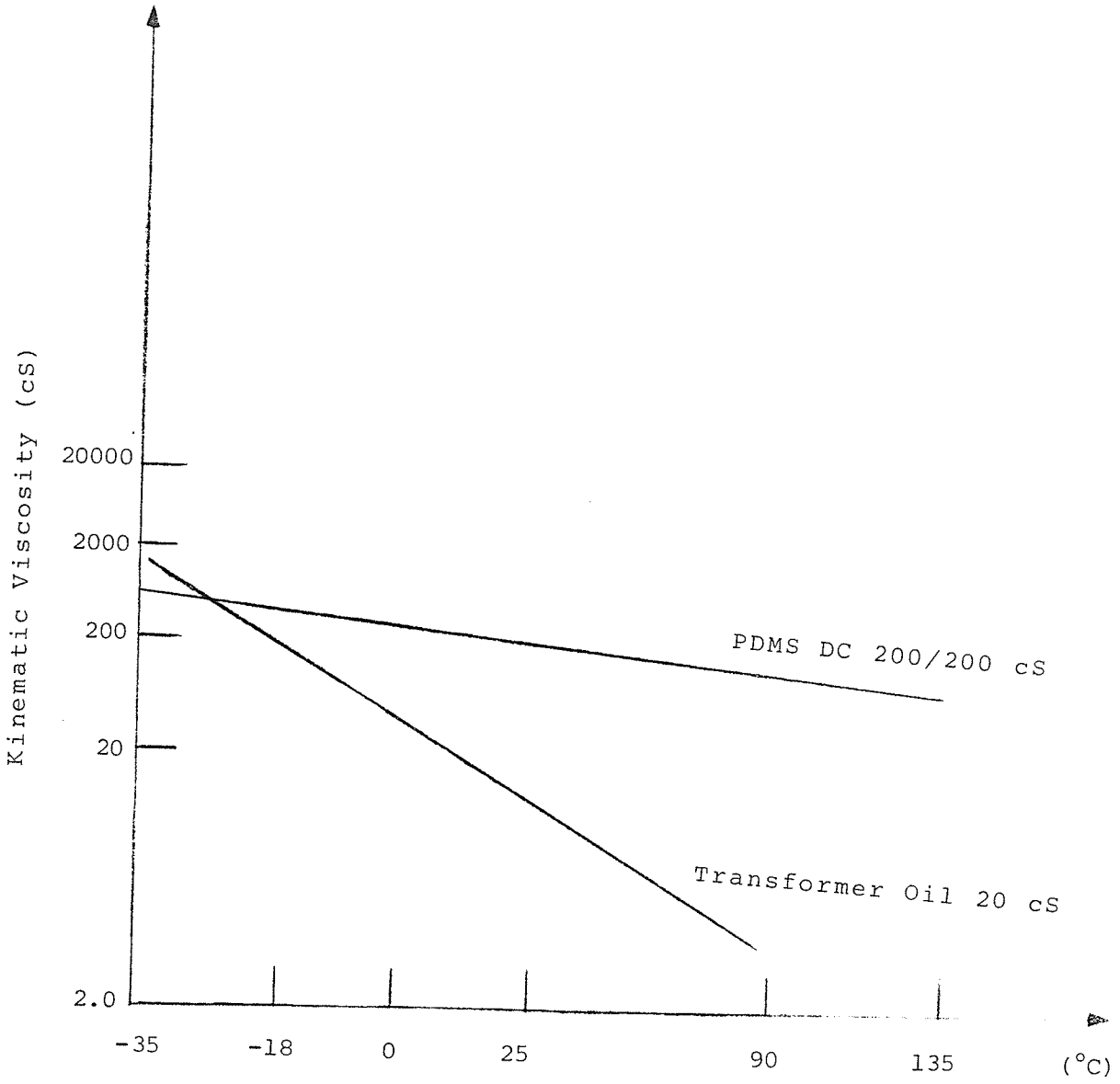

Fig. 4.2: Temperature Coefficient of Viscosity of PDMS DC 200/200 cS [75].

TABLE 4.3: Physical properties of PDMS DC 200/200 cS.

Viscosity 25°C (cS)	200
Viscosity temperature coefficient $1 - \frac{\text{viscosity at } 100^\circ C}{\text{viscosity at } 38^\circ C}$	0.62
Pour point °C	-53
Volatility on heating for 48 hours at 200°C	< 2%
Flash point minimum temperature °C	320
Weight per unit volume	0.81 kg/litre
Refractive index	1.4
Coefficient of thermal expansion x 10^3/°C/25°C to 100°C	0.968

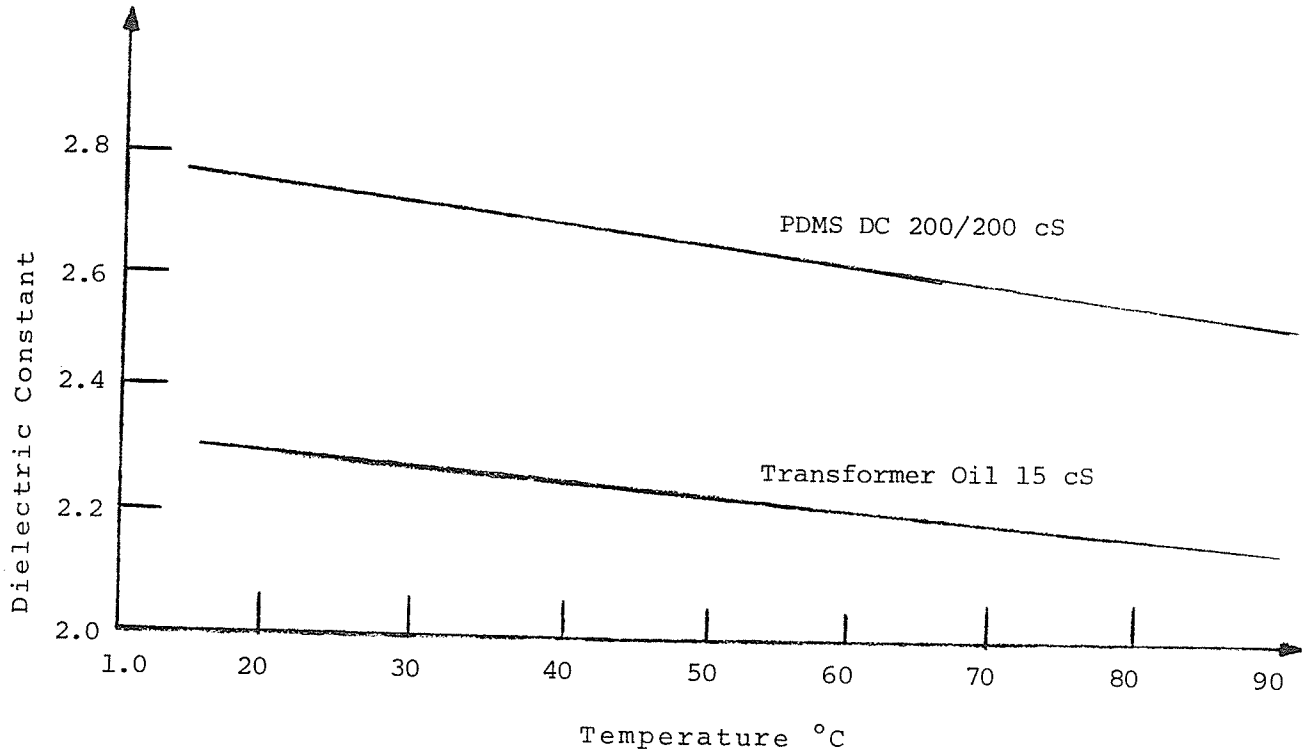

(a)

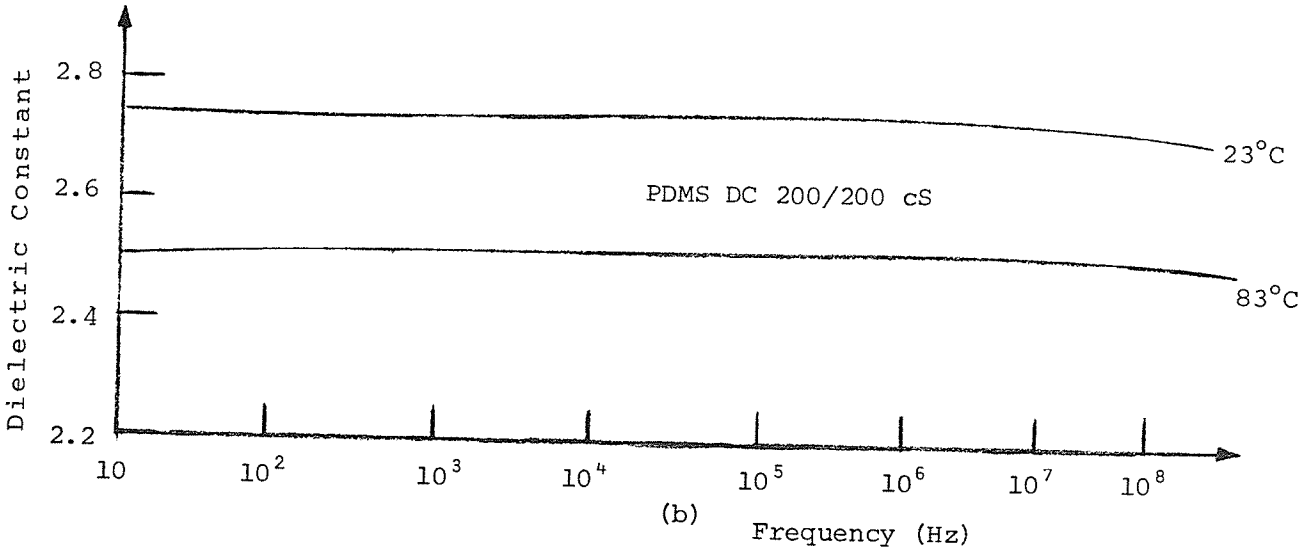

(b)

Fig. 4.3: (a) Dielectric Constant-Temperature Variation.

(b) Dielectric Constant-Frequency Variation [75] - [77].

low and is of the order of 0.0001 at power frequencies. It does not increase appreciably with increasing frequency up to 100 MHz. At higher frequencies there is evidence of rapid increase in the dissipation factor [76]. The dissipation factor increases with temperature but remains lower than that of typical transformer oil [77]. The volume resistivity of PDMS DC 200 fluids is of the order of 10^{14} Ohm-cm and does not drop below 10^{12} Ohm-cm at 200°C. The breakdown strength of PDMS DC 200 fluids like most dielectric liquids decreases with increasing test gap.

The low dissipation factors of these liquid silicones at elevated temperatures or at higher frequencies and their inertness to moisture indicates their applicability in liquid-filled capacitors. In the late 1960's, the unfortunate PCB (poly chlorinated biphenol-askaral) poisoning of people in Japan and the toxicity/environmental studies that followed predicted the eventual elimination of all PCB-based products. Because of the properties outlined above, silicone fluids became the prime candidate to replace PCB's in some applications. Silicone liquid filled capacitors are now being developed at the General Electric Corporation and other Laboratories as well as silicone filled and retro-filled transformers at Ferranti, Dow Corning, Westinghouse, etc. In both cases the low viscosity DC Type 200/50 cS grades or equivalent are being used [78].

Investigations about the possibility of using Electric grade PDMS fluids as impregnants are being carried out at different

laboratories and results on the electrical conduction in, and dielectric properties of, thin liquid films have been reported [79], [80], [81]. Beside high field experiments carried out by Lewis [82], no information is available in literature on breakdown under power frequency voltage of Electric grade PDMS fluids of commercial purity. Furthermore, the behaviour of an XLPE/PDMS interface has not been investigated under any type of voltage. Therefore, it was considered necessary to carry out the study of the electric breakdown of characteristic along an interface of a molded XLPE cable termination filled with PDMS DC 200/200 cS.

4.3 Discussion

In the preceding sections the dielectric and other properties of XLPE and Silicone Oil and their prospect for use as insulants in EHV cables have been reviewed. With improved methods of extrusion and better quality control, the properties of XLPE indicate its extensive use in future as EHV (and higher) cable insulation. Similarly, the properties of silicone oil have made it an increasingly strong competitor for replacing mineral hydrocarbon oils.

CHAPTER V

A REVIEW OF THE FACTORS INFLUENCING BREAKDOWN ALONG A LIQUID/SOLID INTERFACE

In this chapter a review is presented of the different factors that influence the dielectric strength of a liquid in the presence of a solid spacer. Fig. 5.1 shows a cross-section of parallel liquid/solid interface. The intended use of silicone oil (PDMS) together with extruded cross-linked polyethylene (XLPE) in EHV cable terminations necessitates a preliminary study of the breakdown stresses at the PDMS/XLPE parallel interface. This study is experimental (Chapter VI) rather than analytical because no definite theory has yet been developed to explain the reported flashover voltage levels for such an interface. The problem is further compounded by the different results obtained by different researchers in breakdown studies of dielectric liquids. The breakdown strength of a parallel liquid/solid interface is usually lower than that of an equivalent gap filled with the liquid dielectric alone.

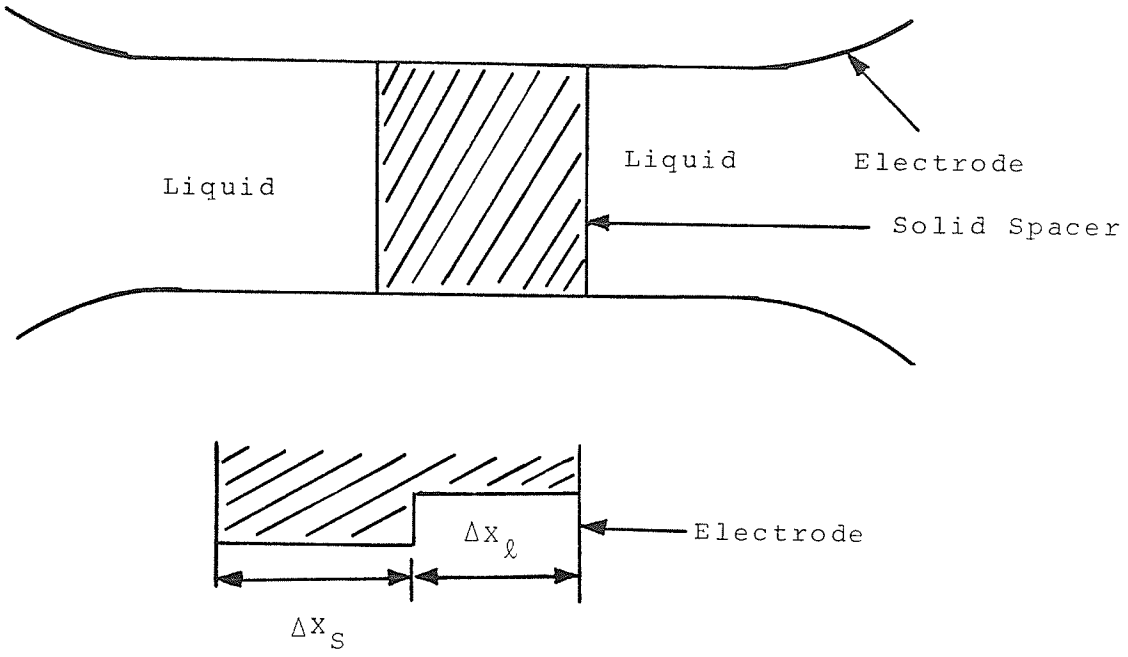

Fig. 5.1: A Parallel Liquid/Solid Interface.

Various theories have been proposed to explain the observed decrease in breakdown stress of a liquid/solid interface compared to the breakdown stress of the liquid itself. The common assumption is that the electric field at some point on the interface is in some way increased above the value of the breakdown field of the liquid, and then surface flashover is initiated by a discharge in the high field region. It has long been known that the ratio of the two dielectric constants (liquid and solid) influences the reduction in breakdown stress along the interface. Other factors which have been found to influence this reduction in breakdown stress include: nature of

surface of the solid spacer, field enhancement at the electrodes, space charge at the liquid/solid interface, the surface resistivity, and motion of the liquid due to electrohydrodynamic forces. Each of these factors is now briefly reviewed.

5.1 Effect of Ratio of Dielectric Constants

With reference to Fig. 5.1, it is seen that at the liquid/solid interface, with uniform field electrodes, the electrostatic field is parallel to the interface. In such a case, both the liquid and the solid spacer would be subjected to the same magnitude of the electric stress. Breakdown would therefore occur by flashover through the liquid (assuming the breakdown strength of the solid spacer is higher than that of the liquid - which is usually the case). Such a flashover through the liquid should be independent of the presence of the solid. This postulation assumes that the surface of the solid spacer is smooth. In practice, there exist points at the liquid/solid interface at which the liquid and the solid are in series. If the surface of the solid spacer is magnified a few times surface pits will be observed. Consider an elemental length ΔX along the liquid/solid interface such that ΔX is made up of length ΔX_s of the solid in series with length ΔX_ℓ of the liquid. Then the potential difference ΔV across ΔX is given by

$$\Delta V = \Delta V_{\ell} + \Delta V_{s}$$

where ΔV_{ℓ} is the incremental voltage across ΔX_{ℓ}; and,

ΔV_{s} is the incremental voltage across ΔX_{s}.

If ΔX is the electrode spacing and ΔV_{b} is the breakdown value of the voltage for the spacing then if $\Delta V_{\ell b}$ is the value of ΔV_{ℓ} at breakdown equation (5.2) results

$$\Delta V_{b} = \Delta V_{\ell b} + \Delta V_{\ell b} \left(\frac{\Delta X_{s} \varepsilon_{\ell}}{\Delta X_{\ell} \varepsilon_{s}}\right) \qquad (5.2)$$

where ε_{ℓ} is dielectric constant of the liquid; and, ε_{s} is dielectric constant of the solid.

Assuming that flashover of the interface occurs in the liquid when a certain critical stress, say, $E_{c\ell}$ is exceeded then equation (5.2) can be rewritten as:

$$\Delta V_{b} = E_{c\ell} \Delta X_{\ell} + E_{c\ell} \left(\frac{\Delta X_{s} \varepsilon_{\ell}}{\varepsilon_{s}}\right) \qquad (5.3)$$

In the absence of the solid spacer the breakdown value of the voltage would be

$$\Delta V_{\ell b} = E_{c\ell} \Delta X \qquad (5.4)$$

The ratio between (5.3) and (5.4) gives the reduction factor of the breakdown voltage of the liquid with and without a spacer for the simplified model of Fig. 5.1:

$$\frac{\Delta V_b}{\Delta V_{\ell b}} = \frac{\Delta X_\ell}{\Delta X} + \frac{\Delta X_s}{\Delta X} \quad \frac{\varepsilon_\ell}{\varepsilon_s} \tag{5.5}$$

In equation (5.5) ΔV_b equals $\Delta V_{\ell b}$ if ΔX_s equals zero, and therefore, $\Delta X = \Delta X_\ell$. This would be the case for an ideal liquid/solid interface. The breakdown field would depend only on the dielectric strength of the liquid irrespective of the presence of the solid. The other limiting case is the idealized series liquid/solid interface. In such a case the voltage ratio in equation (5.5) is proportional to the inverse ratio of the dielectric constants. In practice, a liquid/solid dielectric interface will have points at which the interface is parallel and other points at which the two dielectrics are in series.

While it is agreed that breakdown of a parallel liquid/solid dielectric interface occurs by flashover through the liquid it has not been resolved whether the flashover occurs on the surface of the solid or away from it. Using various dielectric solid spacers in transformer oil, it was found [83] that of the 70 breakdowns obtained, only 6 spacers showed no surface damage. For the spacers whose surfaces were damaged by the flashover, the extent of the damage varied depending on the material used. The experimental breakdown

values for different material along the interface in transformer oil reported in Ref. [83] are reproduced in Table 5.1. The last two columns give the variation of the percentage reduction in breakdown voltage of the liquid with and without a solid spacer. The percentage reduction varies from 6.5% for a spacer material of dielectric constant 3.5 (plexiglass) to 50% for that of dielectric constant 12.2 (phenolic cloth). It was not reported whether the spacers were of the same smoothness. The effect of surface roughness was indicated when a spacer with a pitted surface (epoxy glass) was used. In this case the percentage decrease of the breakdown voltage was three times compared to the percentage decrease when a smooth spacer was used. Although the results show a large scatter (as indicated by the coefficient of variation - calculated by the author) they do indicate the relative dependency of the flashover strength of liquid/solid interface on the strengths and dielectric constants of the liquid and solid spacers and the nature of the surface of the solid. An extreme case is a parallel liquid/solid interface comprised of pure water as the dielectric liquid ($\varepsilon_r = 81$) and a solid of a vastly lower dielectric constant. Here, the liquid/solid interface fails by puncture through the solid.

If the dielectric constant of the spacer material is greater than that of the liquid, the electric field is enhanced in any void at the solid/electrode interface by a factor approximately equal to the dielectric constant of the solid. Elimination of

TABLE 5.1: Breakdown voltage for liquid/solid system in transformer oil (dielectric constant 2.2)

Spacer material	ε_r	B/D Level kV		Decrease %	C.V. %
		Liquid	Liquid/ Spacer		
Polystrene	2.6	87	79	9.0	27.6
Plexiglass	3.5	94	88	6.5	23.5
Polyster Glass	4.7	86	76	11.5	19.2
Epoxy Glass*	4.8	84	49	42.0	16.5
Epoxy Glass**	4.8	91	79	13.0	22.0
Phenolic Paper	4.9	91	81	11.0	30.8
Polyster Glass	5.0	89	79	11.5	25.4
Polyster Glass	8.0	119	98	17.7	19.2
Polyster Glass	11.2	111	74	33.0	19.2
Phenolic Cloth	11.6	87	45	48.0	11.8
Phenolic Cloth	12.2	90	45	50.0	12.9

ε_r: Dielectric Constant

B/D: Breakdown

Decrease: $\frac{\text{B/D Level Liquid - B/D Level Liquid/Spacer}}{\text{B/D Level Liquid}}$

C.V: Coefficient of variation

* With surface pits
** Without surface pits

these voids improves the flashover voltage level but does not bring the strength of the liquid/solid parallel combination to that of the unbridged liquid gap. Furthermore, parallel combinations of the liquid and solid spacer in which the solid has a slightly lower dielectric constant also fail by flashover at strengths lower than that of the liquid gap. It can therefore be concluded here that difference in dielectric constant alone cannot fully account for the lower strength of a liquid/solid parallel combination compared to the strength of an unbridged liquid gap.

5.2 Field Enhancement

Field enhancement has been suggested as a cause of the observed decrease in flashover strength of a parallel liquid/solid interface compared to the breakdown of a liquid gap of similar length [84]. This phenomenon is due to the existence of a weakly bound molecular ion distribution on the surface of the solid insulation such that on application of intense electric field a drift of ions to the electrodes occurs. The resulting accumulation of charged particles at the tri-interface (liquid-solid-electrode) sharply enhances the electric field across the oxide layer on the electrode. Consequently the probability of breakdown being triggered off by field emission from asperities on the electrode surface is increased.

Recessing the solid dielectric into the electrodes reduces the magnitude of the enhanced field at the tri-interface. This was observed when an epoxy rod spacer of 63.5 mm length in transformer oil was recessed 1.5 mm into the electrodes. A flashover voltage increase of 30% with standard impulses was obtained [84]. This voltage increase, however, varies with different solids and liquids. It depends on the ion concentration, degree of charge injection, surface resistivity of the solid and the dielectric constants and strengths of the liquid and solid.

Therefore, in addition to the factors reviewed in the previous section, space charge also influences the flashover voltage value for a parallel liquid/solid interface compared to that of an unbridged liquid gap. Numerical methods for calculating electrostatic fields, despite their usefulness in the design of high voltage dielectric systems, cannot so far account for space charge. Lately the use of the Kerr electroptic cell [85] has made it possible to investigate the changes in field distribution between electrodes in a liquid due to the introduction of a solid. The results of such an investigation are reviewed in the next section.

5.3 Space Charge at Interface and Surface Resistivity

The Kerr electroptic effect has been used to measure the field distortion produced by solid dielectric spacers in pure nitrobenzene [86], [87]. The object was to identify mechanisms responsible for the lowering of flashover strength of a liquid in the presence of the solid dielectric. The use of teflon (polytetraflouroethylene), low density polyethylene, nylon (polyamide) and faradite (barium titanate ceramic) spacers in pure nitrobenzene resulted in a marked degree of distortion of the electric field at the liquid/solid interface. The degree and location of distortion depended upon the spacer material as did the time needed to establish the fringe pattern [86]. The field distortion was found to be greatest at the liquid/solid interface and gradually decreased with increasing distance from the interface. The results so obtained in reference [86] are presented in table form - Table 5.2. For completeness the known values of the dielectric constant and surface resistivity have also been included.

From Table 5.2, it can be concluded that both the field distribution and the time taken to establish a steady-state distribution is different from each solid spacer. Therefore, the liquid by itself is not solely responsible for the field distortion. The observed field distortion can be attributed to space charges on the solid insulator or to an uneven

TABLE 5.2: Electric field distortion in the liquid due to the presence of various solid spacers

Property/Observation	Polyethylene	Teflon	Nylon	Faradite
Dielectric constant	2.3	2.0	3.5-7.5	10^3-10^4
Surface Resistivity (Ohms/square)	1.3×10^9	3.6×10^{12}	2.8×10^9	10^{11}-10^{13}
Maximum field measured (kV/cm)	80 (cathode)	89 (cathode) 89 (anode)	115.0 (cathode)	96.0
Average field in liquid (kV/cm)	75.0	87.5	105.0	87.5
% field enhancement	6.0	1.7	10.0 (cathode) -7.0 (anode)	9.0 (cathode) 7.0 (anode) -8.0 (centre)
Time taken to establish steady-state distribution	<20 ms	<20 ms	40 ms	500 ms

distribution of surface charges on the solid. The field distortions are greatest for nylon and Faradite which have lower surface resitivities than teflon but higher values of the dielectric constant than either teflon or polyethylene. However, from the behaviour of surface charges during static electrification, it would be expected that high surface resistivity materials would be more prone to uneven surface charge distribution and hence would exhibit the largest field distortions if surfaces were predominantly operative. From Table 5.2 this seems to be the reverse, therefore, the field distortion due to the presence of the solid can be attributed to other influences as well such as the bulk polarization of the solid and those reviewed in the previous two sections.

Comparison of Table 5.1 and Table 5.2 reveals that the field enhancement is too small to account directly for the reduction in dielectric strength due to the introduction of a solid spacer in a liquid gap. It should be noted that the dielectric constant of nitrobenzene is higher than that of polyethylene, teflon and nylon so that the field in any voids at the electrode-solid-liquid tri-interface will be lower than the field in the solid dielectric. Furthermore, the field distortion reported in [86] extends across the whole sample and is not limited to the immediate vicinity of the electrode insulator junction.

Use of a liquid of higher ionic content (Aroclor 1242 -

a Monsanto Trade Mark) should result in a higher field distortion in the liquid insulant that could possibly obscure the smaller field distortion solely due to the presence of a solid spacer. However, when this was done [87] the field distortions obtained for teflon in Aroclor were of similar magnitude as obtained for the same solid in nitrobenzene. Also, the field distortions in both cases were greatest at the liquid/solid interface and started to decrease gradually at distances approximately 3mm from the interface. The time taken to establish steady-state field distribution for teflon and phenolic spacers was the same. This suggests that the type of liquid and not the solid is responsible for the field distortions.

Further investigation revealed an enhanced current density in the region close to the liquid/solid dielectric interface. Neither the field enhancements nor the changes in current density are dependent upon spacer material. Both observations can be attributed to the type of liquid dielectric. Values of the surface current density in the liquid and at the liquid/solid interface from the work arising out of reference [87] are shown in Fig. 5.2.

From both studies, [86] and [87], it can further be concluded that although the presence of a solid dielectric in a liquid introduces a field enhancement and increased current density at the liquid/solid interface such changes are not the predominant cause for the reduced flashover strength of

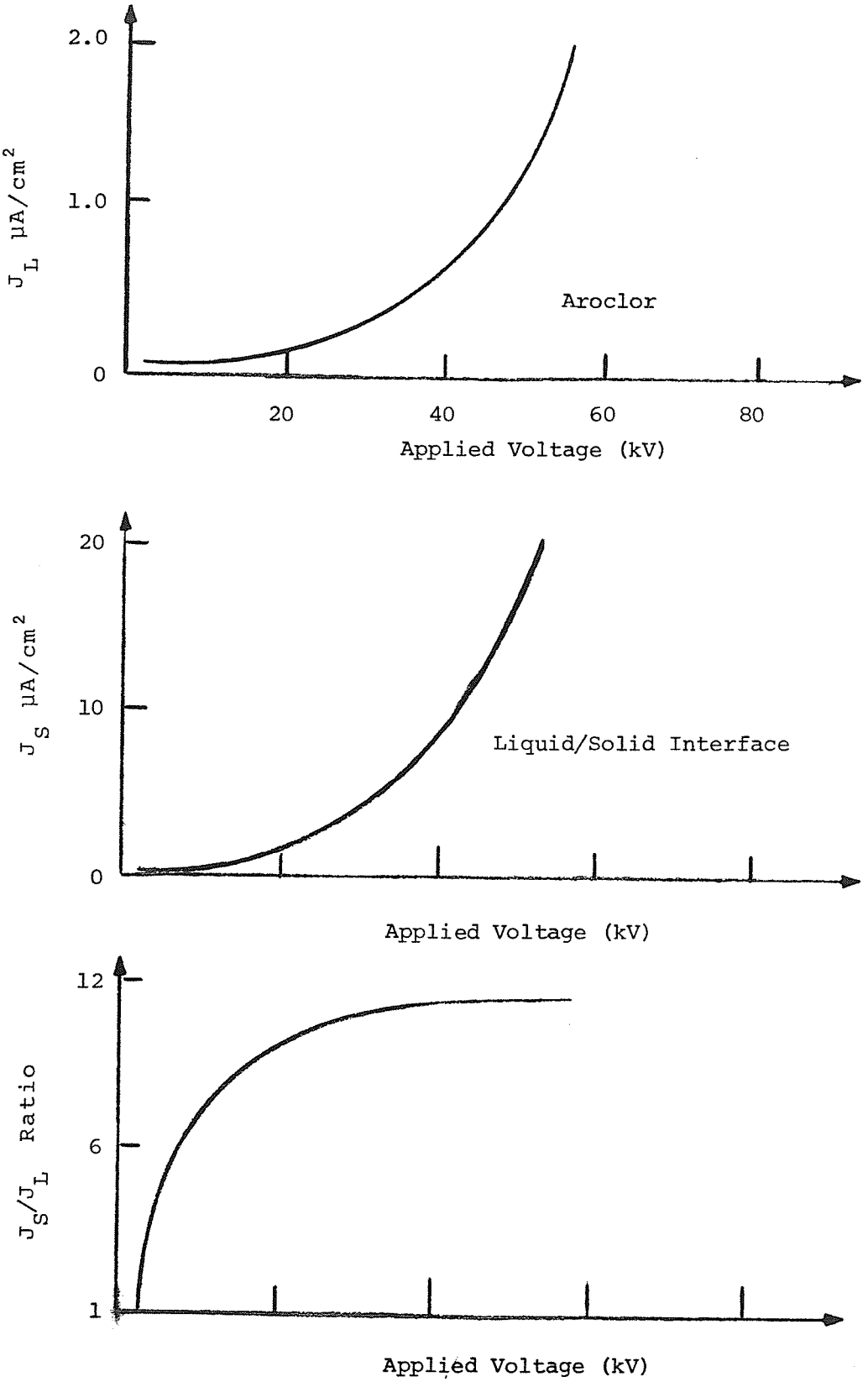

Fig. 5.2: Increase of Current Density at Liquid/Solid Interface [87].

the parallel liquid/solid combination. The amount of field distortion and increase in current density at the liquid/solid interface cannot be attributed to just the type of liquid or type of solid, but to both and other influences to be reviewed in the next section.

5.4 Electrohydrodynamic (EHD) Motion

The existence of turbulence due to unipolar charge injection from an electrode into the liquid has been known since the days of Faraday [88]. But it is only recently that this electrohydrodynamic motion has been suggested as a basic mechanism in the conduction phenomenon in dielectric liquids. Besides turbulence, the existence of a cellular electrohydrodynamic motion equivalent to that in thermal convection has also been suggested [89]. The resulting motion due to the application of a d.c. electric field (EHD) has been proved to be relatively insensitive to the resistivity and permitivity values of the liquid dielectric over several orders of magnitude [90]. The intensity of the EHD motion depends on the factors necessary to establish turbulence such as the applied voltage, gap length, ion mobility, viscosity and Reynold's number. The convective or turbulent convective charge transport during injection of charge carriers into insulating liquids generally dominates over the true mobility. An approximate theory based on the methods of statistical continuum mechanics has been used to explain some of the experimental observations in polar liquids such as nitrobenzene

[89]. It has been argued that turbulence and convective motion are not due to dielectrophoretic forces but to the usual electrostatic force acting on the space charge transported by the liquid (EHD)[88].

In the case of a parallel liquid/solid dielectric interface, it has been suggested that the observed increase in current density at the interface due to the presence of the solid may be due to vorticity which establishes a flow that contours the boundary of the electrode-spacer geometry. At high field strengths, motion of the liquid aids charge injection which further enhances the EHD motion [91]. The resulting pattern should be dependent only upon the geometry and surface smoothness of the spacer and independent of the electrical properties of the solid.

Observations of the liquid circulation at low, intermediate and very high pre-breakdown fields have revealed that the flow is initially columnar in nature; the flow becomes laminar with increasing velocity as voltage is increased [92]. Immediately prior to breakdown the liquid was observed to attain stable vortices of cellular pattern. These observations are similar to those obtained for Aroclor and transformer oil. Further the EHD motion was not affected by change in the composition of spacer material. Fig. 5.3 shows the geometrical representation of these observations. It has therefore been concluded [92] that for EHD flow the solid acts only as a mechanical barrier to liquid flow. In the absence of the solid spacer the intermediate laminar vortices were not observed;

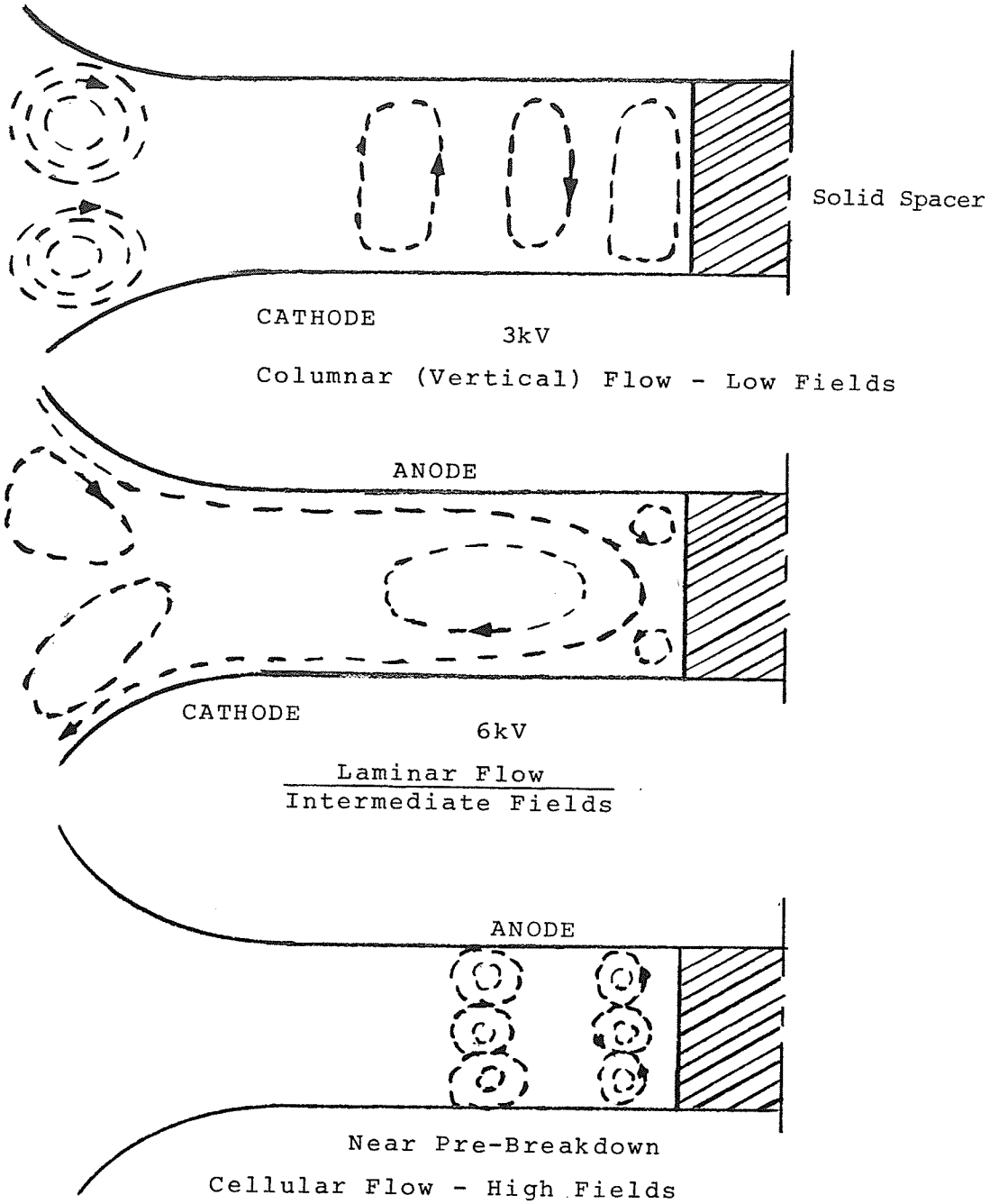

Fig. 5.3: EHD Motion in Liquid in Presence of Solid Spacer - 5mm gap in Aroclor and Transformer Oil; - Teflon Spacer [92].

the EHD motion of the liquid changes from columnar flow to cellular flow prior to breakdown. A higher voltage was required to produce cellular flow instability in the absence of the spacer. Position of the flashover arc was observed with a still camera to be 1 mm away from the interface; the full flashover took less than 0.15μs after initiation.

To further prove that the lower breakdown strength of a liquid in the presence of a dielectric solid spacer is partly a liquid phenomenon, experimental results show that the breakdown of a parallel liquid/solid interface increases with increase in pressure.

5.5 Conclusions

Although the theory of breakdown of liquid/solid interface is still being developed in various laboratories, it can be concluded from the review that the lowered strength of a parallel liquid/solid dielectric combination is influenced by many factors. The dielectric constant of the solid spacer will result in the enhancement of the field in voids at the electrode-solid liquid tri-interface if the ratio $\varepsilon_s/\varepsilon_\ell$ is greater than unity. If the surface of the spacer is not smooth, the field will equally be enhanced in the surface pits of the solid spacer. The observed increase in charge at the liquid/solid interface is due to superposition of fields due to polarization, a positive surface charge and the applied potential difference across the gap. Such a conclusion has been reached for the

case of a solid spacer in vacuum [93]. The obstruction of the flow of the liquid due to EHD forces by the solid spacer distorts the field at the liquid/solid interface and also enhances it by way of increased charge injection into the vortices--hence the increased current density at the interface.

Although the flashover arc was observed at a distance 1 mm away from the interface, the nature of the surface of the spacer plays a role in the initiation of the flashover. The disruption of the flow of the liquid by the spacer and the consequent increase in charge at the liquid/solid interface explains why the interface is weak, electrically, even if the solid has a dielectric constant lower than or equal to that of the liquid.

The behaviour of viscous liquids with a.c. voltage shows that EHD motion as observed for d.c., does exist [90] depending on the frequency and strength of the applied field. Vortices have been observed in nitrobenzene at power frequences for fields of 20 kV/cm [88].

CHAPTER VI

EXPERIMENTAL STUDY OF THE BREAKDOWN STRENGTH OF THE PARALLEL PDMS/XLPE DIELECTRIC INTERFACE

Studies involving breakdown in dielectric liquids have generally branched off into two areas: the study of liquids of technical importance under test conditions of practical significance, and the study of highly purified liquids of doubtful commercial importance in test situations which often have no commercial counterpart. Most of the work reported has fallen into the second category because of the frustration encountered in the past from trying to develop theories explaining the breakdown behaviour encountered in practice. The basic difficulty faced in studying dielectric liquids of commercial purity is that dielectric strength is not a basic property of the material, but is determined by the impurities dissolved or suspended in the liquid; e.g., the amount of gas, moisture and other impurities. Studies in highly purified liquids are aimed at obtaining the intrinsic dielectric strength determined by the basic properties of the liquid dielectric.

The increasingly important role played by silicone fluids in electrical insulation has led to the need for a clearer understanding of the dielectric properties of these liquids. While studies on the thin film properties of PDMS

insulating liquid have been carried out [94], breakdown data on PDMS fluids of commercial purity under impulse and power frequency voltage are not yet available. The suggested use of PDMS for shielding XLPE requires an understanding of the breakdown strength of a PDMS/XLPE parallel interface under power frequency and impulse voltages. This is necessary for proper design of such composite insulations. In cable terminations, the electric stress component along a parallel PDMS/XLPE interface is the dominant factor. Thus, a study of a parallel PDMS/XLPE interface simulates the operating conditions encountered in a termination of an XLPE-insulated cable.

6.1 Experimental Technique and Procedure

In order to simulate the actual operating conditions for a cable termination, it would be necessary to subject a PDMS/XLPE interface to both radial and tangential electric stresses. However, in actual operation the magnitude of the radial stress at the PDMS/XLPE interface is negligible compared to the tangential stress along the interface. Therefore, samples of XLPE solid spacers were obtained from a piece of existing extruded XLPE-insulated medium voltage cable with the shields and conductor removed; and the electrodes were designed so that all the stresses at the interface were tangential to it.

6.1.1 The Test Cell

The test cell consisted of a 4.25 litres pyrex-glass vessel with a brass base and perspex top connected to a bushing. The complete cell is shown in Fig. 6.1 and the details of the glass vessel assembly are shown in Fig. 6.2. The following criteria were considered in the choice of the test cell:

(1) The cell should contain a large volume of PDMS liquid in order that by-products of a breakdown diffusing into the volume of the liquid would have little effect, if any, on subsequent breakdowns.

(2) A means of adjusting the gap length between electrodes without disturbing the liquid sample should be incorporated.

(3) In addition to breakdowns in the test gap, the cell should withstand voltages up to 300 kV.

(4) Means to remove bubbles, which accumulate under the plate electrode after breakdown, should be included.

(5) The electrode orientation should be such that bubbles formed between the XLPE solid spacer and the electrode, near the test gap, are easily removable by tilting the cell.

The pyrex-glass vessel was clamped between a brass plate at the bottom and a perspex plate at the top using nylon screws. A vent in the perspex plate facilitated connection to the evacuation system whose purpose will be detailed later. The brass rod supporting the plate electrode was centred in a

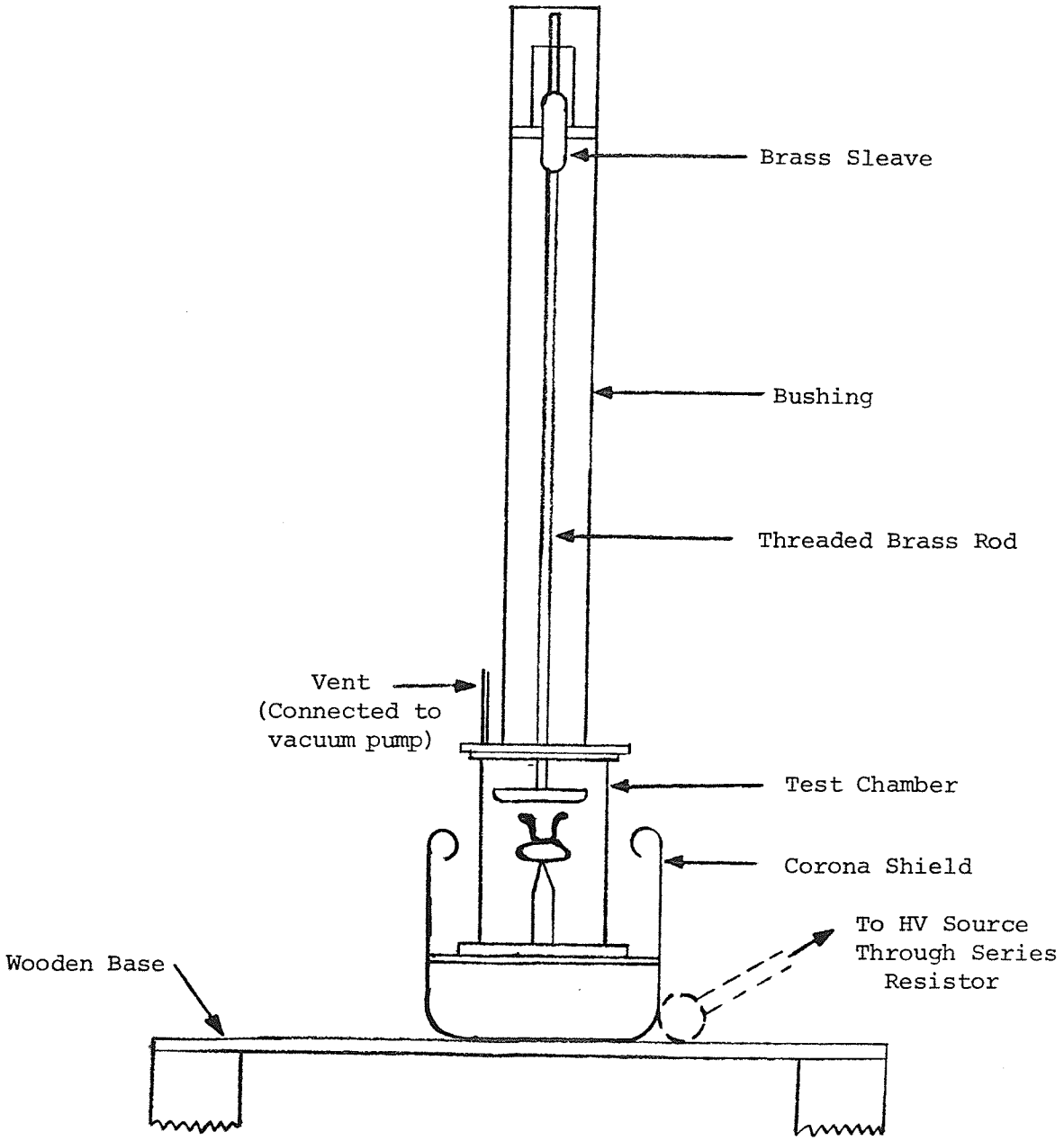

Fig. 6.1: The Test Cell.

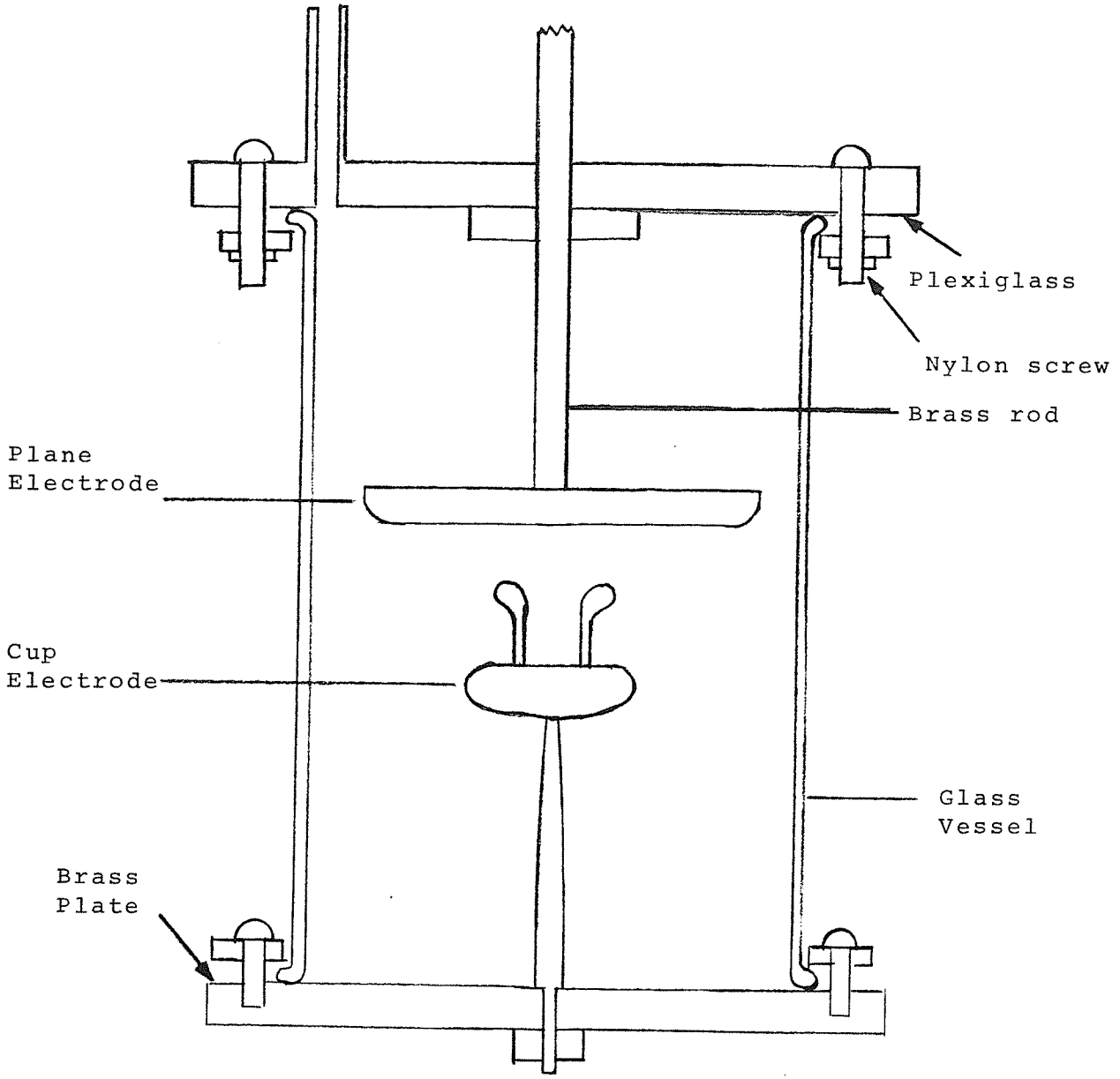

Fig. 6.2: The Test Chamber.

perspex tube filled with silicone oil (PDMS) forming a simple bushing. The top portion of the brass rod was threaded and passed through an internally-threaded base collar. The brass collar was firmly glued to a perspex disc mounted on the bushing cylinder. A special ring prevented the silicone oil in the bushing from leaking into the test cell. (All metal surfaces within the test cell were rounded and all threads shielded to prevent corona discharges).

The usual experience with a parallel solid and liquid insulation is that failure generally occurs at the liquid/solid interface because, as already indicated in Chapter V, the interface is electrically weaker than an equivalent liquid gap in the absence of the solid spacer. In some cases the breakdown level can be reduced as much as fifty percent [83]. In most experiments reported the flashover caused destruction of the solid dielectric along the interface by tracking,leading to degradation of the liquid dielectric. In this work, with the findings of other workers in mind, an electrode system was designed to try and avoid the need to change the solid dielectric following each flashover of the test gap. One electrode was designed in the form of a cup to support the solid dielectric in position and the rim of the cup was tapered off at 6 mm radius resulting in a stress-relief at the parallel liquid/solid interface. The cup electrode was used in an upright position

so that any trapped bubbles between its wall and the in-held spacer would easily move upwards to the bottom surface of the upper electrode. The top electrode was a plate of sufficient diameter to completely overlap the circumference of the rim of the cup electrode. The cup-plane electrode assembly is detailed in Fig. 6.3.

For the purposes of comparison and further understanding of the breakdown strength of the parallel PDMS/XLPE interface other electrode geometries were used. These included two parallel plane electrodes with a 3 mm deep sharp edged recess in one of them, and two parallel electrodes, each with a 3 mm deep recess with rounded off edges. These geometric details are shown in Fig. 6.4. All the elctrodes were made of brass with the exception of a chrome-plated plane electrode used in two test series for comparison. In all cases, the bottom electrode was fixed (Fig. 6.2) and the top electrode which was connected to the brass rod was used to adjust the gap.

6.1.2 Protection System for the Liquid Dielectric

The electric flashover arc associated with the breakdown of a liquid causes irreversible damage to both the liquid dielectric and the electrodes from which the arc emanates. It is therefore necessary to minimize the damage, especially if a series of breakdown tests are to be conducted using a given sample of the liquid.

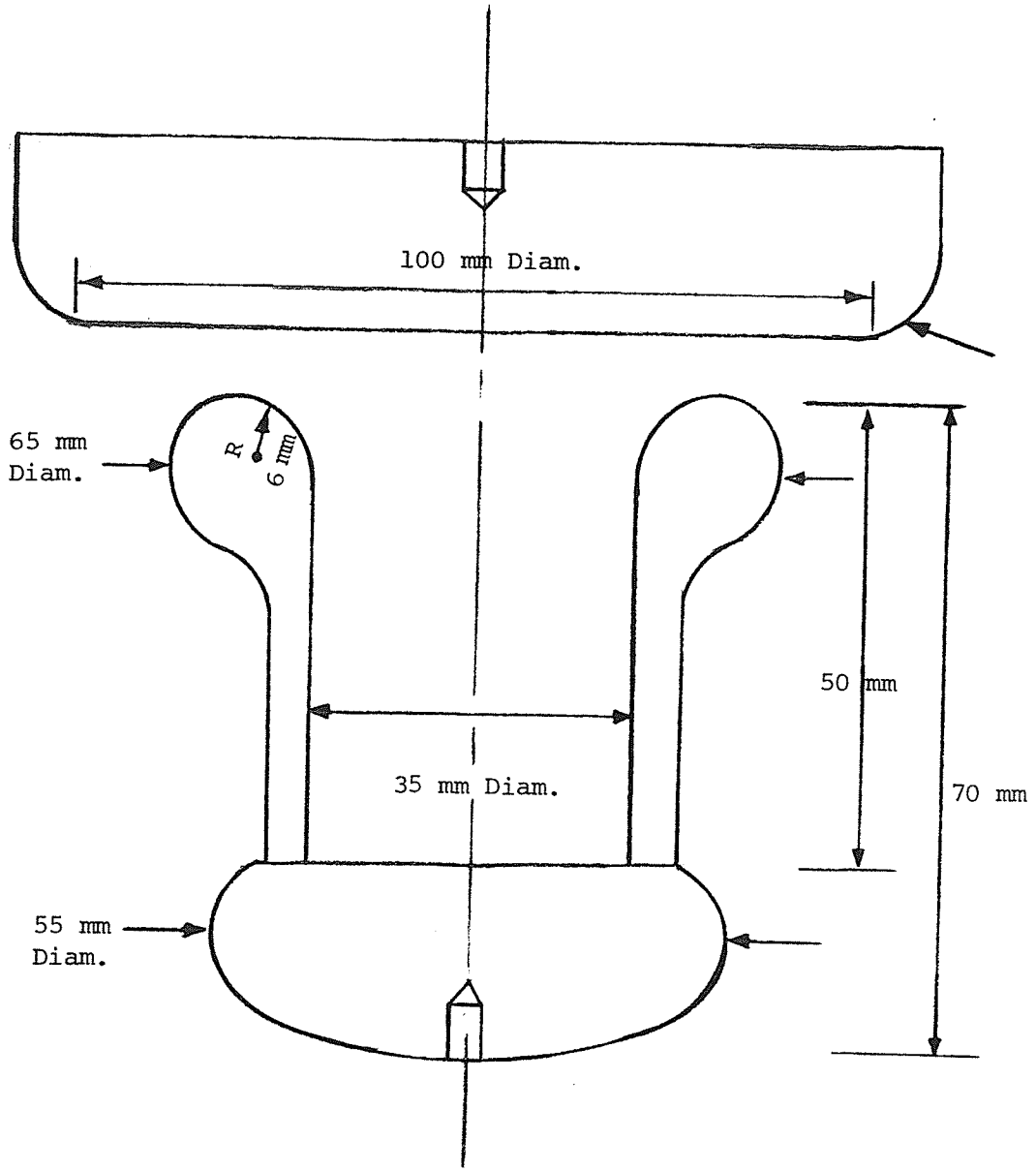

Fig. 6.3: Cup-plane Electrode System.

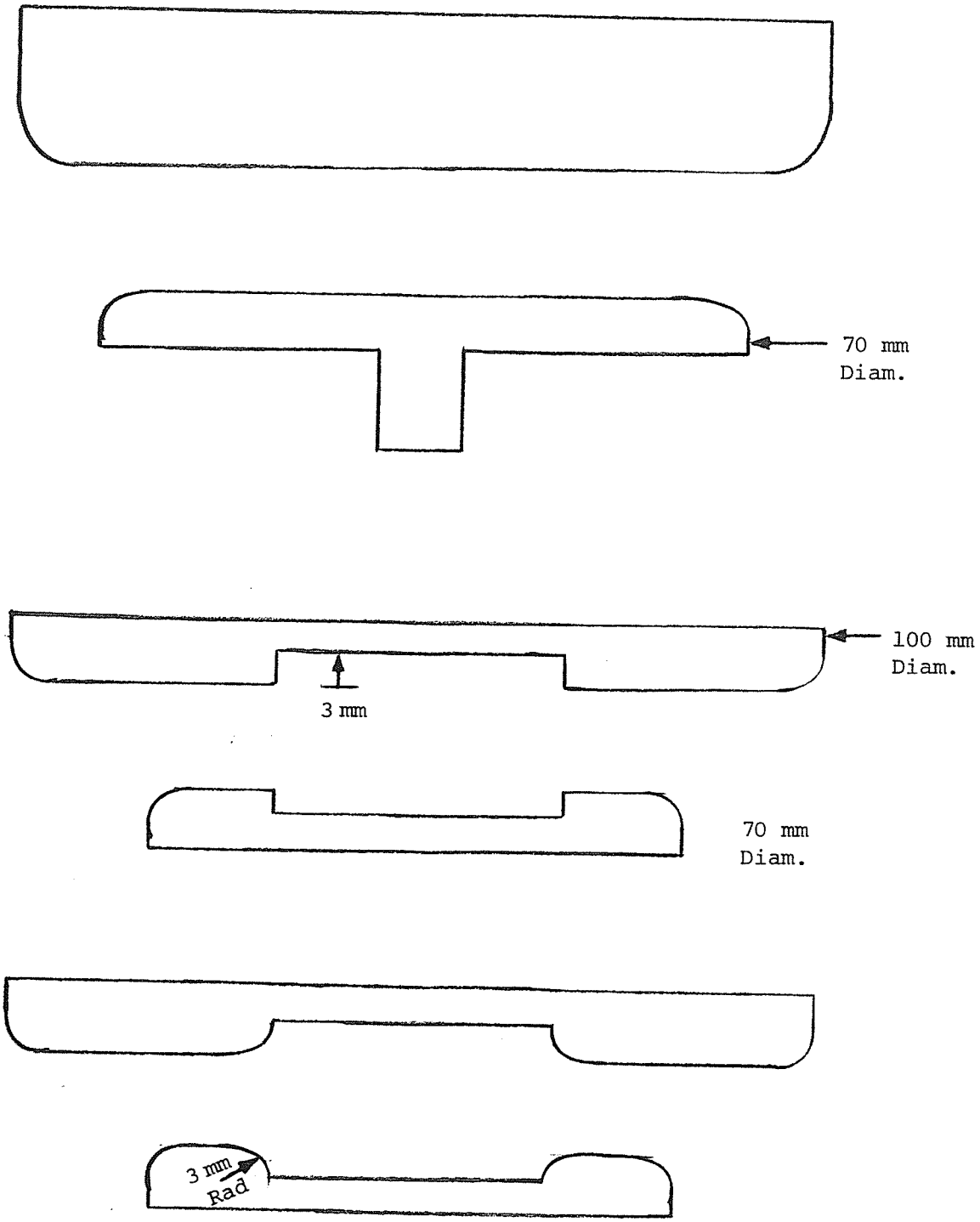

Fig. 6.4: Other Electrode Geometries Used in Power Frequency Tests.

A spark discharge in silicone oil generates intense heat in the proximity of the spark. This heat causes the chemical breakdown of the long chain PDMS molecules leading to the formation of gas bubbles composed of hydrogen (50%), methane, carbon monoxide, carbon dioxide and ethylene gases [94]. In addition polymerized PDMS gelatinous substances are formed on the electrodes. The presence of these bubbles and particles in the liquid gap will alter the breakdown strength of the liquid. The intense heat also creates pits at the root of the spark on the electrode surfaces. These pits alter the stress distribution in the liquid in their vicinity and thus alter the breakdown strength.

During preliminary testing with the circuit breaker trigger circuit, the 100A breaker (see next section) was found to close without any restrikes at the second zero of the sinusoidal voltage. This gives a time-to-close response of the circuit breaker of 10-12 ms. Taking a capacitance of about 5 pF for a 5 mm liquid gap in the absence of the solid, assuming a breakdown voltage of 120 kV the energy dissipated after a flashover is given by

$$\tfrac{1}{2}\, C\, V^2\, t\ \mu J$$

C = capacitance in pF

V = voltage in kV

t = time-to-close ms

Using the half cycle average value of the voltage and the corresponding values of C and t, the energy dissipated in the liquid gap is of the order of 0.1 J. If the duration of the spark can be reduced by orders of magnitude, the energy dissipated will be reduced accordingly. This can be achieved by employing a high voltage fast acting switch.

For lower testing voltages gas-filled thyratrons been used, but above about 30 kV the thyratrons would have to be cascaded, an operation that has been found unacceptable due to the longer time response. Series resistance of high ohmic value has been used to reduce the intensity of the spark but this, beyond a certain value, limits the pre-breakdown current and consequently higher breakdown voltage values result.

In this work, therefore, a trigatron was used to protect the test cell from intense damage by prolonged sparks. It was triggered by a 10 kV hydrogen thyratron. A trigatron is a three-electrode spark-gap consisting of two spherical (or hemispherical) main electrodes together with a trigger electrode of smaller diameter mounted centrally in a hole in one of the main electrodes and insulated from it (usually the one at low voltage). A comparatively small voltage applied to the trigger electrode can cause the main gap to break down at voltages below the normal sparking voltage. Thus, the trigatron acts as a controlled high voltage switch.

When used to protect a test cell, the trigatron is connected in parallel with a series combination of the cell and a resistor. The breakdown current flowing through a small resistance connected in the ground side of the cell results in a pulse voltage which, when adequately amplified can be used to trigger the main trigatron gap. If the main trigatron gap is properly set, the trigger pulse distorts the field resulting in the arc over at the main gap, thus diverting the breakdown current from the test cell--(see later - Fig. 6.6).

Of the research data available to date, about the characteristics of a trigatron spark gap relevant to its use as a fast high voltage switch [95] - [98] reference [98] gives the most elaborate and informative results. Using voltage pulses and appropriate time delays so that the trigger pulse would be available at the trigger-electrode of the trigatron when the high voltage impulse across the main sphere-gap attains crest value, the authors [98] found that the widest operating range was obtained under the negative polarity of the main impulse voltage with a positive trigger pulse. The breakdown values were in close agreement with those obtained for negative-impulse sphere-rod electrode arrangement. With a trigger pulse of negative polarity, the working range was lower and remained between 30 to 40 per cent below the untriggered breakdown value. Positive main impulse voltages with negative trigger pulse gave approximately the same

working range as the negative-negative combination for lower voltages, but the range decreased with higher voltage (> 200 kV). The least efficient combination was the positive main impulse with positive trigger pulse. It can therefore be concluded that the breakdown of the trigatron occurs at a much lower voltage under negative impulse than under positive impulse for a given polarity of the trigger pulse. The authors in [98] suggest that the polarity dependency results from the transformation of the originally uniform field to a non-uniform one by a space charge resulting from the trigger spark. Thus, the field distortion is greater when the trigger pulse is of opposite polarity relative to the main impulse waveform. Their results further show that for the possible combinations, with main voltage of opposite polarity to the trigger pulse, the trigatron may be operated over a wider voltage range. However, for the trigatron to breakdown quickly and consistently in air at normal atmospheric pressure, it should not be operated at voltages less than 70 per cent of the untriggered breakdown value.

For alternating voltages, breakdown may occur on either the positive or negative crest. Therefore, in this case it is necessary, in choosing the polarity of the trigger pulse, to consider both polarities at the high voltage electrode. From the above review, the optimum trigger pulse polarity is the negative one. The trigger pulse can be obtained from

the breakdown current of the sample at the ground side flowing through a very small impedance. This voltage should be amplified and inverted, if necessary, so as to obtain a sufficiently high voltage value at the grid of the thyratron for fast switching action immediately following a breakdown discharge in the sample. To avoid too many amplifier stages, two thyratron were used. A small thyratron on firing made available over 200 V at the grid of the 10 kV thyratron resulting in less than one microsecond operation The details of the circuitry are given in Appendix C.

The facility to vary the input into the small thyratron was very useful at higher voltages (> 100 kV) in avoiding spurious triggering due to corona. The total time delay did not exceed 3.2μs, being much shorter at higher voltage inputs. This time response was measured using a 2 V 2μs-wide rectangular input pulse from a signal generator. Using a sphere gap in air as a test sample, the protection range of this arrangement was investigated. The trigatron consisted of 25 cm spheres with a 10 mm insulated brass rod in the earthed sphere. Five breakdowns in the main gap were initially obtained with the trigger pulse switched out for a given gap. With the trigger pulse switched in, the test gap was readjusted until a limit was reached below which the breakdown of the test gap would not trigger to breakdown the main trigatron gap.

Fig. 5.5 shows the results of this preliminary test. It was found that the best trigger efficiency occurred with

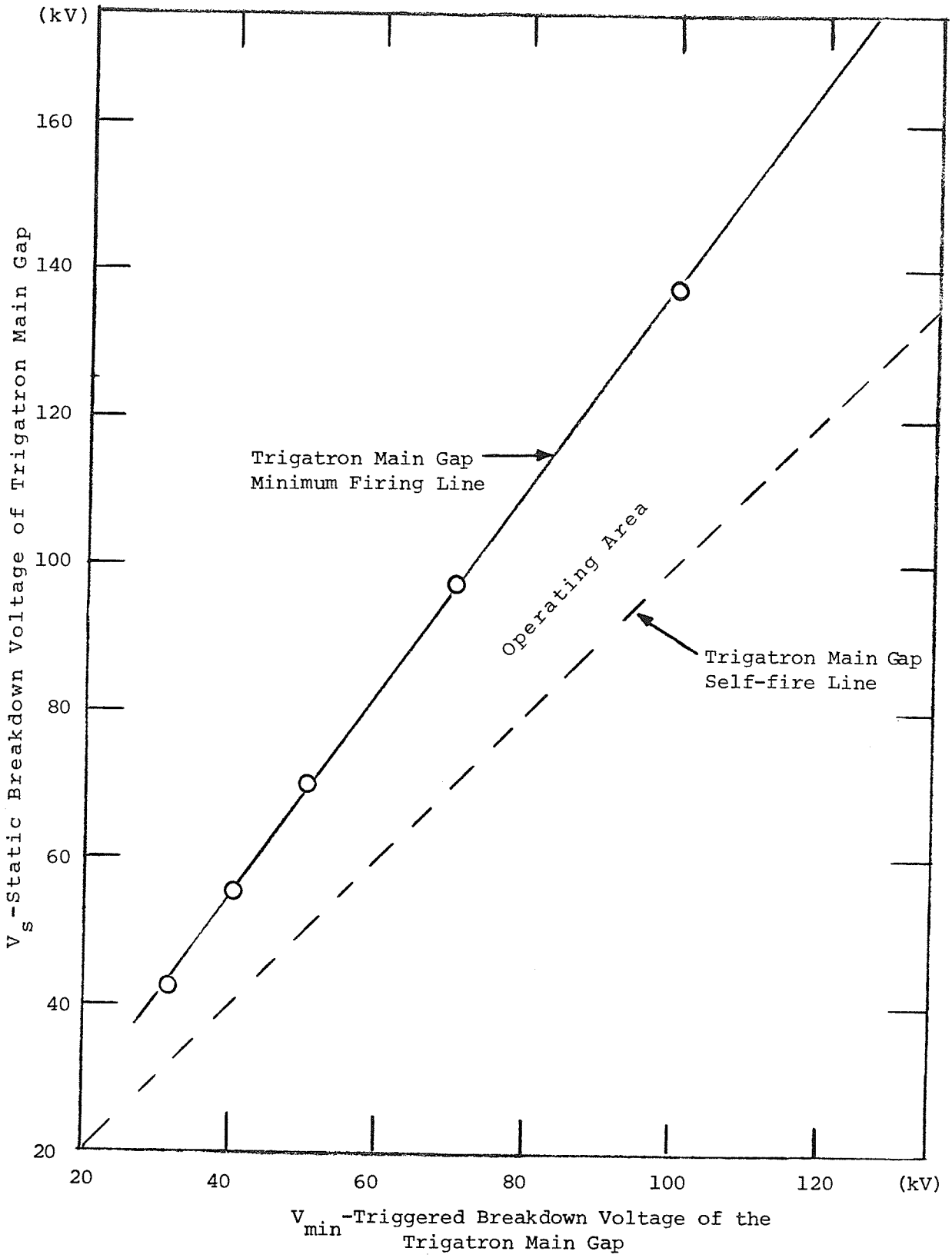

Fig. 6.5: Trigatron Operation Characteristic.

a positive half cycle at the test gap and therefore at the trigatron main gap at the time of trigger. It was also found that the protection unit operated efficiently and reliably when the test gap breakdown voltage was of positive polarity and of magnitude equal to 73% of the voltage required to break down the trigatron main gap in the absence of a trigger pulse. This percentage was higher in the case of breakdowns at the negative half-cycle.

6.1.3 Power Frequency Tests

In order to study the breakdown characteristics at the PDMS/XLPE parallel interface at power frequencies, a high voltage source is required together with a high voltage measuring unit, and a test-cell protection unit. The high voltage source was a 300 kV, 50 kVA, 60 Hz testing transformer. The high voltage measuring system comprised of a gas capacitor connected to a VTVM. The low voltage side of the transformer is supplied by a single-phase 100 A variac. A 100 A mechanical circuit breaker is fitted on the low voltage side. The circuit breaker trip relay is in turn triggered by a pulse across a 1.0 Ω inductor-less resistor connected in the ground side of the test gap as shown in Fig. 5.6.

Preliminary tests showed that a suitable value of ground impedance for the trigatron pulse was ten ohms resistive. Further, it was found that the resistance in series with the

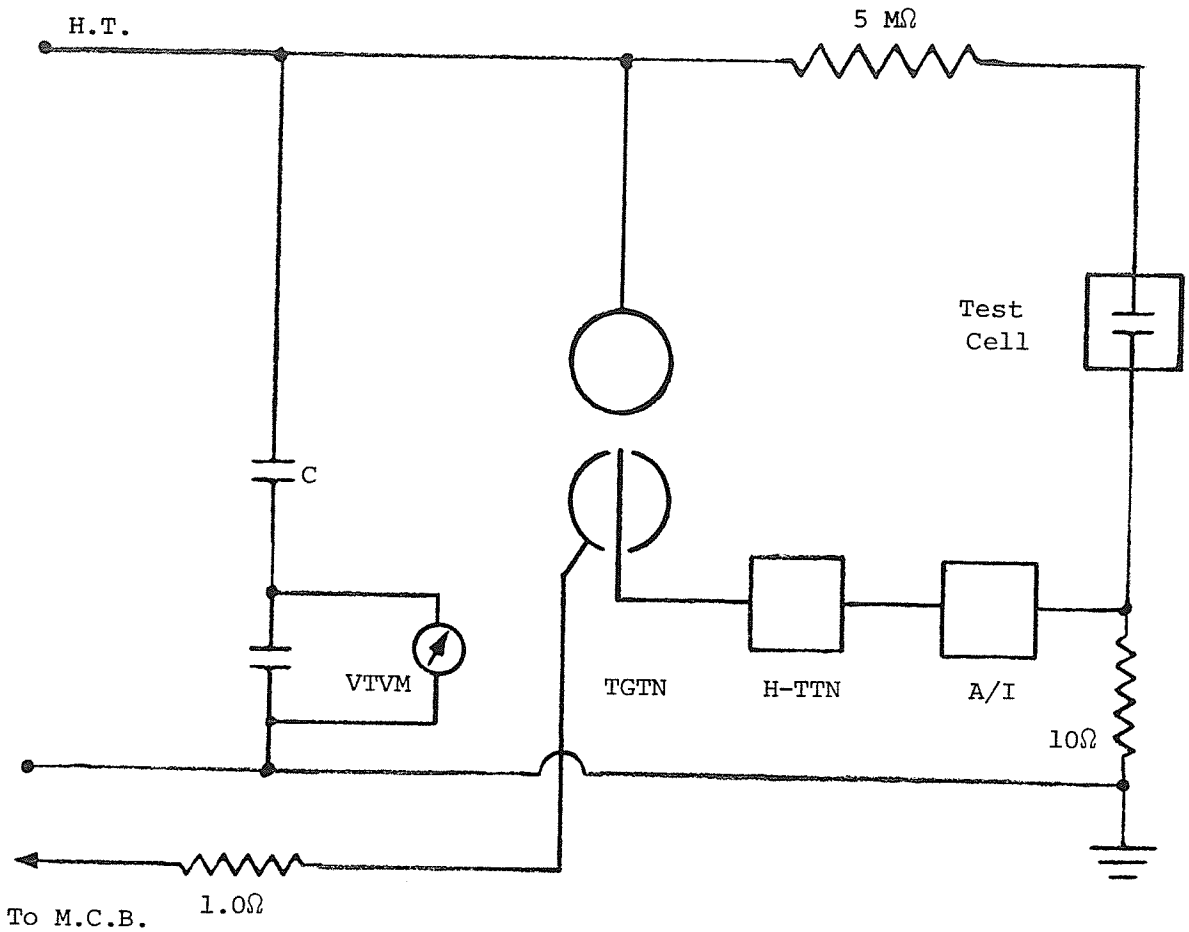

A/I: Amplifier/Inverter

C: High Voltage Gas Capacitor 103.5 pF

H.T: High Voltage Supply 300 kV, 50 kVA Transformer

H-TTN: Hydrogen Thyratron

Fig. 6.6: Power Frequency Test Circuit Diagram.

test gap did not have any significant effect on the breakdown voltage level for values between 500 kΩ and 7 MΩ. Of course the higher the series resistance, the lower the pre-breakdown current and hence the smaller the damage caused to the silicone oil and the electrodes by the breakdown discharge. A value of 5 MΩ was used. The VTVM was initially calibrated using standard IEC tables for disruptive discharge in air with standard sphere-gaps. The results so obtained are shown in the graph of Fig. 5.7. Five breakdowns were obtained for each gap setting.

Preliminary breakdown tests on the silicone oil revealed that some gelatinous substance (polymerized PDMS) was formed on the electrodes at the point of discharge in addition to gas bubbles. Due to the high viscosity of the silicone oil (200 cS) mere stirring of the liquid is not adequate for removal of both the gelatinous substance and the bubbles from the top electrode. A special procedure was therefore used to dislodge the discharge by-products from the electrodes. With the test cell not completely filled with the silicone oil, a partial vacuum was created above the silicone oil level. Consequently, the bubbles grew in size and with proper orientation of the test cell, they dislodged the gelatinous substance during their passage to the top of the liquid surface. This pumping operation lasted up to fifteen minutes after which the vacuum system was shut off and the liquid left to settle before a subsequent breakdown test. Use of

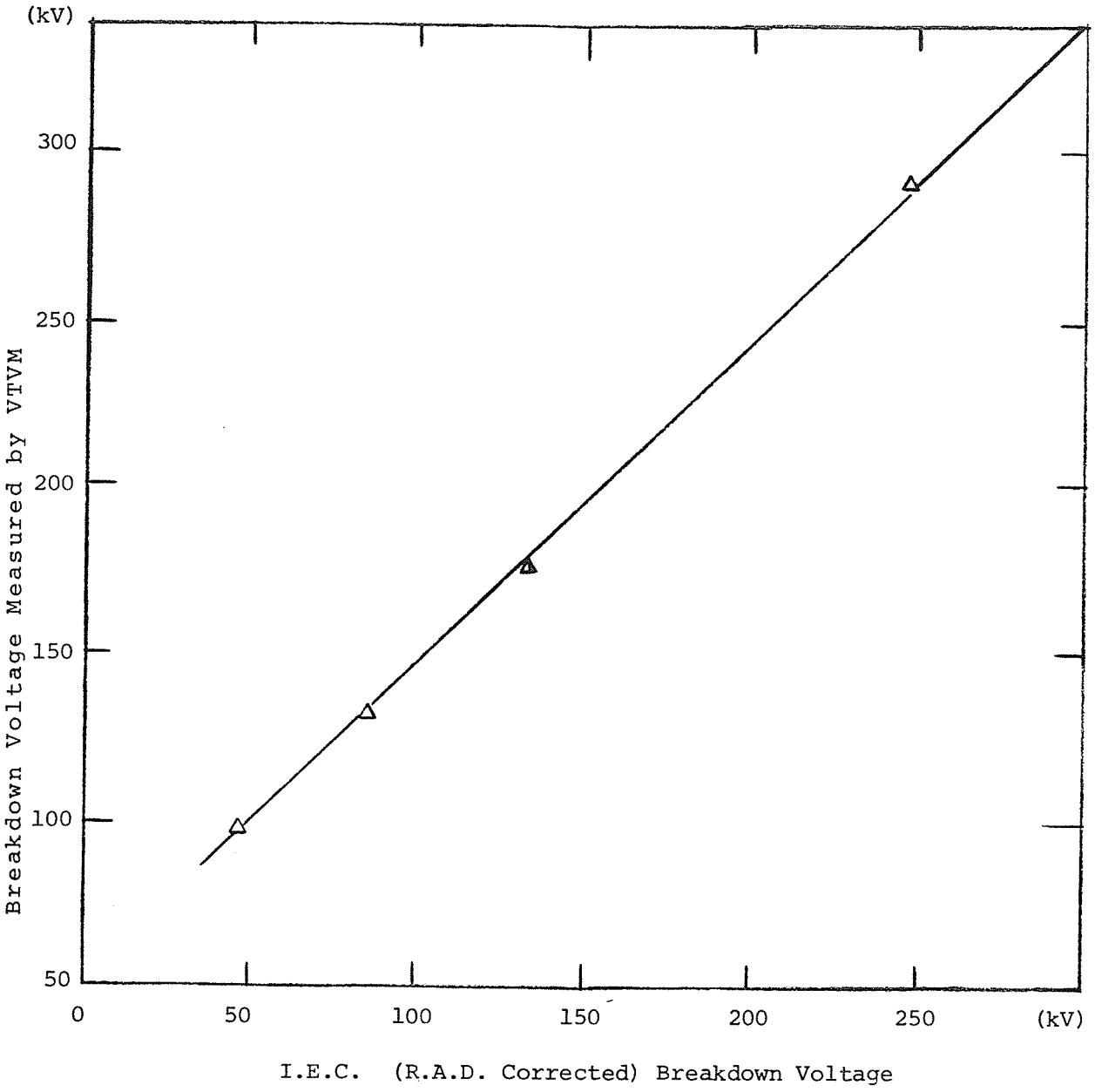

Fig. 6.7: VTVM Calibration Using Standard Gap Settings - 25 cm Spheres as Electrodes

the cell protection system resulted in a reduced amount of discharge by-product being formed.

After a series of tests, it was found necessary to re-finish the electrode surfaces. The following procedure was followed:

(1) Remove pitted surface on lathe, care being taken to maintain the original profile of the electrode.

(2) Polish with various sizes of abrasive (200, 400 then 600 grit or finer) until satisfactory finish is obtained.

(3) Mop with a cloth saturated with liquid abrasive (BRASSO).

(4) Apply clean mop to remove the liquid abrasive.

(5) Repeat (3) and (4) until satisfactory finish is obtained.

For a given gap setting (up to 7.5 mm due to high voltage supply limitation) the test procedure was as follows: A series of breakdown voltages were obtained for the liquid gap in absence of the spacer. The trigatron gap being set according to Fig. 5.5 for an estimated breakdown voltage. With the XLPE solid spacer in place, the procedure was repeated. The number of breakdowns for a given gap spacing depended on the establishment of the criterion for consistency - a low value of the coefficient of variation (ratio between standard deviation and the arithmetic mean). The rate of application of the high voltage did not appear to influence

the breakdown voltage level. An average value of about 3 kV/s was used.

6.1.4 Impulse Voltage Test Assembly and Procedure

A 24 stage, 100 kV per stage, impulse generator was available for this part of the tests. The schematic diagram of the testing circuit is shown in Fig. 5.8. The impulse generator was adjusted to supply a 1.2/50μs impulse voltage wave-form. The voltage divider was the R-C type manufactured by Heafley. A fast storage oscilloscope was available for recording both the amplitude and the wave-form of the voltage after a successful discharge of the generator.

It was found difficult to preset the trigatron gap so as not to fire on pre-breakdown corona currents. However, with proper setting of the trigatron main gap the protection system did operate extremely fast. In applying the impulses to the test sample, the 'normal technique' was used [99]; 10 - 20 successful breakdowns being obtained for each gap setting. For each liquid gap setting, breakdown tests were carried out with and without the XLPE solid spacer.

6.2 Experimental Results - Power Frequency

With a PDMS liquid gap setting of 5 mm, in the absence of the XLPE solid spacer, a series of breakdowns were obtained. The cup-plane electrode arrangement was used for this test series. Over 100 breakdowns were obtained on the same liquid

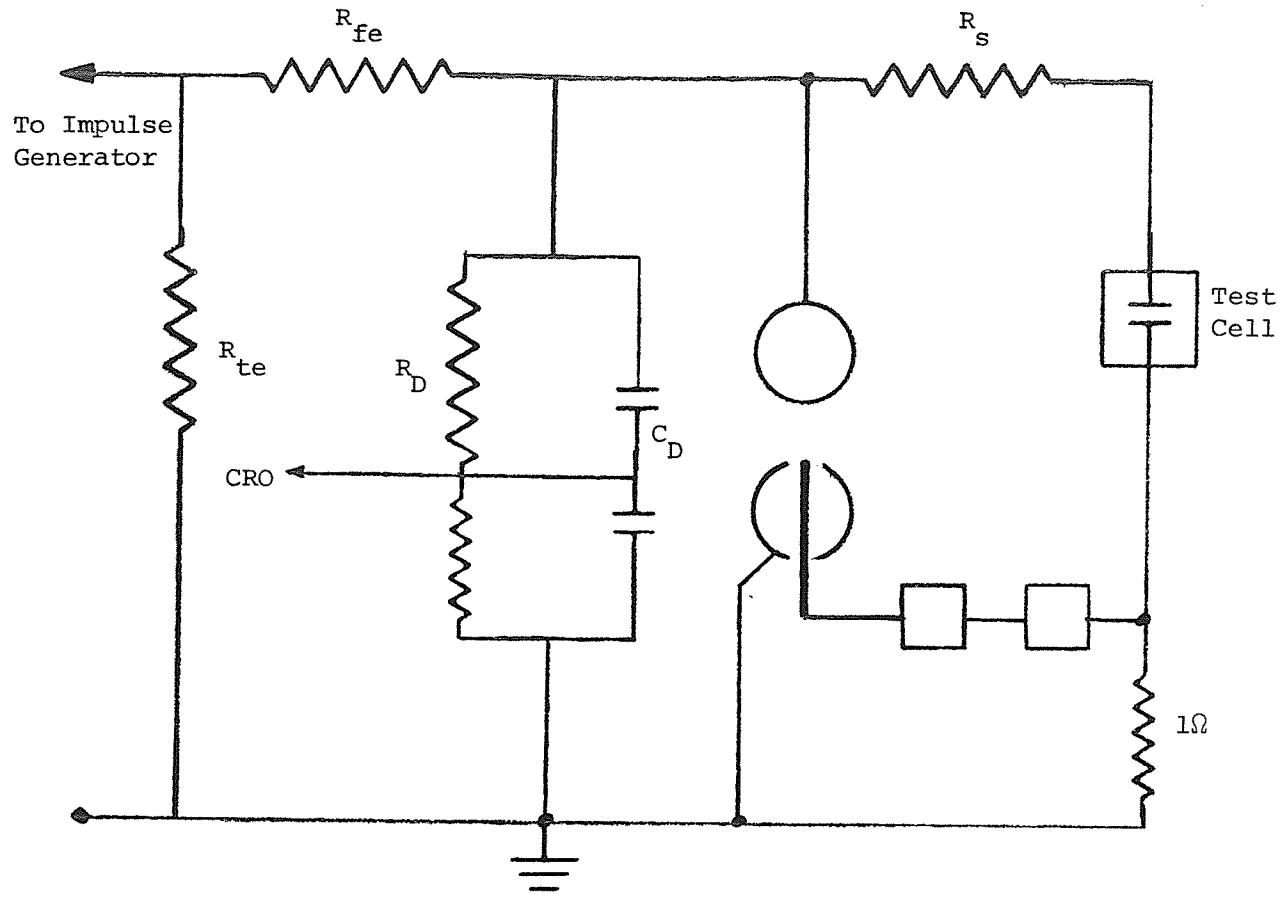

C_D = 800 pF

R_D = 38.7 KΩ

R_{fe} = 305Ω

R_{te} = 11960Ω

R_s = 523Ω

Fig. 6.8: Impulse Tests Circuit Diagram.

sample without detecting any deterioration in the breakdown strength. Following each breakdown, a gelatinous substance (polymerized PDMS) was left deposited on the plate electrode at the point of spark origin or contact. After disloging the gelatinous substance and visible bubbles from the electrodes, a subsequent breakdown usually occurred at a new site. As expected, all liquid breakdowns occurred in the area of shortest gap length; i.e., between the rim of the cup electrode and the plane electrode. Fig. 6.9 shows the results of this test series. It will be noticed that the scatter of the results is confined between 100 kV and 120 kV (peak). The average breakdown value for 40 breakdowns is 117 kV (peak) with a coefficient of variation of 5%.

Above 100 breakdowns in the PDMS liquid sample, on close examination, particles of the gelatinous substance could be seen suspended in the bulk of the liquid although there was no detectable change in the breakdown strength of the liquid. Next it was decided to investigate the effect of filtering the PDMS liquid. A slow ashless (99.98%) filter paper was used. Over twelve hours were necessary to filter about three litres of PDMS. Using the same electrode arrangement as before (cup-plane) a series of breakdowns were obtained using the filtered PDMS liquid for gap settings of 2.5 and 5 mm. Fig. 6.10 shows the results for a 2.5 mm gap setting. The breakdown voltage lies between 60 kV (peak) and 80 kV (peak).

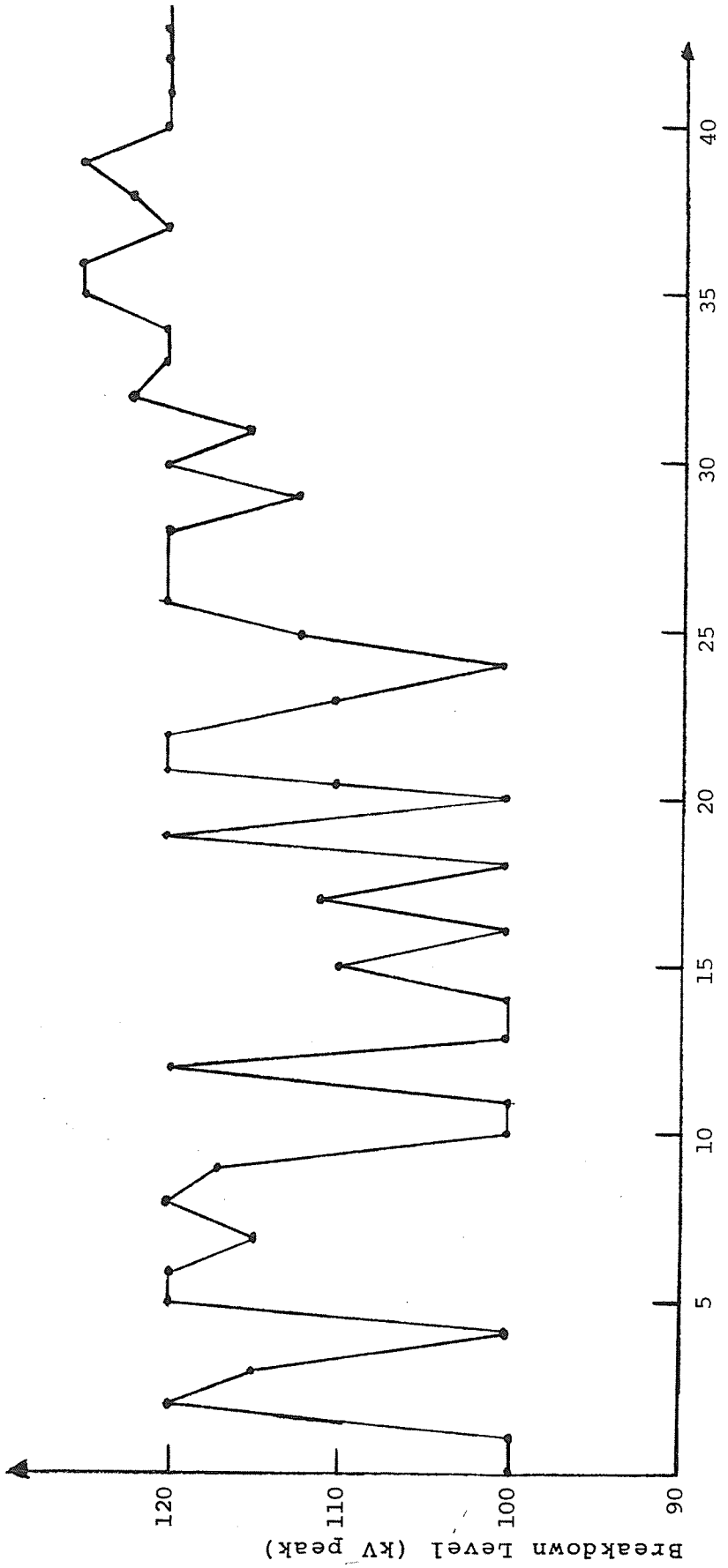

Fig. 6.9: PDMS Breakdown Level 5 mm Gap Cup-Plane Electrode System.

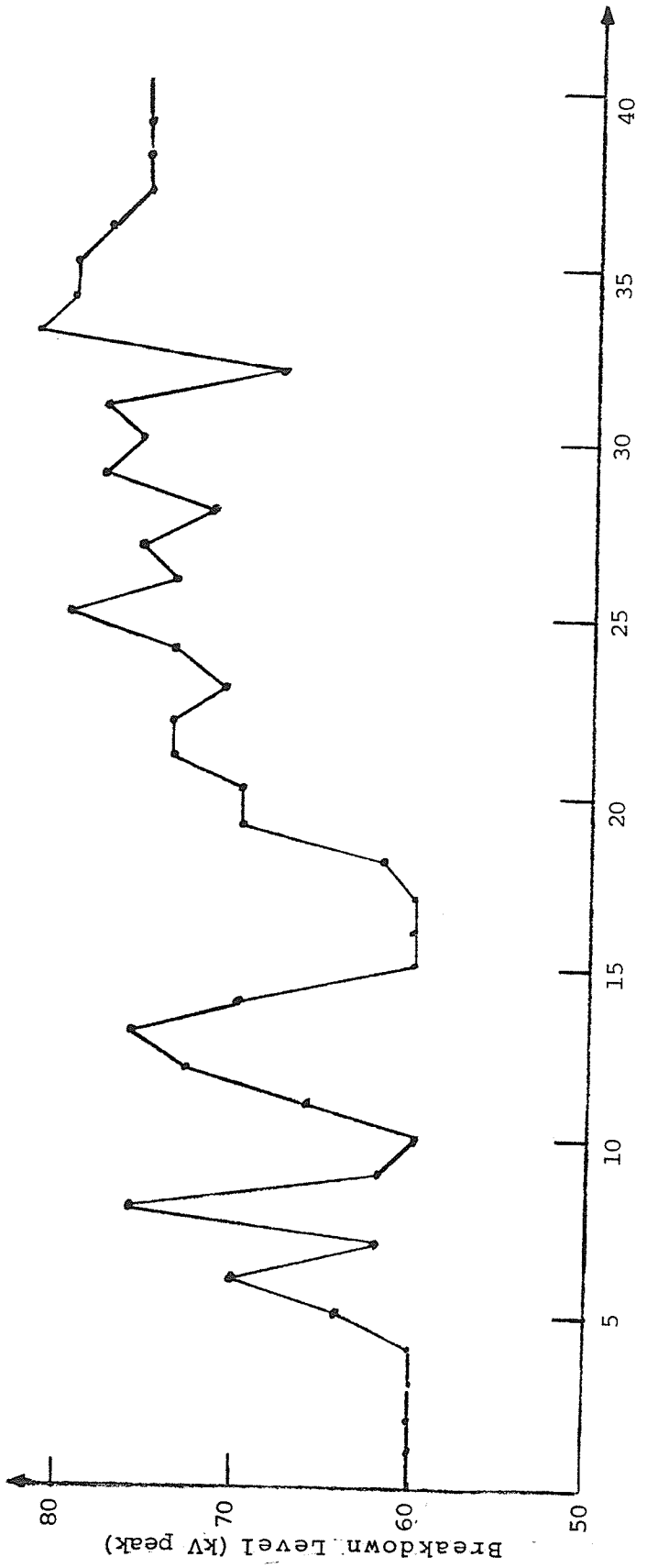

Fig. 6.10: Filtered PDMS Breakdown Level 2.5 mm Gap Cup-Plane Electrode System.

The average breakdown value is 75 kV with a coefficient of variation of 4%. The average breakdown voltage for a similar gap with unfiltered PDMS liquid was 74 kV with a coefficient of variation of 5.8%. Therefore for all practical purposes it can be concluded that filtering has a negligible effect on the breakdown strength of the PDMS liquid.

Having thus established the testing procedure, a series of breakdown tests were carried out on the PDMS liquid (in the absence of the XLPE solid spacer) for various gap settings 1.05 mm - 7.5 mm using the cup-plane electrode arrangement. In Table 6.1, the breakdown voltage levels and the stress are listed for the various gap settings. The coefficient of variation lies between 3% and 7%. This order of consistency is comparable to what other researchers have obtained with dehydrated, and pure liquid samples. Each entry of the breakdown voltage is an average of a series of such readings. Appendix D lists the breakdown voltage levels, for different gaps, from which the average breakdown voltage levels listed in Table 6.1 have been calculated.

Introduction of the XLPE spacer in the PDMS liquid gap (cup-plane electrode arrangement) resulted in lower breakdown voltage levels. All breakdowns took place in the area between the rim of the cup electrode and the plane electrode away from the PDMS/XLPE interface--just as was observed with breakdowns in the PDMS liquid without the solid XLPE spacer. No tracking

TABLE 6.1: PDMS breakdown results using cup-plane electrode system in the absence of the spacer

Gap (mm)	Breakdown Level kV peak	Breakdown Stress kV/mm (rms)	Coefficient of Var.(%)	Electrodes
		(rms)		
1.05	40	26.9	4.0	Brass/Brass
2.1	69	23.0	4.0	Brass/Brass
2.5	75	21.2	4.0	Chrome-plated plane/Brass
3.15	85	19.1	7.0	Brass/Brass
4.2	111	18.7	7.0	Brass/Brass
5.0	120	17.0	5.0	Chrome-plated plane/Brass
5.25	130	17.5	6.9	Brass/Brass
6.3	158	16.8	3.0	Brass/Brass
7.5	173	16.0	4.5	Brass/Brass

was observed on the XLPE surface. Breakdown voltage levels were recorded for various gap settings. Table 6.2 lists the breakdown voltage and stress for various gaps of PDMS liquid bridged by an XLPE solid spacer. The scatter of the PDMS/XLPE results was found to be less than that obtained with the PDMS liquid gap. Fig. 6.11 shows the variation of breakdown stress with gap length for the PDMS liquid in the absence of the spacer and for a parallel PDMS/XLPE interface. The breakdown stress of PDMS in the presence of an XLPE solid spacer is fairly independent of the gap length; whereas, that of the PDMS liquid gap (in the absence of solid spacer) decreases with the gap length as expected.

6.2.1 Effect of Electrode Geometry

In order to study the effect of shielding at the PDMS/XLPE interface due to the cup-plane electrode arrangement breakdown, tests were carried out with three other electrode geometries (Fig. 6.4). In each case the average breakdown voltage of the PDMS liquid for a given gap setting was determined with and without an XLPE solid spacer. When electrodes with sharp edged recesses were used, the discharge did not originate from these edges. Rather, the discharge took place anywhere in the region where the gap length was the shortest. Table 6.3 shows the breakdown stress of PDMS liquid for the three plane electrode geometries with and without an XLPE spacer. Also included in Table 6.3 are

TABLE 6.2: PDMS/XLPE parallel interface breakdown results using cup-plane electrode system

Gap (mm)	Breakdown Level kV (peak)	Breakdown Stress kV r.m.s./mm	Coefficient of Variation (%)
2.5	56	15.8	4.0
3.1	70	15.9	-
4.2	98	16.0	3.0
5.1	100	15.28	-
6.0	125	14.7	4.0
7.5	160	15.1	-

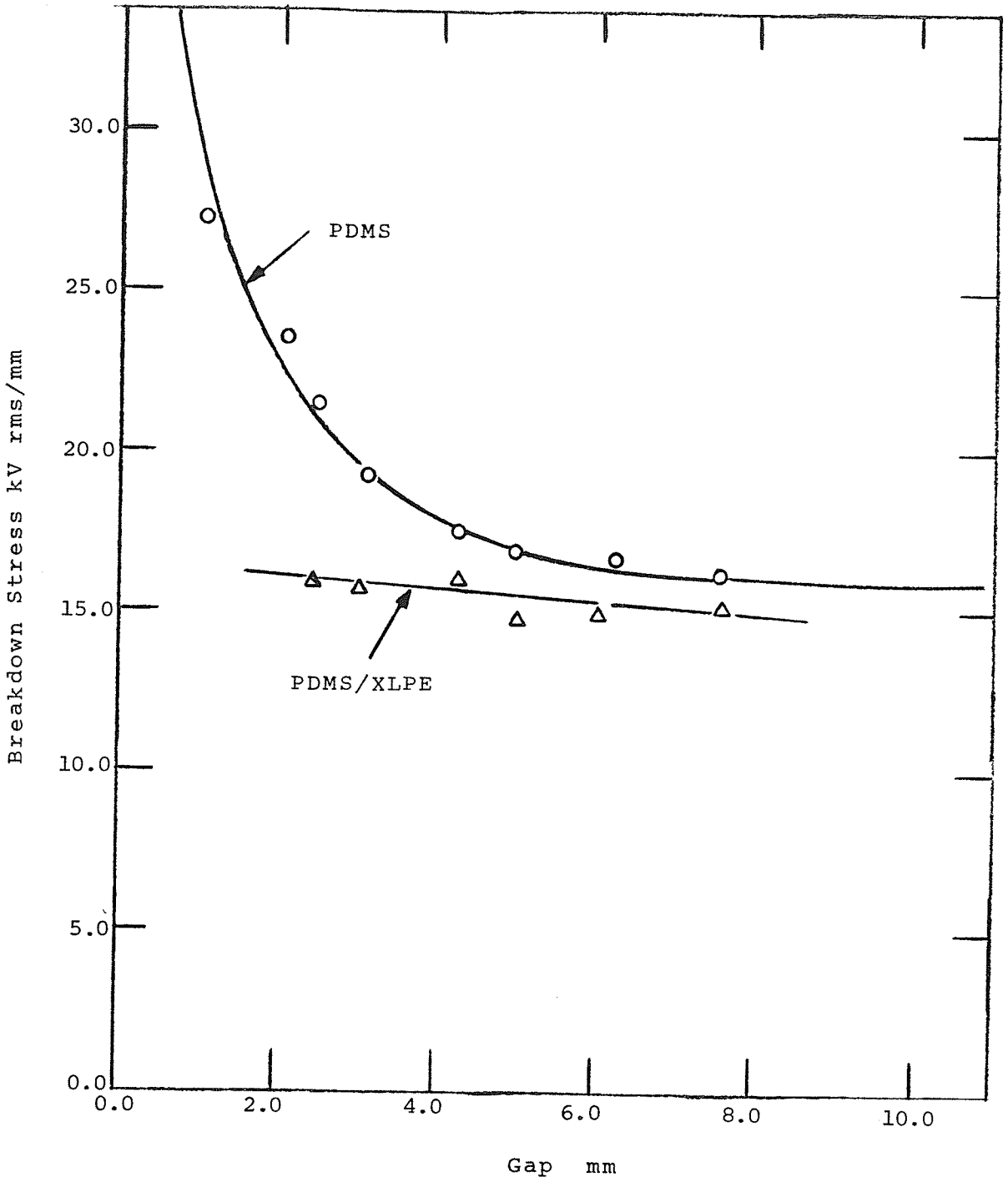

Fig. 6.11: Power Frequency Breakdown Stress of PDMS (Cup-Plane Electrodes).

TABLE 6.3: Breakdown stress of PDMS and PDMS/XLPE using different electrode geometries

Type of Geometry	Breakdown Stress kV r.m.s./mm		Reduction (%)
	PDMS	PDMS/XLPE	
Cup-plane 5 mm Gap			
Brass HV - Chrome LV	16.4	14.1	14.0
Brass HV - Brass LV	17.0	15.2	16.5
Plane-Plane Brass Electrodes: 5 mm Gap	13.1	11.3	13.7
Plane-Plane Brass Electrodes with 3 mm Sharp-edged recess : 5 mm Gap	13.1	11.3	13.7
Plane-Plane Brass Electrodes with 3 mm recess with edges rounded off: 5 mm Gap	13.4	11.4	14.9

the comparative results obtained by using a cup-plane electrode system with a Chrome-plated plane electrode. It is seen that the breakdown voltage levels are relatively higher when Brass electrodes were used for a given gap setting. The three electrode geometries, for a given gap, give lower breakdown levels than the cup-plane electrode system. This decrease in breakdown strength of the PDMS liquid can be attributed to the fact that more liquid is under maximum stress in the plane-plane electrode system than in the cup-plane system. A similar volume effect has been observed in transformer oil [100]. As expected, there is no field enhancement at the electrode-solid-liquid tri-interface.

6.2.2 Effect of Material of Solid Spacer

Using the cup-plane electrode system nylon (Polyamide) and plexiglass (Polymethyl Methacrylite) solid spacers were introduced into the PDMS liquid gap of 5 mm. The results show that both nylon and plexiglass when introduced in the PDMS liquid gap, distort the electric field, thus resulting in lower breakdown voltage levels of the interface. Due to their higher dielectric constants the field distortion is expected. Table 6.4 shows the results together with the dielectric properties.

To investigate the effect of surface roughness, a sample of XLPE was roughened and introduced into a 5 mm PDMS liquid gap. As expected, there was no difference in breakdown stress, since XLPE has a slightly lower dielectric constant than PDMS.

TABLE 6.4: Breakdown stress of liquid/solid interface for various solids - cup/plane electrode system used

	XLPE	Nylon	Plexiglass
ε_r	2.3	7.5	3.5
Surface resistivity	1.2×10^{15}	3.8×10^{9}	10^{16}
Breakdown stress of 5 mm interface gap length (kV/cm)	15.2	12.2	14.0
*Percent reduction	10.6	28.2	17.6

*Breakdown of PDMS liquid - 5 mm gap 17.0 kV/mm

6.2.3 Transformer Oil-XLPE Interface

For purposes of comparison, a series of breakdown tests were obtained using the cup-plane electrode system comprising of transformer oil (ε_r = 2.2, viscosity 15-20 cS) and XLPE as the spacer for a 2.5 mm gap setting. The transformer oil was of commercial grade VOLT ESSO 35. The test results are fairly consistent and Fig. 6.12 shows the scatter of results. To obtain 70 breakdowns, four samples of oil had to be used. The results are scattered between 70 kV and 105 kV (peak) giving an average breakdown stress of 21.5 kV r.m.s./mm, and a coefficient of variation of 7.0%.

Introducing an XLPE solid spacer in the transformer oil gap (2.5 mm) resulted in a decrease of the breakdown stress to 17 kV r.m.s./mm. This is a 21% reduction in breakdown stress due to the presence of an XLPE solid spacer in the transformer oil although the two materials (liquid and solid) have dielectric constants of practically equal magnitude.

6.3 Experimental Results: Impulse Tests

With the cup-plane electrode system (cup electrode grounded), results of the breakdown stress of the PDMS liquid gap and a PDMS/XLPE parallel interface of 2.5 mm, 5 mm, 7.5 mm gap lengths under positive standard impulse stress are tabulated in Table 6.5. Fig. 6.13 shows the breakdown stress variation with gap length. It can be seen that the breakdown

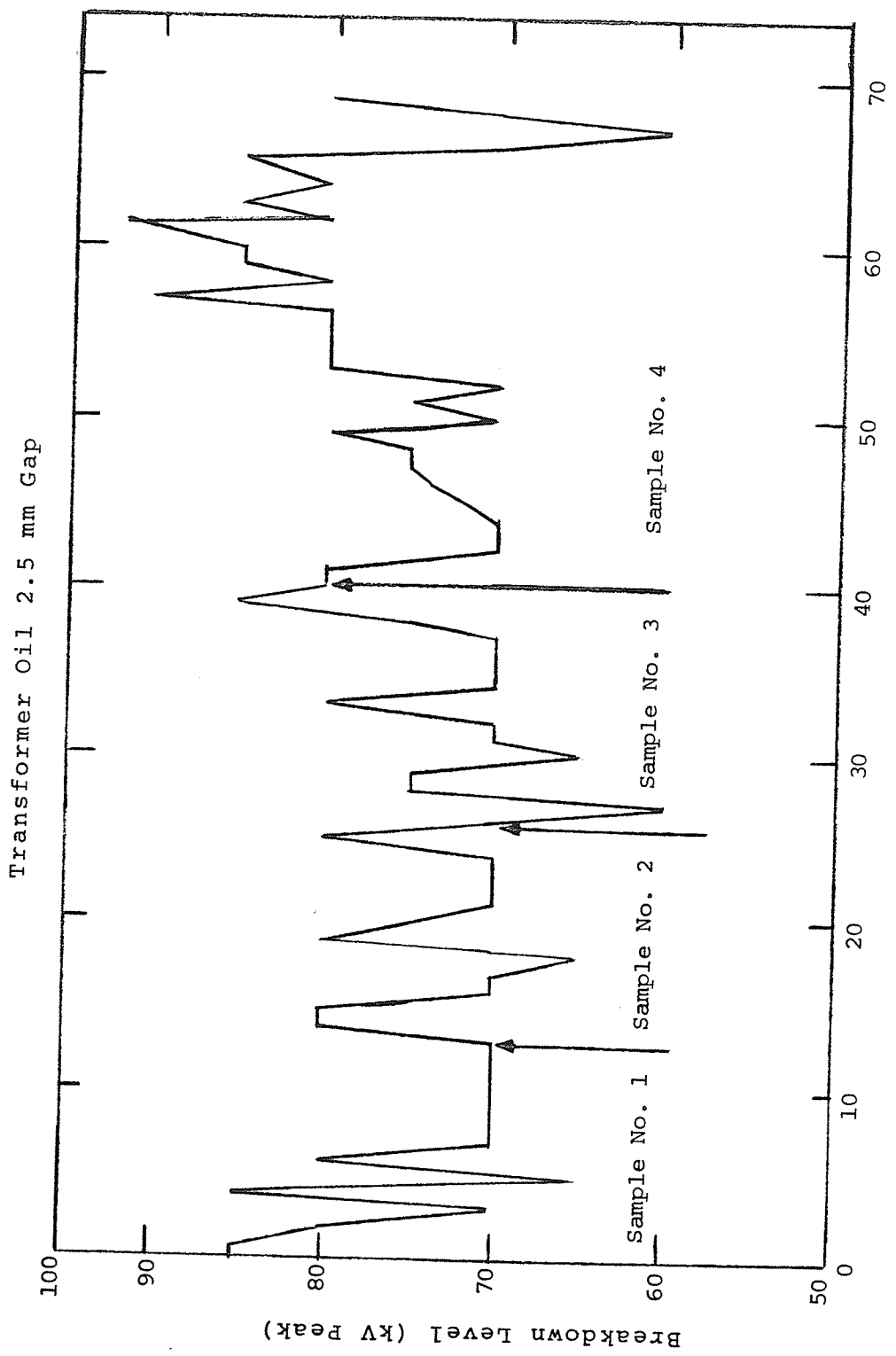

Fig. 6.12: Breakdown Level of Transformer Oil 2.5 mm Gap Cup-Plane Electrodes.

TABLE 6.5: (a) Standard impulse breakdown results for PDMS

Gap (mm)	Breakdown Level kV (Peak)	Breakdown Stress kV/mm	Coefficient of Variation
2.5	134	53	7.0
5.0	235	47	6.0
7.5	284	37.9	3.9

TABLE 6.5: (b) Standard impulse breakdown results for PDMS/XLPE

Gap (mm)	Breakdown Level kV (peak)	Breakdown Stress kV/mm	Coefficient of Variation
2.5	125	50	4.0
5.0	230	46	7.0
7.5	262	25.0	2.9

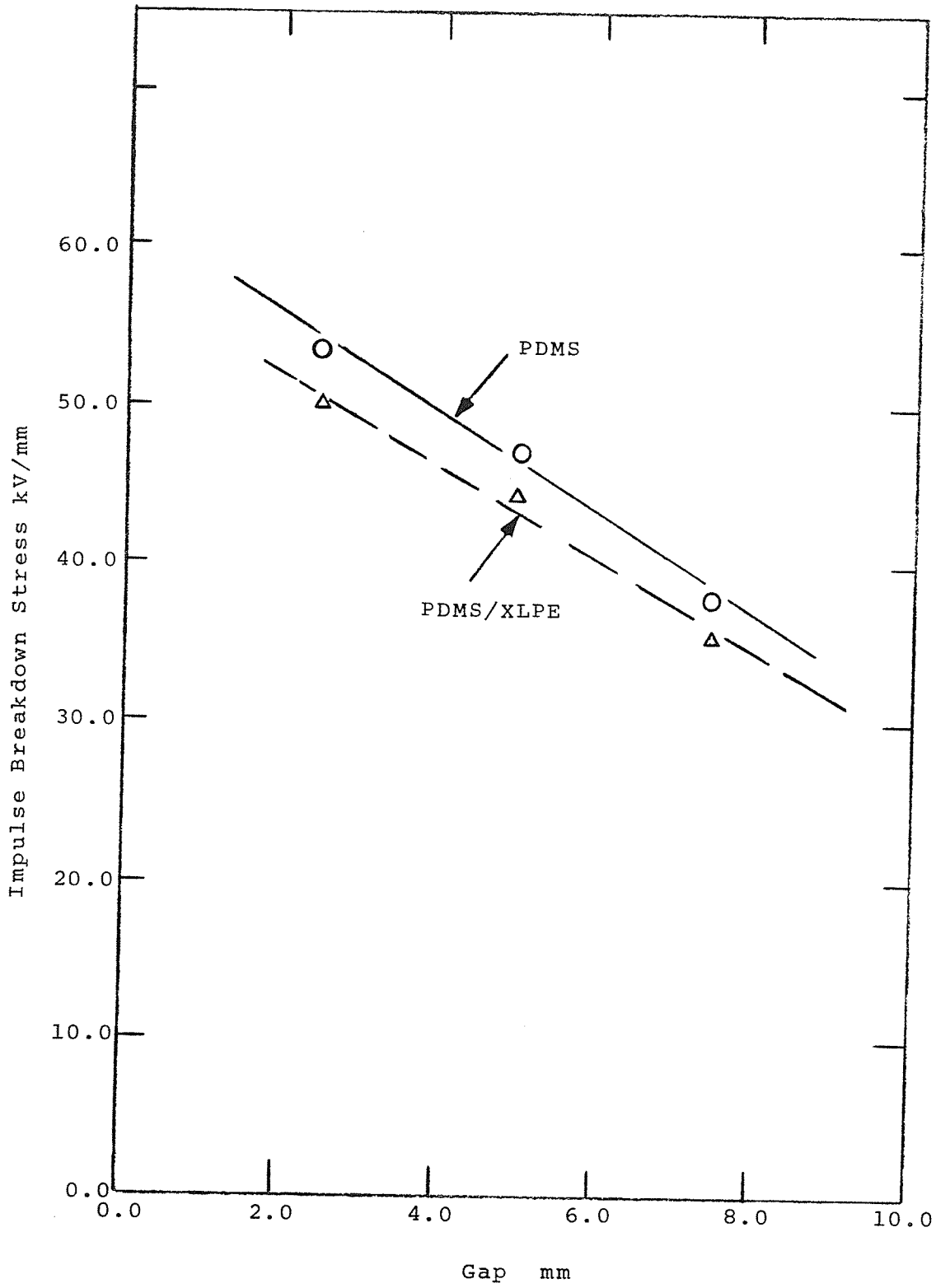

Fig. 6.13: PDMS Breakdown Stress with Standard Impulse.

stress of the PDMS/XLPE interface is lower than that of the PDMS liquid gap for all the three spacings. However, this difference is much less pronounced than the power frequency results. Again all breakdowns took place in the region of shortest gap distance away from the solid spacer. The scatter of the results is comparable to what was obtained for power frequency tests.

To investigate the effect of polarity, negative impulses were used (cup grounded) for a 5 mm PDMS liquid gap. There is a polarity dependency of the breakdown strength of the PDMS liquid used.

6.4 Conclusions

The results given in the preceding sections of this chapter indicate that using a given sample of PDMS liquid, a number of breakdowns can be studied without any detectable deterioration as measured by the scattering of the results. The value of the coefficient of variation obtained ($\simeq$ 5%) indicates that the experimental technique is good and the use of the protection system afforded high reproducibility. In comparison with transformer oil this marked degree of consistency for liquids of commercial purity may be due to the high viscosity and also due to the fact that silicone oil can contain far more water than Askarel or transformer oil without reducing its breakdown strength drastically [78].

Furthermore, water absorption by silicone oil exposed to the atmosphere is not rapid even at relative humidities as high as 54%.

Different electrode geometries show a volume dependence of the breakdown stress of PDMS liquid. The smaller the amount of liquid under maximum stress, the higher the breakdown stress. This has been described to be a statistical property for transformer oil [100]. Brass/Brass electrodes gave a slightly higher breakdown stress of PDMS than did Chrome-plated/Brass for the dome-cup electrode system with a Brass cup electrode in both cases. Similar results have been obtained for other liquids by other workers.

The reductions of the breakdown stress of the PDMS liquid in the presence of the XLPE solid spacer can only be attributed to the inhibition of the liquid motion due to EHD forces. This is because in the case of PDMS/XLPE interface there is no field enhancement of any sort since the dielectric constant of the XLPE solid is slightly lower than that of the PDMS liquid. Furthermore, for power frequency voltages and within the range of gaps investigated, the breakdown stress of the PDMS/XLPE parallel interface is fairly constant. The fact that all breakdowns took place in the PDMS liquid away from the interface further confirms the notion that the presence of the XLPE solid affects the field in the entire liquid as indicated in Chapter V.

With a nylon solid spacer the reduction in the breakdown

strength of PDMS is more than twice that obtained for an XLPE spacer. This is because of the much higher dielectric constant of nylon. However, all the breakdowns took place in the region of the shortest gap distance away from the interface. That the dielectric constant is not the predominant factor in reducing the breakdown stress of PDMS in the presence of the spacer is further confirmed by the fact that the reduction due to the presence of a plexiglass spacer is about two-thirds of that due to nylon, although their dielectric constants are 3.7 and 7.5 respectively.

The small influence on the breakdown stress of the PDMS liquid by the presence of a XLPE solid spacer with impulse voltages is not surprising given the findings of previous researchers - [92]. The authors found that the breakdown mechanism in a liquid in the presence of a solid spacer due to d.c. fields was too slow to respond to 1/50μs impulse. For parallel liquid/solid interfaces with a solid spacer of higher dielectric constant than the liquid, the consequent field distortion does result in fairly large reductions in the breakdown stress of the liquid with impulse voltages.

CHAPTER VII

SUMMARY

In studying the electric stress problem in underground EHV cable terminations the objectives were twofold:

(a) To find a mathematical equation describing the stress relief profile in terms of the specified maximum longitudinal stress.

(b) To evaluate the silicon oil (poly-dimethyl siloxane) and cross-linked polyethylene interface in an EHV cable termination experimentally and in particular the tangential stress at that interface.

A review of the literature concerning the terminal stress problem and cable termination procedures revealed that the complex nature of the electrostatic field in the cable termination does not lend itself to analytical field calculations. Thus, numerical methods had to be used. Further, the infinitely extending nature of the cable termination field requires special numerical methods that cater to the exterior problem in the unbounded region. Of the appropriate numerical methods for such a problem, the Finite Element Combined PDE (Partial Differential Equation) and IE (Integral Equation) formulation was studied. In order to evaluate the accuracy of this method numerical experiments were conducted and it was suggested that the normal derivative of the electrostatic potential function may not be adequately represented by that obtained by taking the normal

derivative of the finite element approximation of the potential function. Improvements that can be made in this method so as to attain better accuracy will be pointed out later.

It was realized that the geometry of the unbounded region of the cable termination is of such a nature that it can be bounded by a flux line drawn orthogonally from a point at the stress relief profile to a point on the corona shield. The flux line approximation was used to bound the infinitely extending region of the cable termination. The relative accuracy of the cable termination field solution using the flux line approximation was demonstrated by changing the position of the flux line and noting changes (if any) in the value of the electrostatic field in the region of interest; i.e., the longitudinal stress at points on the stress relief profile. For example the shifting of the corona shield (see Chapter III) five units axially in the positive z direction resulted in a change of less than three percent in the value of the maximum longitudinal stress at the stress cone profile.

Using the finite element numerical method and the flux line boundary in the unbounded region of the cable termination, a computer-aided design procedure was employed to obtain an equation of the stress relief profile for compact EHV cables in terms of a specified maximum longitudinal stress. This equation can be used to design stress relief profiles for other EHV cables as well. By changing the index n another relationship between A and the maximum stress g_m can be obtained by the computer program in

Appendix B. Therefore, this design procedure can be applied to any kind of cable geometries. Changes in the index n affect not only the volume of the termination but also the maximum stress g_m.

Although developed using dimensions of the 132 kV compact cable, the stress relief equation has been used to define the profile of a 345 kV compact XLPE-insulated cable (161.3 mm^2, 76 mm diameter - General Cable Corporation) termination. Table 7.1 gives the longitudinal stress distribution along the stress relief profile. The specified maximum longitudinal stress g_m was 5.5 kV/cm (giving a value of $A = f(g_m)$ of 125 using the linear relationship given in Chapter III). The obtained value of g_m was 6.5 kV/cm. This difference between the specified g_m and the obtained value can be attributed to the different discritization procedure. However, in actual practice the specified value of g_m would be much lower than the withstand value of the insulation. The point of occurrence of g_m from the point of termination of the insulation sheath was within the limits predicted.

Thus the stress relief profile equation can be used to determine profiles for terminations of a wide range of solid-type insulated EHV cables. The equation presented is particularly suited for molded XLPE termination profiles for XLPE - insulated EHV cables. Indeed, the equation may be used to determine stress relief profiles for other types of cable terminations in which the termination insulation is of higher dielectric constant than the cable insulation.

Prior to conducting experimental studies of the electrical

TABLE 7.1: Stress distribution at the stress relief profile of a 345 kV cable termination

Axial Distance (x 2.54 cm)	Radial Distance (x 2.54 cm)	Longitudinal Stress (kV/cm)
1.5	1.5	0.0
2.0	1.50101	0.52
3.0	1.51392	0.54
4.0	1.52683	1.22
5.0	1.55539	1.78
6.0	1.59756	2.43
8.0	1.73951	3.0
9.0	1.85261	4.0
10.5	2.16533	4.56
11.0	2.22372	4.94
11.5	2.36220	5.35
13.0	2.96399	6.5
13.5	3.43287	6.0
14	3.61121	5.8
14.5	4.05365	5.0
15.5	5.31670	4.9
16.0	6.23281	4.5

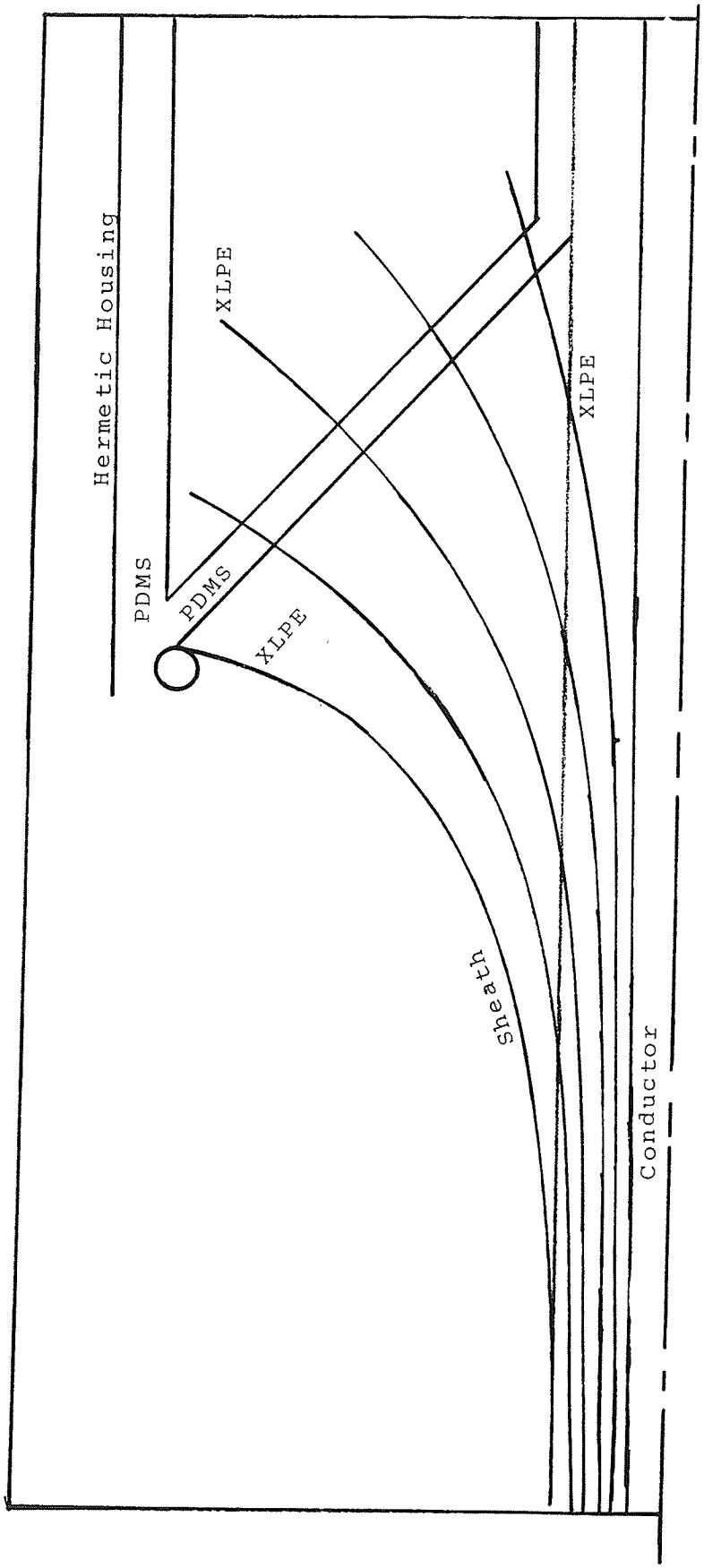

Fig. 7.1: 345 kV XLPE-Cable Termination Showing Equipotential Contours and the PDMS/XLPE Interface.

strength of the tangential interface between silicon oil and XLPE a review of their physical and dielectric properties was carried out. This review revealed that the potential development and use of these cable insulants will result in compact EHV and possibly UHV cables. Such a development is currently being conducted at the General Cable Company in New Jersey.

The experimental results indicate that the parallel PDMS/XLPE interface has a breakdown stress lower than that of the PDMS liquid obtained in the absence of the solid. The difference in breakdown stress is higher for smaller gap settings; ranging from 30% to less than 10% for corresponding gap lengths of 2 mm to 7.5 mm. The power frequency breakdown stress of a PDMS/XLPE parallel interface is independent of gap setting (for the gap length range covered).

Of the mechanisms that have been suggested for the decrease in breakdown strength of a liquid/solid parallel combination, the possible mechanism in the case of PDMS/XLPE parallel interface is that of field distortion at the interface due to obstruction by the XLPE spacer of the EHD motion of the PDMS liquid.

Experimental results indicate that the PDMS/XLPE interface of the cable termination can operate at tangential stresses as high as 10 kV/cm without any fear of discharge inception at the interface (using a factor of safety of 10). From a knowledge of the electrostatic potential distribution in the termination a contour of the PDMS/XLPE interface can be drawn ensuring that the

maximum electrostatic tangential stress of 10 kV/cm is not exceeded. Fig. 7.1 shows such a contour for 345 kV XLPE cable. The determination of the maximum termination diameter and therefore the dimensions of the hermatic housing is beyond the scope of this work.

Other electrical breakdown properties of PDMS include a significant dependency of the breakdown stress on the volume of the liquid under maximum stress, just as has been reported for transformer oil. Under impulse voltages a polarity dependency of the breakdown stress was also noticed.

Suggestions for Further Work

(i) The combined PDE IE-constrained formulation for unbounded field problems may be improved by a mixed formulation. In such a case both the field function and its normal derivatives are specified at node points. This will result in a more adequate approximation of the normal derivative rather than the normal derivative of the approximation to the field function.

(ii) Using the proposed stress profile equation for cable terminations, a molded stress cone should be constructed and tested using the usual test procedure for cable terminations. This of course requires liaison between the researchers and industry.

(iii) In addition, long-term compatibility tests should be carried out on the PDMS/XLPE tangential interface.

(iv) The behaviour of the PDMS/XLPE interface under switching surges and at cable operating temperatures should also be investigated.

(v) Although not directly related to the work presented here, the possibility of XLPE impregnated tapes should be investigated - with PDMS as the impregnant.

BIBLIOGRAPHY

[1] P.V. Hunter and J.T. Hazell, "Development of Power Cables", Gorge Newness Ltd., (London), 1956.

[2] C.C. Barnes, "Power Cables - Their Design and Installation", Chapman and Hall Ltd. (London), 1966.

[3] A. Schwaiger and R.W. Sorensen, "Theory of Dielectrics", John Wiley and Sons (New York), 1932.

[4] British Patent Specification No. 181796.

[5] R.W. Atkinson and D.M. Simmons, "Oil-Filled Cable and Accessories", Trans. A.I.E.E., Vol. 50, (1931).

[6] J.K. Webb, "The Condenser Cone - A New Device for Use in Connection with High Tension Cable Terminations and Joints", Electrical Comm., Vol. 12, (Oct. 1933), p. 92-103.

[7] J.K. Webb, "Condenser Cones for Cable Testing", Electrical Comm., Vol. 15, (April 1937), p. 354-361.

[8] Ch. A. Flamand, "The Use of Capacitor Plates for Extra-High-Tension Cable Ends", The International Conference on Large Electric Systems (C.I.G.R.E.), 1950, Paper 209.

[9] L.I. Komives, "Joints and Terminals for High Tension Cables", ibid., 1952, Paper 226.

[10] L. Domenach, "Evolution in the Technique of Very High Voltage Cable Terminals", ibid., Paper 211.

[11] P.G. Priaroggia, "The Use of 'Field Shields' in Extra High Voltage Cable Sealing Ends", ibid., Paper 212.

[12] A. Giaro "A Study of the Capacitive Network and a Generalized Method of Calculation of Capacitor Bushings for High Voltage Cables", ibid., Paper 209.

[13] E.M. Allan and A.L. McKean, "138 KV Prefab Capacitive-Graded Joint for Oil-Filled Cable Systems", IEEE Trans., Vol. PAS-96, No. 1, p. 20-26, 1977.

[14] L-G. Virsberg and P.H. Ware, "A New Termination for Underground Distribution", IEEE Trans., Vol. PAS-86, No. 9, p. 1129-1135, 1967.

[15] E.J. Merrell, "Semiconducting Shielding for A-C Power Cable", Trans. A.I.E.E., Vol. 65, p. 605-608, 1946.

[16] R.D. Fulcomer and G.A. Foote, "A Simple Non-Stress Cone Stress-Relieving Wrap for Terminating Extruded Dielectric Shielded Power Cable", Underground Transmission Conference, Atlantic City, New Jersey, Oct. 1976, p. 367-372.

[17] H.D. Short, "A Theoretical and Practical Approach to the Design of High Voltage Cable Joints", Trans. A.I.E.E., Vol. 68, 1949, p. 1275-1283.

[18] H.D. Short, "The HST Termination for UD Cables in Theory and Practice", IEEE Special Technical Conf. on Underground Distribution, Anaheim, California, May 1969, Paper 69 C1-PWR, p. 298-352.

[19] Rome PSR-1 Pennant, "15 KV URD Terminating Kits", Rome Cable Division Product Engineering Bulletin No. PSR-1, March 1963.

[20] J.H. Nicholas, Discussion on Reference [18], p. 348-349.

[21] D. McDonald, "The Electrolytic Analogue in the Design of High Voltage Power Transformers", Proc. I.E.E., Vol. 100, Part II, 1953.

[22] K.J. Binns and P.J. Lawrenson, "Analysis and Computation of Electric and Magnetic Field Problems", MacMillan, New York, 1963.

[23] B.A. Wensley and F.W. Parker, "The Solution of Electric Field Problems Using a Digital Computer", Electrical Energy, 1960, pp. 12-16.

[24] S.P. Frankel, "Convergence Rates of Iterative Treatments of Partial Differential Equations", Math. Tab., Washington, Vol. IV, No. 30, 1950, pp. 65-75.

[25] J.T. Storey and M.J. Billings, "General Digital-Computer Program for the Determination of Three-Dimensional Electrostatic Axially Symmetric Fields", Proc. I.E.E., Vol. 114, No. 10, 1967, pp. 1551-1555.

[26] R.H. Galloway, H. McL. Ryan and M.F. Scott, "Calculation of Electric Fields by Digital Computer", Proc. I.E.E., Vol. 114, No. 6, 1967, p. 824.

[27] I.A. Cermak and P. Silvester, "Boundary-Relaxation Analysis of Rotationally Symmetric Electric Field Problems", Trans. I.E.E.E., Vol. PAS-89, 1970, p. 925.

[28] E. Weber, "Electromagnetic Fields - Theory and Applications: Vol. I", John Wiley, 1950.

[29] A.M-S Katahoire, "Boundary Relaxation for Infinitely Extending Symmetric Fields", Univ. of Windsor, E.E. Dept., Internal Report, May 1977.

[30] F. Sandy and J. Sage, "Use of Finite Difference Approximations for Problems Having Boundaries at Infinity", Trans. I.E.E.E., Vol. MTT-19, 1971, pp. 484-486.

[31] H. Singer, H. Steinbigler and P. Weiss, "A Charge Simulation Method for Calculation of High Voltage Fields", Trans. I.E.E.E., Vol. PAS-

[32] M.S. Abou-Seada, and E. Nasser, "Digital Computer Calculation of the Electric Potential and Field of a Rod Gap", Proc. I.E.E.E., Vol. 56, 1968, pp. 813-820.

[33] A. Yializis, E. Kuffel and P.H. Alexander, "An Optimized Charge Simulation Method for the Calculation of High Voltage Fields", Trans. I.E.E.E., Vol. PAS-97, 1978, p. 2434.

[34] G.W. Carter and S.C. Loh, "The Approximate Calculation of the Electric Field Between a Rod and a Concentric Ring by Means of Toroidal Functions", Proc. I.E.E., Vol. 104, Part II, 1957, pp. 13-17.

[35] D.H. Norrie and G. de Vries, "The Finite Element Method in Engineering Science", Academic Press, 1973.

[36] O.C. Zienkiewicz, A.K. Bahrani and P.L. Arlett, "Solution of Three-Dimensional Field Problems by the Finite Element Method", The Engineer, Oct. 27, 1967, p. 547.

[37] O.C. Zienkiewicz, "The Finite Element Method in Engineering Science", McGraw-Hill, 1971.

[38] K.H. Huebner, "The Finite Element Method for Engineers, John Wiley, New York, 1975.

[39] C.S. Desai and J.F. Abel, "Introduction to the Finite Element Method", V. Nostrand Reinhold, 1972.

[40] P.L. Arlett, A.K. Bahrani, O.C. Zienkiewicz, "Application of Finite Elements to the Solution of Helmoltz's Equation", Proc. I.E.E., Vol. 115, No. 12, 1968, p. 1762.

[41] P. Silvester and A. Konrad, "Axisymmetric Triangular Finite Elements for the Scalar Helmholtz Equation", Int. Journ. Num. Methods in Engg. Vol. V, 1973, p. 481.

[42] P. Silvester, "Higher-Order Polynomial Triangular Finite Elements for Potential Problems", Int. J. Engg Sci., Vol. 7, pp. 849-861.

[43] B. Carnahan, H.A. Luther and J.O. Wilkes", Applied Numerical Methods", John Wiley, 1969.

[44] J.K. Reid, "Large Sparse Sets of Linear Equations", Academic Press, 1971.

[45] T.A. Cruse, "Application of the Boundary-Integral Equation Solution in Solid Mechanics", Published in "Variational Methods in Engineering, Vol. II", C.A. Brebbid, H. Tottenham, Eds.

[46] O.D. Kellog, "Foundations of Potential Theory", Dover, 1954.

[47] A.J. Burton and G.F. Miller, "The Application of Integral Equation Methods to the Numerical Solution of Some Exterior Boundary-Value Problems", Proc. Roy. Soc. Lond. Vol. 323A, 1971, pp. 201-210.

[48] J.A. Stratton, "Electromagnetic Theory", McGraw-Hill, 1941.

[49] C.G. Williams and G.K. Cambrell, "Efficient Numerical Solution of Unbounded Field Problems", Electronics Letters, Vol. 8, No. 9, 1972, p. 247.

[50] B.H. Mcdonald and A. Wexler, "Finite Element Solution of Unbounded Field Problems", Trans. I.E.E.E., Vol. MTT-20, No. 12, 1972, p. 841.

[51] O.C. Zienkiewicz, D.W. Kelly and P. Bettess, "The Coupling of the Finite Element Method and Boundary Solution Procedures", Int. J. Num. Meth. Engg., Vol. 11, 1977, p. 355.

[52] P. Silvester, et al, "Exterior Finite Elements for 2-Dimensional Field Problems with Open Boundaries", Proc. I.E.E., Vol. 124, No. 12, 1977, p. 1267.

[53] R.H. Gallagher, "Finite Element Analysis-Fundamentals", Prentice Hall, 1975, p. 196.

[54] B.H. Mcdonald, "Constrained Variational Solution of Field Problems", Ph.D. Thesis, Univ. of Manitoba, 1975, p. 58.

[55] S. Washisu, I. Fukai and M. Suzuki, "Extension of Finite-Element Method to Unbounded Field Problems", Elect. Lett. Vol. 15, No. 24, November 1979, pp. 772-774.

[56] O.W. Andersen, "Laplacian Electrostatic Field Calculations by Finite Elements with Automatic Grid Generation", Trans. IEEE, Vol. PAS-92, No. 5, 1973, pp. 1485-1491.

[57] R.C. Weast and S.M. Selby (Ed.) "Handbook of Tables for Mathematics", The Chemical Rubber Co., 1970, Cleveland.

[58] J.C. de Vos and J. Vermeer, "Contribution to The Development of Power Cables for High and Extra-High Voltage with a Composite Insulation of Synthetic High Polymer Materials and Oil", The Int. Conf. on Large Electric Systems (C.I.G.R.E.), 17th Convention 1958, Vol. II, Paper No. 207.

[59] E.R.A. Annual Report 1956/57, Electrical Review, July 1957.

[60] C.A. Harper, Ed-in-Chief, "Handbook of Plastics and Elastomers", McGraw-Hill.

[61] R. Jocteur, M. Osty, H. Lemainque and G. Terramorsi, "Research and Development in France in the Field of Extruded Polyethylene Insulated High Voltage Cables", C.I.G.R.E., 24th Session 1972, Vol. I, Paper No. 21-06.

[62] J.W. Shackleton, "General Characteristics of Polyethylene", Trans. A.I.E.E., Vol. 64, 1945, p. 912-916.

[63] W. Jackson and J.S.A. Forsyth, "The Development of Polyethylene as a High Frequency Dielectric", Proc. IEE, Vol. 92, Part III, 1945, pp. 23-37.

[64] Wm. A. Del Mar, "Dielectric Strength of Polyethylene", Trans. A.I.E.E., Vol. 64, 1945, pp. 918-921.

[65] J.C. de Vos and J. Vermeer, "On the Impulse Strength of a Composite Insulation of Synthetic High Polymer Materials and Oil as a Dielectric for High and Extra-High Voltage Cables", C.I.G.R.E., 18th Convention 1960, Vol. II, Paper No. 226.

[66] J.A.M. Gibbons, P.R. Howard, D.J. Skipper, R.S. Body and W.G. Hawley, "Gas-Pressurised Polyethylene Tape Dielectric for Extra-High-Voltage Cables", C.I.G.R.E., 20th Mtg, 1964, Vol. II, Paper No. 20).

[67] H. Birnbreier, et al, "High-Power Cables with Internal or External Water Cooling", C.I.G.R.E., 1974, Vol. I, Paper No. 21-09, Also the Group 21 discussion.

[68] G.J. Crowdes, G.H. Hunt, P.H. Ware, "Research Work and Progress in the Application of Solid Dielectrics to High-Voltage Cable", C.I.G.R.E., 20th Mtg, 1964, Vol. II, Paper No. 220.

[69] S. Fujiki, H. Furusawa, T. Kuhara, and H. Matsuba, "The Research in Discharge Suppression of High Voltage Cross-linked Insulated Power Cable", Trans. I.E.E.E., Vol. PAS 90, 1971, p. 2703.

[70] R. Bernard, G. Martin, and G. Weissenberger, "Laying of Paper Insulated Lead Covered Cables at Low Temperatures", C.I.G.R.E., 1964, Paper 206, 1964.

[71] W.J. Plate, T.H. Ling, J.F. Nuccio, "Reassessment of Polyethylene Power Cable", Trans. I.E.E.E., Vol. PAS-82, 1963, pp. 990-1002.

[72] F.H. Kreuger, "Endurance Tests with Polyethylene Insulated Cables - Methods and Criteria", C.I.G.R.E., 1968, Vol. I, Paper No. 21-02.

[73] A.L. McKean, F.S. Oliver, and S.W. Trill, "Cross-Linked Polyethylene for Higher Voltages", Trans., I.E.E.E., Vol. PAS-86, No. 1, 1967, pp.1-10.

[74] G.A. Vincent, F.W.G. Fearon, and T. Orbeck,"Structure Property Relationships in Silicone Fluid Dielectrics", Conf. on Elect. Insul. and Diel. Phenomena, Montreal, Oct. 1973, pp. 17-23.

[75] S.L. Bass, M.J. Hunter, and T.A. Kauppi, "Silicones as Electrical Insulating Materials", Trans. Electro-Chemical Soc., Vol. 90, 1947, pp. 311-330.

[76] M. Ueda and M. Ito, "Electric Breakdown of Liquid Silicones in High Frequency Field", Electrotechnical Journ. of Japan, Vol. 5, No. 2, 1959, pp. 56-60.

[77] M. Hakim, R.G. Olivier and H. St-Onge, "The Dielectric Properties of Silicone Fluids", Trans. I.E.E.E., Vol. EI-12, No. 5, 1977, pp. 360-370.

[78] W.C. Page, T. Michaud, "Development of Methods to Retro-fill Transformers with Silicone Transformer Liquid", Dow Corning Corporation, Midland, Michigan.

[79] H. Shimokawa, A. Ohashi and M. Ueda, "The Electrical Conduction in Silicone Liquid Films", 6th Int. Conf. on Conduction and Breakdown in Dielectric Liquids", pp. 169-174.

[80] A. Ohashi, H. Shimokawa, and M. Ueda, "Dielectric Properties of Silicone Liquid Films", I.E.E.E., Int. Symposium on Electrical Insulation, Philadephia, 1978, pp. 245-248.

[81] C. Hosticka, "Insulating Characteristics of Dimethyl Silicone in Bare and Insulated Uniform Field Gaps", Trans. I.E.E.E., Vol. EI-12, No. 6, 1977, pp. 389-394.

[82] T.J. Lewis, "The Electric Strength of Silicone Liquids", Proc. I.E.E., Vol. 104-pt. B, 1957, p. 493.

[83] K. Wechsler and M. Riccitiello, "Electric Breakdown of a Parallel Solid and Liquid Dielectric System", Tran. A.I.E.E., Vol. 80 Pt. III, 1961, pp. 365-369.

[84] E.A. Cherney, "High Voltage Flashover Along a Solid-Liquid Interface", Conf. on Electric Insulation and Dielectric Phenomena, 1970 Annual Report. pp. 187-190.

[85] J. Kerr, "A New Relation Between Electricity and Light: Dielectric Media Birefringent", Phil. Mag., Vol. 50, 1875, pp. 337-348.

[86] J.D. Cross and R. Tobazeon, "Electric Field Distortions Produced by Solid Dielectric Spacers Separating Uniform Field Electrodes in Nitrobenzene", Trans. I.E.E.E., Vol. E I-8, No. 1, 1973, pp. 25-29.

[87] E.A. Cherney and J.D. Cross, "Space Charge Effects in Chlorobiphenyls and at Solid/Liquid Interfaces", Conf. Elec. Insul. Dielectr. Phenom., 1972, Annual Report, pp. 84-90.

[88] N.J. Felici, "D.C. Conduction in Liquid Dielectrics - (Part II) Electrohydrodynamic Phenomena", Direct Current, Vol. 2, No. 4, 1974, pp. 147-165.

[89] N.J. Felici, "Phénomènes Hydro et Aérodynamiques dan la Conduction des Diélectriques Fluides", Rev. Gén´de l'Elect. (French), Vol. 78, 1969, pp. 717-734.

[90] P. Atten, "EHD Instabilities Induced by Space Charge in Dielectric Liquids of Very Low Conductivity", 4th Int. Conf. on Conduction and Breakdown Dielectric Liquids, Dublin, July 25-27, 1972, pp. 85-96.

[91] E.A. Cherney and J.D. Cross, "Electric Field Distortions at Solid-Liquid Dielectric Interfaces", Trans. I.E.E.E., Vol. EI-9, No. 2, 1974, pp. 37-42.

[92] E.A. Cherney and J.D. Cross, "Electrical Breakdown at Solid-Liquid Interface", Trans. I.E.E.E., Vol. EL-12, No. 3, 1977, pp. 214-218.

[93] T.S. Sudarshan and J.D. Cross, "D.C. Electric-Field Modifications Produced by Solid Insulators Bridging a Uniform-Field Vacuum Gap", Trans. I.E.E.E., Vol. EI-8, No. 4, 1973, pp. 122-128.

[94] H. Kuwahara, et al, "Partial Discharge Characteristics of Silicone Liquids", I.E.E.E., Trans. Vol. EI-11, No. 3, 1976, p. 86.

[95] T.J. Lewis, "Electrical Breakdown in Organic Liquids", Proc. I.E.E., Vol. 100, Pt. IIA, 1953, p. 141.

[96] R.Hancox and H.Tropper, "The Breakdown of Transformer Oil Under Impulse Voltages", Proc. I.E.E., Vol. 105A, 1958, p. 250.

[97] A.M. Sletten and J.J. Lewis, "Characteristics of the Trigatron Spark-Gap", Proc. I.E.E., Vol. 104C, 1957, p. 54.

[98] E. Kuffel and M.M. Bera, "Breakdown in Triggered Spark Gaps in Air", I.E.E.E., Trans. Vol. PAS-87, No. 7, 1968, p. 1628.

[99] J.A. Bakken, "Determination of Characteristic Voltages in Impulse and Switching Surge Testing", Trans. I.E.E.E., Vol. PAS-86, No. 8, 1967, p. 962.

[100] W.R. Wilson, "A Fundamental Factor Controlling the Unit Dielectric Strength of Oil", Trans. A.I.E.E., Vol. 72, Part III, 1953, p. 68-74.

APPENDIX A

PDE IE-CONSTRAINED COMPUTER PROGRAM

This is a Fortran Computer program used to implement the PDE IE-constrained finite element formulation.

OUTPUT: Nodal potential and all input data

MAIN: Calculates the finite element system matrix [S]

DATA: Elemental assembly

→ COORDS: Global coordinates of the nodes in the continuum

→ SOLN: Solves the augmented matrix

→ STRAIN: Calculates the integral equation constraints - matrix [C]

→ RING: Coordinates of the integration Contour I_C

→ LINU3F: Matrix inversion IMSL Library

```
C**                                                    USUB,NUMAR,ING
C**
C**THE FINITE ELEMENT METHOD
C**
      COMMON X(76),Y(76),NODE(28,6),C(28,76)
      COMMONRC1(28),RC2(28),ZC1(28),ZC2(28)
      COMMON S(76,76),V(76)
      COMMON G(28)
      COMMON ENM(28)
      REAL*8 EP(28)
      REAL*8 EXACTV(76)
      REAL*8 G
      REAL*8 ENM
      REAL*8 XE(3),YE(3)
      REAL*8 SE(6,6)
      INTEGER NO(6)
      DOUBLE PRECISION X,Y,C,RC1,RC2,ZC1,ZC2,S,V
      DOUBLE PRECISION DABS,RBAR,AA,CONST,PI,DEL
      DOUBLE PRECISION B1,B2,B3,C1,C2,C3
      DOUBLE PRECISION X1,X2,X3,Y1,Y2,Y3,V1,V2,V3
C**
C**SPECIFY TYPE OF PROBLEM  : 2-DIMENSION (NCASE=1)
C**OR 3-DIMENSION AXI-SYMMETRIC (NCASE=2)
C**
      READ(5,105) NCASE
      IF(NCASE.EQ.2) GO TO 33
      WRITE(6,202)
      GO TO 60
   33 WRITE(6,303)
   60 CONTINUE
C**
C**INITIALIZE TO ZERO S(I,J) ,SE(I,J),V(I),X Y(I) ,XE,YE
C**
      READ(5,100) NE,NN
      DO 1 I=1,NN
      DO 1 J=1,NN
    1 S(I,J)=0.D0
      DO 2 I=1,NN
      X(I)=0.D0
      Y(I)=0.D0
    2 V(I)=0.D0
      DO 3 I=1,3
      DO 3 J=1,3
      XE(I)=0.DC
      YE(I)=0.D0
    3 CONTINUE
      DO 4 I=1,6
      DO 4 J=1,6
    4 SE(I,J)=0.D0
      PI=3.14159265
C**
C**READ IN NODE NUMBERS &NODAL COORDINATES
C**
      DO 5 K=1,NE
      READ(5,110) NODE(K,1),NODE(K,2),NODE(K,3),
     1NODE(K,4),NODE(K,5),NODE(K,6)
      PRINT,NODE(K,1),NODE(K,2),NODE(K,3),NODE(K,4)
     1,NODE(K,5),NODE(K,6),K
    5 CONTINUE
      CALL COORDS
      WRITE(6,999) (I,X(I),Y(I),I=1,NN)
  999 FORMAT('0',I16,2F16.5)
      DO 11 I=20,35
      V(I)=-36.0673605*DLOG((X(I)-0.375D0)**2+(Y(I)-0.375D0)**2)
      V(I)=V(I)*2.D0/3.D0
```

```
50       11 CONTINUE
      C
      C*** ASSIGN DIELECTRIC CONSTANT VALUES EP(K) FOR EACH ELEMENT K
      C
51           DO 80 K=1,NE
52           EP(K)=1.D0
53       80 CONTINUE
      C**
      C**PRINT ALL THE INPUT DATA
      C**
54           WRITE(6,200) NE,NN
55           WRITE(6,210) (V(I),I=1,NN)
      C**
      C**CALCULATION OF MATRIX ELEMENTS FOR EACH FINITE ELEMENT
      C**
56           DO  35 K=1,NE
      C**
57           XE(1)=X(NODE(K,1))
58           XE(2)=X(NODE(K,2))
59           XE(3)=X(NODE(K,3))
      C**
60           YE(1)=Y(NODE(K,1))
61           YE(2)=Y(NODE(K,2))
62           YE(3)=Y(NODE(K,3))
      C**
63           B1=YE(3)-YE(2)
64           B2=YE(1)-YE(3)
65           B3=YE(2)-YE(1)
      C**
66           C1=XE(2)-XE(3)
67           C2=XE(3)-XE(1)
68           C3=XE(1)-XE(2)
69           DEL=DABS(0.500*(XE(1)*(YE(2)-YE(3))+XE(2)*(YE(3)-YE(1))+
            1XE(3)*(YE(1)-YE(2))))
70           PRINT,K,DEL
71           RBAR=(XE(1)+XE(2)+XE(3))/3.D0
72           AA=EP(K)
73           IF(NCASE.EQ.2)AA=AA*2.D0*PI*RBAR**2
74           CONST=AA/(4.D0*DEL)
75           SE(1,1)=(B1*B1+C1*C1)*CONST
76           SE(1,2)=(B1*B2+C1*C2)*CONST
77           SE(1,3)=(B1*B3+C1*C3)*CONST
78           SE(1,2)=SE(1,2)/(-3.D0)
79           SE(1,3)=SE(1,3)/(-3.D0)
8            SE(2,1)=SE(1,2)
81           SE(2,2)=(B2*B2+C2*C2)*CONST
82           SE(2,3)=(B2*B3+C2*C3)*CONST
83           SE(2,3)=SE(2,3)/(-3.D0)
84           SE(3,1)=SE(1,3)
85           SE(3,2)=SE(2,3)
86           SE(3,3)=(B3*B3+C3*C3)*CONST
      C
87           SE(1,4)=(B1*B2+C1*C2)*CONST*4.D0/3.D0
88           SE(1,5)=0.D0
89           SE(1,6)=(B1*B3+C1*C3)*CONST*4.D0/3.D0
      C
90           SE(2,4)=SE(1,4)
91           SE(2,5)=(B2*B3+C2*C3)*CONST*4.D0/3.D0
92           SE(2,6)=0.D0
      C
93           SE(3,4)=0.D0
94           SE(3,5)=SE(2,5)
95           SE(3,6)=SE(1,6)
      C
96           SE(4,1)=SE(1,4)
97           SE(4,2)=SE(2,4)
```

```
 98            SE(4,3)=SE(3,4)
 99            SE(4,4)=2.D0*SE(1,4)+8.D0*(SE(1,1)+SE(2,2))/3.D
100            SE(4,5)=SE(2,4)+2.D0*SE(1,6)+4.D0*SE(2,2)/3.D0+SE(2,5)
101            SE(4,6)=4.D0*SE(1,1)/3.D0+SE(1,6)+SE(1,4)+2.D0*SE(2,5)
       C
102            SE(5,1)=SE(1,5)
103            SE(5,2)=SE(2,5)
104            SE(5,3)=SE(3,5)
105            SE(5,4)=SE(4,5)
106            SE(5,5)=2.D0*SE(2,5)+8.D0*(SE(2,2)+SE(3,3))/3.D
107            SE(5,6)=2.D0*SE(1,4)+SE(1,6)+SE(2,5)+4.D0*SE(3,3)/3.D
       C
108            SE(6,1)=SE(1,6)
109            SE(6,2)=SE(2,6)
110            SE(6,3)=SE(3,6)
111            SE(6,4)=SE(4,6)
112            SE(6,5)=SE(5,6)
113            SE(6,6)=2.D0*SE(1,6)+8.D0*(SE(1,1)+SE(3,3))/3.D
       C
       C**
       C**ASSEMBLE SYSTEM EQUATIONS WITHOUT BOUNDARY CONDITIONS
       C**
114            DO 28 J=1,6
115            NO(J)=NODE(K,J)
116         28 CONTINUE
       C
117            DO 30 IE=1,6
118            I=NO(IE)
119            DO 30 JE=1,6
120            J=NO(JE)
121            S(I,J)=S(I,J)+SE(IE,JE)
122         30 CONTINUE
       C**
       C**RECYCLE FOR NEXT ELEMENT
       C**
123         35 CONTINUE
       C**
       C**ACCOUNT FOR SPECIFIED BOUNDARY CONDITIONS
       C**
124            DO 40 I=20,35
125            DO 40 J=1,NN
126            IF(I.NE.J)GO TO 36
127            GO TO 37
128         36 S(I,J)=0.D0
129            GO TO 40
130         37 S(I,J)=1.D0
131         40 CONTINUE
132            DO 140 J=20,35
133            DO 140 I=1,NN
134            IF(I.NE.J)GO TO 136
135            GO TO 137
136        136 CONTINUE
137            V(I)=V(I)-S(I,J)*V(J)
138            S(I,J)=0.D0
139            GO TO 140
140        137 S(I,J)=1.D0
141        140 CONTINUE
142            DO 211 I=20,35
143            V(I)=-38.067376C5*DLOG((X(I)-0.375D0)**2+(Y(I)-0.375D0)**2)
144            V(I)=V(I)*2.D0/3.D0
145        211 CONTINUE
146            WRITE(6,210) (V(I),I=1,NN)
       C**
       C** SOLVE THE CONSTRAINED SYSTEM OF EQUATIONS
       C**
147            CALL SOLN
```

```
148           DO 215 I=1,NN
149           EXACTV(I)=-36.067376C5*DLOG((X(I)-0.375D0)**2+
             1(Y(I)-0.375D0)**2)
150           EXACTV(I)=EXACTV(I)*2.DC/3.DC
151           WRITE(6,111)I,EXACTV(I),V(I)
152       111 FORMAT('0','EXACTV (',I3,') = ',F20.10,F28.10)
153       215 CONTINUE
          C**
          C**FORMATS : READ 100 TO 199 ,WRITE 200 TO 28
          C**
154       100 FORMAT(2I4)
155       105 FORMAT(I2)
156       11  FORMAT(6I4)
          C**
157       200 FORMAT(6X,2(I4,8X))
158       202 FORMAT('0',16X,'THIS IS A TWO-DIMENSIONAL PROBLEM')
159       210 FORMAT('0',8D15.8)
160       303 FORMAT('0',16X,'THIS IS A THREE-DIMENSIONAL AXI-SYMMETRIC PR
             1)
161           STOP
162           END

163           SUBROUTINE COORDS
          C
          C**
          C** COORDS GENERATES NODAL COORDINATES OF THE CONTINUUM
          C**
164           COMMON X(76),Y(76),NODE(28,6),C(28,76)
165           COMMENRC1(28),RC2(28),ZC1(28),ZC2(28)
166           COMMON S(76,76),V(76)
167           COMMON G(28)
168           COMMON ENM(28)
169           REAL*8 ENM
170           REAL*8 G
171           REAL*8 DSQRT
172           DOUBLE PRECISION X,Y,C,RC1,RC2,ZC1,ZC2,S,V
173           PI=3.14159265
          C
174           DO 1  I=1,7
175           Y(I)=0.D
176           X(I)=0.D0+0.5D0*(I-1)/2
177       1   CONTINUE
178           X(16)=
179           Y(16)=0.5D0
180           X(18)=0.5D
181           Y(18)=0.5D
          C
182           X(37)=1.D0
183           X(39)=1.5D
184           Y(37)=0.5D0
185           Y(39)=0.5D
          C
186           X(54)=0.D0
187           X(56)=0.5D
188           X(59)=1.D0
189           X(61)=1.5D0
          C
190           Y(54)=1.D0
191           Y(56)=1.D0
192           Y(59)=1.D
193           Y(61)=1.D0
          C
194           DO 2 I=7 ,76
195           Y(I)=1.5D0
196           X(I)=0.D0+0.5D0*(I-76)/2
197       2   CONTINUE
```

```
      C
198           DO 6 I=24,34,2
199           Y(I)=0.25D0*DSIN((I-24)*PI/8.D0)+0.75D0
200           X(I)=0.25D0*DCOS((I-24)*PI/8.D0)+0.75D0
201         6 CONTINUE
202           X(20)=0.75D0
203           Y(20)=0.5D0
204           X(22)=0.25D0/DSQRT(2.D0)+0.75D0
205           Y(22)=-0.25D0/DSQRT(2.D0)+0.75D0
      C
      C
206           DO 7 I=21,33,2
207           X(I)=X(I-1)+(X(I+1)-X(I-1))/2.D0
208           Y(I)=Y(I-1)+(Y(I+1)-Y(I-1))/2.D0
209         7 CONTINUE
210           X(35)=X(34)+(X(20)-X(34))/2.D0
211           Y(35)=Y(34)+(Y(20)-Y(34))/2.D0
      C**
212           X(8)=0.D0
213           Y(8)=0.25D0
214           Y(15)=0.25D0
215           X(15)=1.5D0
      C
216           X(46)=0.D0
217           X(47)=1.5D0
218           Y(46)=0.75D0
219           Y(47)=0.75D0
      C
220           X(62)=0.D0
221           X(69)=1.5D0
222           Y(62)=1.25D0
223           Y(69)=1.25D0
224           DO 55 I=1,76
225           X(I)=X(I)/2.D0
226           Y(I)=Y(I)/2.D0
227        55 CONTINUE
228           RETURN
229           END

230           SUBROUTINE RING
      C
      C** RING GENERATES COORDINATES OF THE INTEGRATION CONTOUR
      C       AS RC1(K),RC2(K), & ZC1(K),ZC2(K)
      C
231           COMMON X(76),Y(76),NODE(28,6),C(28,76)
232           COMMONRC1(28),RC2(28),ZC1(28),ZC2(28)
233           COMMON S(76,76),V(76)
234           COMMON G(28)
235           COMMON ENM(29)
236           REAL*8 ENM
237           REAL*8 G
238           DOUBLE PRECISION X,Y,C,RC1,RC2,ZC1,ZC2,S,V
239           NE=28
240           DO 3 K=1,NE
241           RC1(K)=0.D0
242           RC2(K)=0.D0
243           ZC1(K)=0.D0
244           ZC2(K)=0.D0
245         3 CONTINUE
246           RC1(2)=0.25D0
247           ZC1(2)=0.25D0
248           RC2(2)=0.5D0
249           ZC2(2)=0.25D0
250           ENM(2)=1.D0
      C
251           RC1(3)=0.5D0
```

```
252           ZC1(3)=0.25D0
253           RC2(3)=0.625D0
254           ZC2(3)=0.25D0
255           ENM(3)=1.D0
      C
256           RC1(4)=0.625D0
257           RC2(4)=0.875D0
258           ZC1(4)=0.25D0
259           ZC2(4)=0.25D0
260           ENM(4)=1.D0
      C
261           RC1(5)=0.875D0
262           RC2(5)=1.D0
263           ZC1(5)=0.25D0
264           ZC2(5)=0.25D0
265           ENM(5)=1.D0
      C
266           RC1(6)=1.D0
267           RC2(6)=1.25D0
268           ZC1(6)=0.25D0
269           ZC2(6)=0.25D0
270           ENM(6)=1.D0
      C
271           ZC1(7)=0.25D0
272           ZC2(7)=0.5D0
273           RC1(7)=1.25D0
274           RC2(7)=1.25D0
275           ENM(7)=-1.D0
      C
276           ZC1(14)=0.5D0
277           ZC2(14)=0.625D0
278           RC1(14)=1.25D0
279           RC2(14)=1.25D0
280           ENM(14)=-1.D0
      C
281           ZC1(15)=0.625D0
282           ZC2(15)=0.875D0
283           RC1(15)=1.25D0
284           RC2(15)=1.25D0
285           ENM(15)=-1.D0
      C
286           ZC1(21)=0.875D0
287           ZC2(21)=1.D0
288           RC1(21)=1.25D0
289           RC2(21)=1.25D0
290           ENM(21)=-1.D0
      C
291           ZC1(28)=1.D0
292           ZC2(28)=1.25D0
293           RC1(28)=1.25D0
294           RC2(28)=1.25D0
295           ENM(28)=-1.D0
      C
296           RC1(27)=1.25D0
297           RC2(27)=1.D0
298           ZC1(27)=1.25D0
299           ZC2(27)=1.25D0
300           ENM(27)=-1.D0
      C
301           RC1(26)=1.D0
302           RC2(26)=0.875D0
303           ZC1(26)=1.25D0
304           ZC2(26)=1.25D0
305           ENM(26)=-1.D0
      C
306           RC1(25)=0.875D0
```

```
307           RC2(25)=0.625D0
308           ZC1(25)=1.25D0
309           ZC2(25)=1.25D0
310           ENM(25)=-1.D0
      C
311           RC1(24)=0.625D0
312           RC2(24)=0.5D0
313           ZC1(24)=1.25D0
314           ZC2(24)=1.25D0
315           ENM(24)=-1.D0
      C
316           RC1(23)=0.5D0
317           RC2(23)=0.25D0
318           ZC1(23)=1.25D0
319           ZC2(23)=1.25D0
320           ENM(23)=-1.D0
      C
321           ZC1(22)=1.25D0
322           ZC2(22)=1.D0
323           RC1(22)=0.25D0
324           RC2(22)=0.25D0
325           ENM(22)=1.D0
      C
326           ZC1(16)=1.D0
327           ZC2(16)=0.875D0
328           RC1(16)=0.25D0
329           RC2(16)=0.25D0
330           ENM(16)=1.D0
      C
331           ZC1(8)=0.875D0
332           ZC2(8)=0.625D0
333           RC1(8)=0.25D0
334           RC2(8)=0.25D0
335           ENM(8)=1.D0
      C
336           ZC1(9)=0.625D0
337           ZC2(9)=0.5D0
338           RC1(9)=0.25D0
339           RC2(9)=0.25D0
340           ENM(9)=1.D0
      C
341           ZC1(1)=0.5D0
342           ZC2(1)=0.25D0
343           RC1(1)=0.25D0
344           RC2(1)=0.25D0
345           ENM(1)=1.D0
      C
      C
346           DO 5 K=1,NE
347           RC1(K)=RC1(K)/2.D0
348           RC2(K)=RC2(K)/2.D0
349            ZC1(K)=ZC1(K)/2.D0
350           ZC2(K)=ZC2(K)/2.D0
351         5 CONTINUE
352           RETURN
353           END

354           SUBROUTINE STRAIN
      C
      C** COMPUTATION OF THE CONSTRAINTS MATRIX ELEMENTS C(I,J)
      C
355           COMMON X(76),Y(75),NODE(28,6),C(28,76)
356           COMMONRC1(28),RC2(28),ZC1(28),ZC2(28)
357           COMMON S(76,76),V(76)
358           COMMON G(28)
359           COMMON ENM(28)
```

```
360           REAL*8 G
361           REAL*8 ENM
362           DOUBLE PRECISION X,Y,C,RC1,RC2,ZC1,ZC2,S,V
363           REAL*8 AN(3),BN(3),CN(3)
364           REAL*8 VOLTG1(6),VOLTG2(6)
365           DOUBLE PRECISION PI
366           DOUBLE PRECISION X1,X2,X3,Y1,Y2,Y3,DELT,XX,YY,DABS
367           DOUBLE PRECISION DELTAZ,DELTAR,HX,HY,Z,T,ENOMO
368           DOUBLE PRECISION R1,R2,R3,RI1,RI2,RI3,DLOG
369           DOUBLE PRECISION F1,F2,F3,FF1,FF2,FF3,ENTGR1,ENTGR2
370           DOUBLE PRECISION TEMPR1,TEMPR2,TEMPZ1,TEMPZ2
371           REAL*8 EN1(3),EN2(3),EN3(3),ELA(6),ELB(6),ELC(6)
372           REAL*8 DN1(3),DN2(3),DN3(3),DNA(6),DNB(6),DNC(6)
373           REAL*8 HXHY
374           NN=76
375           NE=28
376           NC=28
377           PI=3.14159265
      C
      C** INITIALIZE
      C
378           DO 1 I=1,NC
379           G(I)=0.D0
380           DO 1 J=1,NN
381         1 C(I,J)=0.D0
382           I1=1
383           I2=8
384           I3=1
385           IK=0
386        35 CONTINUE
387           DO 40 I=I1,I2,I3
388           IK=IK+1
389           KI=0
390           CALL RING
391           K1=1
392           K2=9
393           K3=1
394        15 CONTINUE
395           DO 20 K=K1,K2,K3
396           ENOMO=ENM(K)
397           KI=KI+1
      C
      C** ELEMENT PATTERN AND COORDS
      C
398           X1=X(NODE(K,1))
399           X2=X(NODE(K,2))
400           X3=X(NODE(K,3))
      C**
401           Y1=Y(NODE(K,1))
402           Y2=Y(NODE(K,2))
403           Y3=Y(NODE(K,3))
      C
      C** COEFFICIENTS OF THE SHAPE FUNCTION
      C
404           AN(1)=X2*Y3-X3*Y2
405           AN(2)=X3*Y1-X1*Y3
406           AN(3)=X1*Y2-X2*Y1
      C**
407           BN(1)=Y2-Y3
408           BN(2)=Y3-Y1
409           BN(3)=Y1-Y2
      C**
410           CN(1)=X3-X2
411           CN(2)=X1-X3
412           CN(3)=X2-X1
413           DELT=DABS(0.5D0*(X1*(Y2-Y3)+X2*(Y3-Y1)+X3*(Y1-Y2)))
```

```
      C
414           TEMPR1=RC1(K)
415           TEMPR2=RC2(K)
416           TEMPZ1=ZC1(K)
417           TEMPZ2=ZC2(K)
418           IPC=2
419           DELTAZ=(ZC2(K)-ZC1(K))/IPC
420           DELTAR=(RC2(K)-RC1(K))/IPC
      C**
421           DO 33 LL=1,6
422           RC1(K)=TEMPR1
423           RC2(K)=TEMPR2
424           ZC1(K)=TEMPZ1
425           ZC2(K)=TEMPZ2
426           VOLTG1(LL)=0.D0
427           VOLTG2(LL)=0.D0
      C
428           DO 91 II=1,IPC
429           RC2(K)=RC1(K)+DELTAR
430           ZC2(K)=ZC1(K)+DELTAZ
431           HX=RC2(K)-RC1(K)
432           HY=ZC2(K)-ZC1(K)
433           HXHY=1.D-3
434           IF(DABS(HX).LE.HXHY.AND.DABS(HY).LE.HXHY)GO TO 20
435           HX=HX/2.D0
436           HY=HY/2.D0
437           X1=RC1(K)
438           Y1=ZC1(K)
439           Z=X(I)
440           T=Y(I)
441           R2=(Z-X1-HX)**2+(T-Y1-HY)**2
442           R1=(Z-X1)**2+(T-Y1)**2
443           R3=(Z-X1-2.D0*HX)**2+(T-Y1-2.D0*HY)**2
      C
444           DO 4 L=1,3
445           EN1(L)=(AN(L)+BN(L)*X1+CN(L)*Y1)/(2.D0*DELT)
446           EN2(L)=(AN(L)+BN(L)*(X1+HX)+CN(L)*(HY+Y1))/(2.D0*DELT)
447           EN3(L)=(AN(L)+BN(L)*(X1+2.D0*HX)+CN(L)*(Y1+2.D0*HY))/
             1(2.D0*DELT)
448         4 CONTINUE
      C
449           DO 5 L=1,3
450           ELA(L)=EN1(L)*(2.D0*EN1(L)-1.D0)
451           ELB(L)=EN2(L)*(2.D0*EN2(L)-1.D0)
452           ELC(L)=EN3(L)*(2.D0*EN3(L)-1.D0)
453         5 CONTINUE
      C
454           ELA(4)=4.D0*EN1(1)*EN1(2)
455           ELB(4)=4.D0*EN2(1)*EN2(2)
456           ELC(4)=4.D0*EN3(1)*EN3(2)
      C
457           ELA(5)=4.D0*EN1(2)*EN1(3)
458           ELB(5)=4.D0*EN2(2)*EN2(3)
459           ELC(5)=4.D0*EN3(2)*EN3(3)
      C
460           ELA(6)=4.D0*EN1(3)*EN1(1)
461           ELB(6)=4.D0*EN2(3)*EN2(1)
462           ELC(6)=4.D0*EN3(3)*EN3(1)
      C
463           DO 6 L=1,3
464           DN1(L)=-DLOG(R1)*(BN(L)*DABS(HY)+CN(L)*DABS(HX))/(2.D0*DELT)
465           DN2(L)=-DLOG(R2)*(BN(L)*DABS(HY)+CN(L)*DABS(HX))/(2.D0*DELT)
466           DN3(L)=-DLOG(R3)*(BN(L)*DABS(HY)+CN(L)*DABS(HX))/(2.D0*DELT)
467         6 CONTINUE
      C
468           DO 7 L=1,3
```

```
469           DNA(L)=(4.D0*EN1(L)-1.D0)*DN1(L)
470           DNB(L)=(4.D0*EN2(L)-1.D0)*DN2(L)
471           DNC(L)=(4.D0*EN3(L)-1.D0)*DN3(L)
472         7 CONTINUE
      C
473           DNA(4)=4.D0*EN1(2)*DN1(1)+4.D0*EN1(1)*DN1(2)
474           DN3(4)=4.D0*EN2(2)*DN2(1)+4.D0*EN2(1)*DN2(2)
475           DNC(4)=4.D0*EN3(2)*DN3(1)+4.D0*EN3(1)*DN3(2)
      C
476           DNA(5)=4.D0*EN1(3)*DN1(2)+4.D0*EN1(2)*DN1(3)
477           DN3(5)=4.D0*EN2(3)*DN2(2)+4.D0*EN2(2)*DN2(3)
478           DNC(5)=4.D0*EN3(3)*DN3(2)+4.D0*EN3(2)*DN3(3)
      C
479           DNA(6)=4.D0* EN1(1)*DN1(3)+4.D0*EN1(3)*DN1(1)
480           DNB(6)=4.D0*EN2(1)*DN2(3)+4.D0*EN2(3)*DN2(1)
481           DNC(6)=4.D0*EN3(1)*DN3(3)+4.D0*EN3(3)*DN3(1)
      C
482           RI1=ELA(LL)
483           RI2=ELB(LL)
484           RI3=ELC(LL)
      C
485           F1=DNA(LL)
486           F2=DNB(LL)
487           F3=DNC(LL)
488           ENTGR1=ENOMO*(F1+4.D0*F2+F3)/(12.D0*PI)
489           FF1=RI1*((X(I)-X1)*DABS(HY)+(Y(I)-Y1)*DABS(HX))/R1
490           FF2=RI2*((X(I)-X1-HX)*DABS(HY)+(Y(I)-Y1-HY)*DABS(HX))/R2
491           FF3=RI3*((X(I)-X1-2.D0*HX)*DABS(HY)
             1+(Y(I)-Y1-2.D0*HY)*DABS(HX))/R3
492           ENTGR2=ENOMO*(FF1+4.D0*FF2+FF3)/(6.D0*PI)
493           VOLTG1(LL)=VOLTG1(LL)+ENTGR1
494           VOLTG2(LL)=VOLTG2(LL)+ENTGR2
495           RC1(K)=RC2(K)
496           ZC1(K)=ZC2(K)
497        91 CONTINUE
498           J=NODE(K,LL)
499           C(IK,J)=C(IK,J)+VOLTG1(LL)-VOLTG2(LL)
500        33 CONTINUE
501           PRINT,KI,K
502        20 CONTINUE
503           IF(KI.EQ.9)GO TO 21
504           IF(KI.EQ.12)GO TO 22
505           GO TO 30
506        21 CONTINUE
507           K1=14
508           K2=16
509           K3=1
510           GO TO 15
511        22 CONTINUE
512           K1=21
513           K2=28
514           K3=1
515           GO TO 15
516        30 CONTINUE
517           C(IK,I)=C(IK,I)-1.D0
518        40 CONTINUE
519           PRINT,IK,I
520           IF(IK.EQ.8)GO TO 45
521           IF(IK.EQ.16)GO TO 46
522           IF(IK.EQ.18)GO TO 47
523           IF(IK.EQ.20)GO TO 48
524           IF(IK.EQ.22)GO TO 49
525           GO TO 60
526        45 CONTINUE
527           I1=69
528           I2=76
```

```
529           I3=1
530           GO TO 35
531        46 CONTINUE
532           I1=15
533           I2=16
534           I3=1
535           GO TO 35
536        47 CONTINUE
537           I1=39
538           I2=40
539           I3=1
540           GO TO 35
541        48 CONTINUE
542           I1=47
543           I2=54
544           I3=7
545           GO TO 35
546        49 CONTINUE
547           I1=61
548           I2=62
549           I3=1
550           GO TO 35
551        60 CONTINUE
552           G(25)=100.0000000770
553           G(26)=G(25)
554           G(27)=G(25)
555           G(28)=G(25)
556           C(25,20)=1.D0
557           C(26,24)=1.D0
558           C(27,28)=1.D0
559           C(28,32)=1.D0
560           RETURN
561           END

562           SUBROUTINE SOLN
      C
      C** SOLN SOLVES THE CONSTRRAINED MATRIX  NON-NUMERICALLY
      C
563           COMMON X(76),Y(76),NODE(28,6),C(28,76)
564           COMMONRC1(28),RC2(28),ZC1(28),ZC2(28)
565           COMMON S(76,76),V(76)
566           COMMON G(28)
567           COMMON ENM(28)
568           REAL*8 CT(76,28),SINVCT(76,28),SINVB(76),CSINVB(28)
569           REAL*8 CSNVCT(28,28),LAMDA(28),SLAMDA(76)
570           REAL*8 WKAREA(152),D1,D2
571           REAL*8 G
572           REAL*8 ENM
573           DOUBLE PRECISION X,Y,C,RC1,RC2,ZC1,ZC2,S,V
574           DOUBLE PRECISION D
575           NC=28
576           NN=76
577           D1=-1.D0
578           IJOB=1
579           N2N=2*NN
580           DO 590 I=1,N2N
581           WKAREA(I)=0.D0
582        590 CONTINUE
      C
      C** FORM INVERSE OF S(159,159)
      C
583           CALL LINV3F(S,V,IJOB,NN,NN,D1,D2,WKAREA,IER)
      C
      C** FORM C TRANSPOSED
      C
584           CALL STRAIN
```

```
      C
585         DO 600 I=1,NN
586         DO 600 J=1,NC
587         CT(I,J)=C(J,I)
588   600 CONTINUE
      C
      C**ACCOUNT FOR SPECIFIED BOUNDARY CONDITIONS
      C
      C
      C
      C** FORM S INVERSE TIMES C TRANSPOSED
      C
589         DO 610 I=1,NN
590         DO 610 J=1,NC
591         SINVCT(I,J)=0.D0
592         DO 610 K=1,NN
593         SINVCT(I,J)=SINVCT(I,J)+S(I,K)*CT(K,J)
594   610 CONTINUE
      C
      C** FORM S INVERSE TIMES V
      C
595         DO 615 I=1,NN
596         SINVB(I)=0.D0
597         DO 615 J=1,NN
598         SINVB(I)=SINVB(I)+S(I,J)*V(J)
599   615 CONTINUE
      C
      C** FORM C TIMES SINVB
      C
600         DO 620 I=1,NC
601         CSINVB(I)=0.D0
602         DO 620 J=1,NN
603         CSINVB(I)=CSINVB(I)+C(I,J)*SINVB(J)
604   620 CONTINUE
605         DO 621 I=1,NC
606         CSINVB(I)=CSINVB(I)-G(I)
607         PRINT,I,G(I)
608   621 CONTINUE
      C
      C** FORM C TIMES SINVCT
      C
609         DO 625 I=1,NC
610         DO 625 J=1,NC
611         CSNVCT(I,J)=0.D0
612         DO 625 K=1,NN
613         CSNVCT(I,J)=CSNVCT(I,J)+C(I,K)*SINVCT(K,J)
614   625 CONTINUE
      C
      C** FORM INVERSE OF CSNVCT
      C
615         CALL LINV3F(CSNVCT,LAMDA,IJOB,NC,NC,D1,D2,WKAREA,IER)
616         PRINT,IER
      C
      C** FORM CSNVCT TIMES CSINVB
      C
617         DO 630 I=1,NC
618         LAMDA(I)=0.D0
619         DO 630 J=1,NC
620         LAMDA(I)=LAMDA(I)+CSNVCT(I,J)*CSINVB(J)
621   630 CONTINUE
      C
      C** FORM SINVCT TIMES LAMDA
      C
622         DO 635 I=1,NN
623         SLAMDA(I)=0.D0
624         DO 635 J=1,NC
```

```
625           SLAMDA(I)=SLAMDA(I)+SINVCT(I,J)*LAMDA(J)
626        635 CONTINUE
           C
           C** FORM SINVB MINUS SLAMDA
           C
627           DO 640 I=1,NN
628           V(I)=SINVB(I)-SLAMDA(I)
629        640 CONTINUE
           C
           C** OUTPUT LAMDA
           C
630           DO 645 I=1,NC
631           WRITE(6,650) I,LAMDA(I)
632        645 CONTINUE
           C
633        650 FORMAT('0','LAMDA (',I3,') =',F16.10)
           C**CHECK WHETHER CONSTRAINTS * V EQUALS ZERO
           C
634           DO 700 I=1,NC
635           LAMDA(I)=0.D0
636           DO 700 J=1,NN
637           LAMDA(I)=LAMDA(I)+C(I,J)*V(J)
638        700 CONTINUE
639           DO 750 I=1,NC
640           WRITE(6,650) I,LAMDA(I)
641        750 CONTINUE
642           RETURN
643           END
```

APPENDIX B

COMPUTER-AIDED DESIGN COMPUTER PROGRAM

This Fortran program calculates the longitudinal eletrostatic stress in a cable termination; starting at the stress relief profile.

OUTPUT: Nodal potentials, equipotentials plot, nodal longitudinal stresses and all input data

MAIN: Calculates the finite element system matrix [S]

- DATA: Elemental assembly
- COORDS: Global coordinates of the nodes in the continuum
- GAUSDO: Gauss-Siedel large system matrix iterative solution
- STRESS: Calculates longitudinal stress at each node point
- CONTUA: Plots equipotential contours
  - DASH
  - SYMBOL
  - SIMOCON

```
      C**
      C**
      C**THE FINITE ELEMENT METHOD
      C**
      COMMON X(185),Y(185),NODE(70,6)
      COMMON S(185,186),V(185)
      COMMON G(13)
      REAL*8 EP(70)
      REAL*4 EXACTV(185)
      REAL*8 G
      REAL*8 ENM
      REAL*8 XE(3),YE(3)
      REAL*8 SE(6,6)
      INTEGER ND(6)
      DOUBLE PRECISION X,Y,C,RC1,RC2,ZC1,ZC2,S,V
      DOUBLE PRECISION DABS,RBAR,AA,CONST,PI,DEL
      DOUBLE PRECISION B1,B2,B3,C1,C2,C3
      DOUBLE PRECISION X1,X2,X3,Y1,Y2,Y3,V1,V2,V3
      REAL*8 R1,R2,R3,S11,S12,S13,S22,S23,S33
      REAL*4 ERROR(185)
      C**
      C**SPECIFY TYPE OF PROBLEM  : 2-DIMENSION (NCASE=1)
      C**OR 3-DIMENSION AXI-SYMMETRIC (NCASE=2)
      C**
      READ(5,105) NCASE
      IF(NCASE.EQ.2) GO TO 33
      WRITE(6,202)
      GO TO 60
   33 WRITE(6,303)
   60 CONTINUE
      C**
      C**INITIALIZE TO ZERO S(I,J) ,SE(I,J),V(I),X Y(I) ,XE,YE
      C**
      READ(5,100) NE,NN
      DO 1 I=1,NN
      DO 1 J=1,NN
    1 S(I,J)=0.D0
      DO 2 I=1,NN
      X(I)=0.D0
      Y(I)=0.D0
    2 V(I)=0.D0
      DO 3 I=1,3
      DO 3 J=1,3
      XE(I)=0.D0
      YE(I)=0.D0
    3 CONTINUE
      DO 4 I=1,6
      DO 4 J=1,6
    4 SE(I,J)=0.D0
      PI=3.14159265
      C**
      C**READ IN NODE NUMBERS &NODAL COORDINATES
      C**
      DO 5 K=1,NE
      READ(5,110) NODE(K,1),NODE(K,2),NODE(K,3),
     1NODE(K,4),NODE(K,5),NODE(K,6)
      PRINT,NODE(K,1),NODE(K,2),NODE(K,3),NODE(K,4)
     1,NODE(K,5),NODE(K,6),K
    5 CONTINUE
      CALL COORDS
      WRITE(6,999) (I,X(I),Y(I),I=1,NN)
  999 FORMAT('0',I16,2F16.5)
      DO 11 I=153,185
   11 V(I)=100.D0
      C
```

```
      C
      C*** ASSIGN DIELECTRIC CONSTANT VALUES EP(K) FOR EACH ELEMENT K
      C
49          DO 80 K=1,NE
50          EP(K)=2.3D0
51       80 CONTINUE
      C**
      C**PRINT ALL THE INPUT DATA
      C**
52          WRITE(6,200) NE,NN
53          WRITE(6,210) (V(I),I=1,NN)
      C**
      C**CALCULATION OF MATRIX ELEMENTS FOR EACH FINITE ELEMENT
      C**
54          DO  35 K=1,NE
      C**
55          XE(1)=X(NODE(K,1))
56          XE(2)=X(NODE(K,2))
57          XE(3)=X(NODE(K,3))
      C**
58          YE(1)=Y(NODE(K,1))
59          YE(2)=Y(NODE(K,2))
60          YE(3)=Y(NODE(K,3))
      C**
61          B1=YE(3)-YE(2)
62          B2=YE(1)-YE(3)
63          B3=YE(2)-YE(1)
      C**
64          C1=XE(2)-XE(3)
65          C2=XE(3)-XE(1)
66          C3=XE(1)-XE(2)
67          DEL=DABS(0.5D0*(XE(1)*(YE(2)-YE(3))+XE(2)*(YE(3)-YE(1))+
           1XE(3)*(YE(1)-YE(2))))
68          PRINT,K,DEL
69          RBAR=(YE(1)+YE(2)+YE(3))/3.D0
70          AA=EP(K)
71          IF(NCASE.EQ.2)GO TO 27
72          CONST=AA/(4.D0*DEL)
73          SE(1,1)=(B1*B1+C1*C1)*CONST
74          SE(1,2)=(B1*B2+C1*C2)*CONST
75          SE(1,3)=(B1*B3+C1*C3)*CONST
76          SE(1,2)=SE(1,2)/(-3.D0)
77          SE(1,3)=SE(1,3)/(-3.D0)
78          SE(2,1)=SE(1,2)
79          SE(2,2)=(B2*B2+C2*C2)*CONST
80          SE(2,3)=(B2*B3+C2*C3)*CONST
81          SE(2,3)=SE(2,3)/(-3.D0)
82          SE(3,1)=SE(1,3)
83          SE(3,2)=SE(2,3)
84          SE(3,3)=(B3*B3+C3*C3)*CONST
      C
85          SE(1,4)=(B1*B2+C1*C2)*CONST*4.D0/3.D0
86          SE(1,5)=0.D0
87          SE(1,6)=(B1*B3+C1*C3)*CONST*4.D0/3.D0
      C
88          SE(2,4)=SE(1,4)
89          SE(2,5)=(B2*B3+C2*C3)*CONST*4.D0/3.D0
90          SE(2,6)=0.D0
      C
91          SE(3,4)=0.D0
92          SE(3,5)=SE(2,5)
93          SE(3,6)=SE(1,6)
      C
94          SE(4,1)=SE(1,4)
95          SE(4,2)=SE(2,4)
96          SE(4,3)=SE(3,4)
```

```
      SE(4,4)=2.D0*SE(1,4)+8.D0*(SE(1,1)+SE(2,2))/3.D0
      SE(4,5)=SE(2,4)+2.D0*SE(1,6)+4.D0*SE(2,2)/3.D0+SE(2,5)
      SE(4,6)=4.D0*SE(1,1)/3.D0+SE(1,6)+SE(1,4)+2.D0*SE(2,5)
C
      SE(5,1)=SE(1,5)
      SE(5,2)=SE(2,5)
      SE(5,3)=SE(3,5)
      SE(5,4)=SE(4,5)
      SE(5,5)=2.D0*SE(2,5)+8.D0*(SE(2,2)+SE(3,3))/3.D0
      SE(5,6)=2.D0*SE(1,4)+SE(1,6)+SE(2,5)+4.D0*SE(3,3)/3.D0
C
      SE(6,1)=SE(1,6)
      SE(6,2)=SE(2,6)
      SE(6,3)=SE(3,6)
      SE(6,4)=SE(4,6)
      SE(6,5)=SE(5,6)
      SE(6,6)=2.D0*SE(1,6)+8.D0*(SE(1,1)+SE(3,3))/3.D0
C**
C**AXISYMMETRIC RING ELEMENTS MATRIX ASSEMBLY
C**
      GO TO 29
   27 CONTINUE
      AA=AA*2.D0*PI*RBAR
      CONST=AA/(4.D0*DEL)
C
      SE(1,1)=(B1*B1+C1*C1)*CONST
      SE(1,2)=(B1*B2+C1*C2)*CONST
      SE(1,3)=(B1*B3+C1*C3)*CONST
      SE(2,1)=SE(1,2)
      SE(2,2)=(B2*B2+C2*C2)*CONST
      SE(2,3)=(B2*B3+C2*C3)*CONST
      SE(3,1)=SE(1,3)
      SE(3,2)=SE(2,3)
      SE(3,3)=(B3*B3+C3*C3)*CONST
C
      R1=YE(1)
      R2=YE(2)
      R3=YE(3)
      S11=SE(1,1)
      S12=SE(1,2)
      S13=SE(1,3)
      S23=SE(2,3)
      S33=SE(3,3)
      S22=SE(2,2)
C
      SE(1,1)=S11*(3.D0*R1+R2+R3)/5.D0
      SE(1,2)=-S12*(2.D0*R1+2.D0*R2+R3)/15.D0
      SE(1,3)=-S13*(2.D0*R1+R2+2.D0*R3)/15.D0
      SE(1,4)=S11*(3.D0*R1-2.D0*R2-R3)/15.D0
     1+S12*(14.D0*R1+3.D0*R2+3.D0*R3)/15.D0
      SE(1,5)=S12*(3.D0*R1-R2-2.D0*R3)/15.D0
     1+S13*(3.D0*R1-2.D0*R2-R3)/15.D0
      SE(1,6)=S11*(3.D0*R1-R2-2.D0*R3)/15.D0
     1+S13*(14.D0*R1+3.D0*R2+3.D0*R3)/15.D0
C
      SE(2,2)=S22*(R1+3.D0*R2+R3)/5.D0
      SE(2,3)=-S23*(R1+2.D0*R2+2.D0*R3)/15.D0
      SE(2,4)=S12*(3.D0*R1+14.D0*R2+3.D0*R3)/15.D0
     1+S22*(-2.D0*R1+3.D0*R2-R3)/15.D0
      SE(2,5)=S22*(-R1+3.D0*R2-2.D0*R3)/15.D0+
     1S23*(3.D0*R1+14.D0*R2+3.D0*R3)/15.D0
      SE(2,6)=S12*(-R1+3.D0*R2-2.D0*R3)/15.D0
     1+S23*(-2.D0*R1+3.D0*R2-R3)/15.D0
C
      SE(3,3)=S33*(R1+R2+3.D0*R3)/5.D0
      SE(3,4)=S13*(-R1-2.D0*R2+3.D0*R3)/15.D0
```

```
     1+S23*(-2.D0*R1-R2+3.D0*R3)/15.D0
147   SE(3,5)=S23*(3.D0*R1+3.D0*R2+14.D0*R3)/15.D0
     1+S33*(-R1-2.D0*R2+3.D0*R3)/15.D0
148   SE(3,6)=S13*(3.D0*R1+3.D0*R2+14.D0*R3)/15.D0
     1+S33*(-2.D0*R1-R2+3.D0*R3)/15.D0
      C
149   SE(4,4)=16.D0*(S11*(R1+3.D0*R2+R3)/30.D0+S12*(2.D0*R1
     1+2.D0*R2+R3)/30.D0+S22*(3.D0*R1+R2+R3)/30.D0)
150   SE(4,5)=16.D0*(S12*(R1+2.D0*R2+2.D0*R3)/60.D0+S13*(R1+3.D0*R2
     1+R3)/30.D0+S22*(2.D0*R1+R2+2.D0*R3)/60.D0
     1+S23*(2.D0*R1+2.D0*R2+R3)/60.D0)
151   SE(4,6)=16.D0*(S13*(2.D0*R1+2.D0*R2+R3)/60.D0+S12*(2.D0*R1+R2
     1+2.D0*R3)/60.D0+S23*(3.D0*R1+R2+R3)/30.D0
     1+S11*(R1+2.D0*R2+2.D0*R3)/60.D0)
      C
152   SE(5,5)=16.D0*(S22*(R1+R2+3.D0*R3)/30.D0+S23*(R1+2.D0*R2
     1+2.D0*R3)/30.D0+S33*(R1+3.D0*R2+R3)/30.D0)
153   SE(5,6)=16.D0*(S12*(R1+R2+3.D0*R3)/30.D0+S13*(R1+2.D0*R2
     1+2.D0*R3)/60.D0+S23*(2.D0*R1+R2+2.D0*R3)/60.D0
     1+S33*(2.D0*R1+2.D0*R2+R3)/60.D0)
154   SE(6,6)=16.D0*(S11*(R1+R2+3.D0*R3)/30.D0+S13*(2.D0*R1+R2
     1+2.D0*R3)/30.D0+S33*(3.D0*R1+R2+R3)/30.D0)
      C
155   SE(4,1)=SE(1,4)
156   SE(4,2)=SE(2,4)
157   SE(4,3)=SE(3,4)
158   SE(5,1)=SE(1,5)
159   SE(5,2)=SE(2,5)
160   SE(5,3)=SE(3,5)
161   SE(5,4)=SE(4,5)
162   SE(6,1)=SE(1,6)
163   SE(6,2)=SE(2,6)
164   SE(6,3)=SE(3,6)
165   SE(6,4)=SE(4,6)
166   SE(6,5)=SE(5,6)
      C
167   SE(2,1)=SE(1,2)
168   SE(3,1)=SE(1,3)
169   SE(3,2)=SE(2,3)
      C
170     29  CONTINUE
      C**
      C**ASSEMBLE SYSTEM EQUATIONS WITHOUT BOUNDARY CONDITIONS
      C**
171         DO 28 J=1,6
172         NO(J)=NODE(K,J)
173     28  CONTINUE
      C
174         DO 30 IE=1,6
175         I=NO(IE)
176         DO 30 JE=1,6
177         J=NO(JE)
178         S(I,J)=S(I,J)+SE(IE,JE)
179     30  CONTINUE
      C**
      C**RECYCLE FOR NEXT ELEMENT
      C**
180     35 CONTINUE
      C**
      C**ACCOUNT FOR SPECIFIED BOUNDARY CONDITIONS
      C**
181         DO 40 I=1,45
182         DO 40 J=1,NN
183         IF(I.NE.J)GO TO 36
184         GO TO 37
185     36  S(I,J)=0.D0
```

```
186           GO TO 40
187        37 S(I,J)=1.D0
188        40 CONTINUE
189           DO 45 I=153,185
190           DO 45 J=1,NN
191           IF(I.NE.J)GO TO 41
192           GO TO 42
193        41 S(I,J)=0.D0
194           GO TO 45
195        42 S(I,J)=1.D0
196        45 CONTINUE
197           DO 140 J=1,45
198           DO 140 I=1,NN
199           IF(I.NE.J)GO TO 136
200           GO TO 137
201       136 CONTINUE
202           V(I)=V(I)-S(I,J)*V(J)
203           S(I,J)=0.D0
204           GO TO 140
205       137 S(I,J)=1.D0
206       140 CONTINUE
207           DO 145 J=153,185
208           DO 145 I=1,NN
209           IF(I.NE.J)GO TO 141
210           GO TO 142
211       141 CONTINUE
212           V(I)=V(I)-S(I,J)*V(J)
213           S(I,J)=0.D0
214           GO TO 145
215       142 S(I,J)=1.D0
216       145 CONTINUE
217           DO 211 I=1,45
218       211 V(I)=0.D0
219           DO 212 I=153,185
220       212 V(I)=100.D0
221           WRITE(6,210) (V(I),I=1,NN)
          C**
          C** SOLVE THE CONSTRAINED SYSTEM OF EQUATIONS
          C**
222           CALL GAUSDO
223           AVG=0.0
224           DO 215 I=1,NN
225           EXACTV(I)=V(I)
226           ERROR(I)=0.D0
227           WRITE(6,111)I,EXACTV(I),ERROR(I),V(I)
228       111 FORMAT('0','EXACTV (',I3,') = ',F20.10,2F28.10)
229           AVG=AVG+ERROR(I)
230       215 CONTINUE
231           AVG=AVG/NN
232           PRINT,AVG
233           CALL STRESS
          C**
          C**PLOT EQUIPOT. CONTOURS
          C**
234           NOPLOT=0
235           CALL CONTUA(NOPLOT)
          C**
          C**FORMATS : READ 100 TO 190 ,WRITE 200 TO 280
          C**
236       100 FORMAT(2I4)
237       105 FORMAT(I2)
238       110 FORMAT(6I4)
          C**
239       200 FORMAT(8X,2(I4,8X))
240       202 FORMAT('0',16X,'THIS IS A TWO-DIMENSIONAL PROBLEM')
241       210 FORMAT(' ',8D15.8)
```

```
242       303 FORMAT('0',16X,'THIS IS A THREE-DIMENSIONAL AXI-SYMMETRIC PR
              1)
243           STOP
244           END

245           SUBROUTINE COORDS
          C
          C**
          C** COORDS GENERATES NODAL COORDINATES OF THE CONTINUUM
          C**
246           COMMON X(185),Y(185),NODE(7 ,6)
247           COMMON S(185,186),V(185)
248           COMMON G(13)
249           REAL*8 ENM
250           REAL*8 G
251           REAL*8 DSQRT
252           DOUBLE PRECISION X,Y,C,RC1,RC2,ZC1,ZC2,S,V
253           PI=3.14159265
254           NE=7
255           A=5 .D
256           EN=1.6
          C
257           X(3)=1.D0
258           X(5)=2.D0
259           Y(1)=1.D
260           Y(3)=1.D0
261           Y(5)=1.D0
262           X(7)=3.D
263           Y(7)=1.D0
264           DO 2  I=7,23,2
265       2   X(I)=3.D0+(I-7)*0.25D0
266           DO 3  I=25,45,2
267       3   X(I)=7.25D +(I-25)* .125D
268           DO 1  I=5,45,2
269       1   Y(I)=A*DCOSH((X(I)-1.5D0)/(A-(X(I)-1.5D )**EN))-(A-1.D )
270           X(62)=5.5D0
271           Y(62)=0.75D0
272           X(69)=6.5D0
273           Y(69)=1.D0
274           X(75)=7.D0
275           Y(75)=1.D
276           X(98)=7.5D0
277           Y(98)=1.25D
278           X(101)=8.D0
279           Y(101)=1.5D0
280           X(103)=8.5D0
281           Y(105)=Y( 35)
282           Y(103)=Y( 31)
283           X(105)=8.75D
284           X(107)=9.D0
285           Y(107)=Y( 37)
286           X(116)=9.5D
287           Y(116)=2.D0
288           X(109)=9.5D
289           Y(109)=Y( 39)
290           X(123)=10.5D0
291           Y(123)=4.6875D
292           X(125)=11.D0
293           Y(125)=2.D0
294           X(127)=11.D
295           Y(127)=3.5D0
296           X(135)=12.D0
297           Y(135)=3.875D
298           X(138)=12.5D0
299           Y(138)=2.D0
300           X(140)=12.5D0
```

```
301           Y(140)=3.5D0
302           Y(146)=1.25D0
303           X(146)=14.D0
304           X(148)=14.D0
305           Y(148)=2.125D0
306           DO 4  I=153,181,2
307         4 Y(I)=1.5D0
308           X(181)=14.625D0
309           X(183)=14.75D0
310           X(185)=15.D0
311           Y(183)=0.75D0
312           Y(185)=1.D0
313           DO 6  I=155,159,2
314         6 X(I)=1.5D0+(I-155)*0.5D0
315           DO 7  I=165,171,2
316         7 X(I)=5.D0+(I-165)*0.5D0
317           X(161)=4.D0
318           X(163)=4.5D0
319           DO 8  I=173,179,2
320         8 X(I)=9.5D0+(I-173)*0.75D0
      C
321           DO 5  K=1,NE
322           X1=X(NODE(K,1))
323           X2=X(NODE(K,2))
324           X3=X(NODE(K,3))
      C
325           Y1=Y(NODE(K,1))
326           Y2=Y(NODE(K,2))
327           Y3=Y(NODE(K,3))
      C
328           X(NODE(K,4))=X1+(X2-X1)/2.0
329           X(NODE(K,5))=X2+(X3-X2)/2.0D0
330           X(NODE(K,6))=X3+(X1-X3)/2.0D0
      C
331           Y(NODE(K,4))=Y1+(Y2-Y1)/2.0D0
332           Y(NODE(K,5))=Y2+(Y3-Y2)/2.0D0
333           Y(NODE(K,6))=Y3+(Y1-Y3)/2.0D0
      C
334         5 CONTINUE
335           RETURN
336           END

337           SUBROUTINE GAUSDD
      C**
      C** GAUSDD IMPLEMENTS THE GAUSS-SEIDEL ITERATIVE METHOD
      C**
      C**     FOR SOLVING LARGE SYSTEMS OF LINEAR EQUATIONS
      C**
338           COMMON X(185),Y(185),NODE(70,6)
339           COMMON S(185,186),V(185)
340           COMMON G(13)
341           INTEGER CHEKPT
342           REAL*8 SV(185),DABS,ASTAR,XSTAR,EPS
343           REAL*8 X,Y,C,RC1,RC2,ZC1,ZC2,S,V,G,ENM
344           NN=185
345           NN1=NN+1
346           ITMAX=400
347           EPS=0.001D0
348           DO 2  I=1,NN
349           SV(I)=50.D0
350           S(I,NN1)=V(I)
351         2 CONTINUE
352           WRITE(6,202) (SV(I),I=1,NN)
      C***
      C   NORMALIZATION OF DIAGONAL ELEMENTS
      C***
```

```
353           DO 3 I=1,NN
354           ASTAR=S(I,1)
355           DO 3 J=1,NN1
356         3 S(I,J)=S(I,J)/ASTAR
          C***
          C    GAUSS-SEIDEL ITERATIONS
          C***
357           DO 9 ITER=1,ITMAX
358           CHEKPT=1
359           DO 7 I=1,NN
360           XSTAR=SV(I)
361           SV(I)=S(I,NN1)
          C***
          C    NEW SOLN VALUE SV(I)
          C***
362           DO 5 J=1,NN
363           IF(I.EQ.J)GO TO 5
364           SV(I)=SV(I)-S(I,J)*SV(J)
365         5 CONTINUE
          C***
          C    TEST SV(I) FOR CONVERGENCE
          C***
366           IF(DABS(XSTAR-SV(I)).LE.EPS)GO TO 7
367           CHEKPT=0
368         7 CONTINUE
369           IF(CHEKPT.NE.1)GO TO 9
370           WRITE(6,205) ITER
371       205 FORMAT('0','CONVERGED AFTER ',I3,' ITERATIONS')
372           WRITE(6,203) (SV(I),I=1,NN)
373           GO TO 10
374         9 CONTINUE
375           WRITE(6,206) ITER
376       206 FORMAT('0','DID NOT CONVERGE AFTER ',I3,' LESS ONE')
377           WRITE(6,204) (SV(I),I=1,NN)
378        10 CONTINUE
379           DO 15 I=1,NN
380        15 V(I)=SV(I)
          C***
          C    FORMAT STATEMENTS
          C***
381       202 FORMAT('0',' INITIAL SV(I)',11F10.5)
382       203 FORMAT('0',8X,'SOLN',11F10.5)
383       204 FORMAT('0',' NO CONVERGENCE',11F10.5)
384           RETURN
385           END

386           SUBROUTINE STRESS
          C
          C**
          C** STRESS CALCULATES TANGENTIAL STRESS AT STRESS-CONE
          C**
387           COMMON X(185),Y(185),NODE(70,6)
388           COMMON S(185,186),V(185)
389           COMMON G(13)
390           REAL*8 EZ(185),ER(185),EZR(185),DX,XG,YG,DELI
391           REAL*8 ENM
392           REAL*8 G
393           REAL*8 DSQRT,X1,X2,X3,Y1,Y2,Y3,V1,V2,V3,V4,V5,V6,C1,C2
394           REAL*8 AN(3),BN(3),CN(3),EN1(3),ELA(6)
395           LOGICAL LI,NCHKPT
396           DOUBLE PRECISION X,Y,C,RC1,RC2,ZC1,ZC2,S,V
397           PI=3.14159265
398           NN=185
399           NE=70
          C
400            DO 20 I=1,NN
```

```
401           DO 21 K=1,NE
402           X1=X(NODE(K,1))
403           X2=X(NODE(K,2))
404           X3=X(NODE(K,3))
      C::
405           Y1=Y(NODE(K,1))
406           Y2=Y(NODE(K,2))
407           Y3=Y(NODE(K,3))
      C**
408           AN(1)=X2*Y3-X3*Y2
409           AN(2)=X3*Y1-X1*Y3
410           AN(3)=X1*Y2-X2*Y1
      C**
411           BN(1)=Y2-Y3
412           BN(2)=Y3-Y1
413           BN(3)=Y1-Y2
      C**
414           CN(1)=X3-X2
415           CN(2)=X1-X3
416           CN(3)=X2-X1
417           DELT=DABS(0.5D0*(X1*(Y2-Y3)+X2*(Y3-Y1)+X3*(Y1-Y2)))
      C**
418           DX=0.05D0
419           XG=X(I)+DX
420           YG=Y(I)
421           DO 4 L=1,3
422           EN1(L)=(AN(L)+BN(L)*XG+CN(L)*YG)/(2.D0*DELT)
423         4 CONTINUE
424           DO 5 L=1,3
425           ELA(L)=EN1(L)*(2.D0*EN1(L)-1.D0)
426         5 CONTINUE
427           ELA(4)=4.D0*EN1(1)*EN1(2)
428           ELA(5)=4.D0*EN1(2)*EN1(3)
429           ELA(6)=4.D0*EN1(3)*EN1(1)
      C**
430           LI=NCHKPT(X1,Y1,X2,Y2,X3,Y3,XG,YG,DELT)
431           IF(.NOT.LI)GO TO 21
      C**
432           V1=V(NODE(K,1))
433           V2=V(NODE(K,2))
434           V3=V(NODE(K,3))
435           V4=V(NODE(K,4))
436           V5=V(NODE(K,5))
437           V6=V(NODE(K,6))
438           EZ(I)=ELA(1)*V1+ELA(2)*V2+ELA(3)*V3+
             1        ELA(4)*V4+ELA(5)*V5+ELA(6)*V6
439           EZ(I)=(EZ(1)-V(I))/(DX*2.54D0)
440           PRINT,I,EZ(I)
441           GO TO 20
442           ER(I)=4.D0*(BN(1)*(EN1(1)-.25D0)*V1
             1  +BN(2)*(EN1(2)-.25D0)*V2+BN(3)*(EN1(3)-.25D0)*V3
             1  +(BN(1)*EN1(2)+BN(2)*EN1(1))*V4
             1  +(BN(2)*EN1(3)+BN(3)*EN1(2))*V5
             1  +(BN(3)*EN1(1)+BN(1)*EN1(3))*V6)
             1  /(2.D0*DELT*2.54D0)
443           ER(I)=4.D0*(CN(1)*(EN1(1)-.25D0)*V1
             1  +CN(2)*(EN1(2)-.25D0)*V2+CN(3)*(EN1(3)-.25D0)*V3
             1  +(CN(1)*EN1(2)+CN(2)*EN1(1))*V4
             1  +(CN(2)*EN1(3)+CN(3)*EN1(2))*V5
             1  +(CN(3)*EN1(1)+CN(1)*EN1(3))*V6)
             1  /(2.D0*DELT*2.54D0)
444           EZR(I)=DSQRT(EZ(I)**2+ER(I)**2)
445           WRITE(6,500) I,EZ(I),ER(I),EZR(I)
446      500  FORMAT('0','STRESS AT NODE',I4,2X,'IS',2X,F20.1,2X,'KV/CM',
             1  2F20.1)
447           GO TO 20
```

```
448       21   CONTINUE
449       20   CONTINUE
450            RETURN
451            END

452            LOGICAL FUNCTION NCHKPT(X1,Y1,X2,Y2,X3,Y3,XG,YG,DELT)
          C
          C**         FUNCTION SUBPROGRAM NCHKPT LOCATES
          C**           ELEMENTS CORRESPONDING TO EACH GRID POINT
          C
453            REAL*8 X1,Y1,X2,Y2,X3,Y3,XG,YG,C1,C2,DELT
454            C1=((XG-X3)*(Y2-Y3)-(X2-X3)*(YG-Y3))/(2.D0*DELT)
455            C2=((X1-X3)*(YG-Y3)-(XG-X3)*(Y1-Y3))/(2.D0*DELT)
456            IF(C1.GE.-1.D-6.AND.C2.GE.-1.D-6.AND.
              1   (C1+C2-1.D0).LE.1.D-6)GO TO 10
457            NCHKPT=.FALSE.
458            RETURN
459       10   CONTINUE
46             NCHKPT=.TRUE.
461            RETURN
462            END

463            SUBROUTINE CONTUA(NOPLOT)
          C
          C**CONTUA PLOTS EQUIPOTENTIALS AT SPECIFIED GRID POINTS
          C
          C**      INPUT NOPLOT: NOPLOT=0   PLOTTER JCL REQUIRED
          C**                    NOPLOT=1   DEFAULT
          C
464            COMMON X(185),Y(185),NODE(70,6)
465            COMMON S(185,186),V(185)
466            COMMON G(13)
467            REAL*8 X,Y,S,V,C,RC1,RC2,ZC1,ZC2
468            REAL*8 GV(61,21),GX(61),GY(21)
469            REAL*8 AN(3),BN(3),CN(3),ENI(3),ELA(6)
47             LOGICAL LI,NCHKPT
471            LOGICAL*1 D(21,61)/1281*.TRUE./
472            DIMENSION IBUF(4000)
473            REAL*8 XMIN,XMAX,YMIN,YMAX,XINT,YINT,FCURVE,DELTV
474            REAL*8 X1,X2,X3,Y1,Y2,Y3,V1,V2,V3,V4,V5,V6,DELT
475            REAL*8 C1,C2,XG,YG,CURVE
476            DIMENSION GVS(61,21)
477            NY=21
478            NX=61
479            NE=70
480            DO 17 I=1,NY
481            GY(I)=0.D0
482            DO 17 J=1,NX
483            GX(J)=0.D0
484            GV(J,I)=100.D0
485       17   CONTINUE
486            DO 18 I=1,NY
487            DO 18 J=1,40
488       18   GV(J,I)=0.D0
          C
          C**      CALCULATION OF GRID POTS & GRID COORDS.
          C
489            XMIN=0.D0
490            XMAX=15.D0
491            YMIN=0.5D0
492            YMAX=5.5D0
493            XINT=(XMAX-XMIN)/FLOAT(NX-1)
494            YINT=(YMAX-YMIN)/FLOAT(NY-1)
495            DO 19   I=1,NY
496            GY(I)=YMIN+(I-1)*YINT
497            DO 20 J=1,NX
```

```
498           GX(J)=XMIN+(J-1)*XINT
      C
      C
499           DO 21 K=1,NE
500           X1=X(NODE(K,1))
501           X2=X(NODE(K,2))
502           X3=X(NODE(K,3))
      C::
503           Y1=Y(NODE(K,1))
504           Y2=Y(NODE(K,2))
505           Y3=Y(NODE(K,3))
      C**
506           AN(1)=X2*Y3-X3*Y2
507           AN(2)=X3*Y1-X1*Y3
508           AN(3)=X1*Y2-X2*Y1
      C**
509           BN(1)=Y2-Y3
510           BN(2)=Y3-Y1
511           BN(3)=Y1-Y2
      C**
512           CN(1)=X3-X2
513           CN(2)=X1-X3
514           CN(3)=X2-X1
515           DELT=DABS(0.5D0*(X1*(Y2-Y3)+X2*(Y3-Y1)+X3*(Y1-Y2)))
      C**
516           XG=GX(J)
517           YG=GY(I)
518           DO 4 L=1,3
519           EN1(L)=(AN(L)+BN(L)*XG+CN(L)*YG)/(2.D0*DELT)
520         4 CONTINUE
521           DO 5 L=1,3
522           ELA(L)=EN1(L)*(2.D0*EN1(L)-1.D0)
523         5 CONTINUE
524           ELA(4)=4.D0*EN1(1)*EN1(2)
525           ELA(5)=4.D0*EN1(2)*EN1(3)
526           ELA(6)=4.D0*EN1(3)*EN1(1)
      C**
527           LI=NCHKPT(X1,Y1,X2,Y2,X3,Y3,XG,YG,DELT)
528           IF(.NOT.LI)GO TO 21
      C**
529           V1=V(NODE(K,1))
530           V2=V(NODE(K,2))
531           V3=V(NODE(K,3))
532           V4=V(NODE(K,4))
533           V5=V(NODE(K,5))
534           V6=V(NODE(K,6))
535           GV(J,I)=ELA(1)*V1+ELA(2)*V2+ELA(3)*V3+
             1          ELA(4)*V4+ELA(5)*V5+ELA(6)*V6
536           WRITE(6,500) K,GX(J),GY(I)
537           GO TO 20
538        21 CONTINUE
539        20 CONTINUE
540        19 CONTINUE
541           WRITE (6,400) ((GV(J,I),J=1,NX),I=1,NY)
542       400 FORMAT(10(2X,F10.4) /////)
543       500 FORMAT(6X,'ELEMENT # ',I3,10X,'X :',F8.3,2X,'Y :',F8.3/)
      C
      C**      PLOT EQUIPOTENTIAL CONTOURS
      C**           ON GRID POINTS
      C
      C**        IF NOPLOT=1  NO PLOT OUTPUT
      C
544           IF(NOPLOT.EQ.1)GO TO 25
      C
545           NXPLOT=NX
546           NYPLOT=NY
```

```
547           DO 55 I=1,NXPLOT
548           DO 55 J=1,NYPLOT
549           GVS(I,J)=SNGL(GV(I,J))
550        55 CONTINUE
      C**
551           FCURVE=0.00
552           DELTV=20.00
553           NCURVE=6
554           CALL PLOTS(IBUF,4000)
555           CALL PLOT(0.0,-11.0,-3)
556           CALL DASH(0.0,10.0,2,10)
557           CALL DASH(10.0,10.0,2,10)
558           CALL DASH(10.0,0.0,2,10)
559           CALL DASH(0.0,0.0,2,10)
      C**
560           DO 23 I=1,NCURVE
561           CURVE=FCURVE+(I-1)*DELTV
562           CURVES=SNGL(CURVE)
563           CALL SMOCON(GVS,NXPLOT,NYPLOT,.0125,CURVES,0,7.7,3)
564        23 CONTINUE
565           CALL SYMBOL(0.00,10.2,.21,'POTENTIAL CONTOUR',0.0,17)
566           CALL PLOT(12.0,0.0,999)
      C::
567        25 RETURN
568           END

569           LOGICAL FUNCTION NCHKPT(X1,Y1,X2,Y2,X3,Y3,XG,YG,DELT)
      C
      C**        FUNCTION SUBPROGRAM NCHKPT LOCATES
      C**          ELEMENTS CORRESPONDING TO EACH GRID POINT
      C
570           REAL*8 X1,Y1,X2,Y2,X3,Y3,XG,YG,C1,C2,DELT
571           C1=((XG-X3)*(Y2-Y3)-(X2-X3)*(YG-Y3))/(2.D0*DELT)
572           C2=((X1-X3)*(YG-Y3)-(XG-X3)*(Y1-Y3))/(2.D0*DELT)
573           IF(C1.GE.-1.D-6.AND.C2.GE.-1.D-6.AND.
             1  (C1+C2-1.D0).LE.1.D-6)GO TO 10
574           NCHKPT=.FALSE.
575           RETURN
576        10 CONTINUE
577           NCHKPT=.TRUE.
578           RETURN
579           END
```

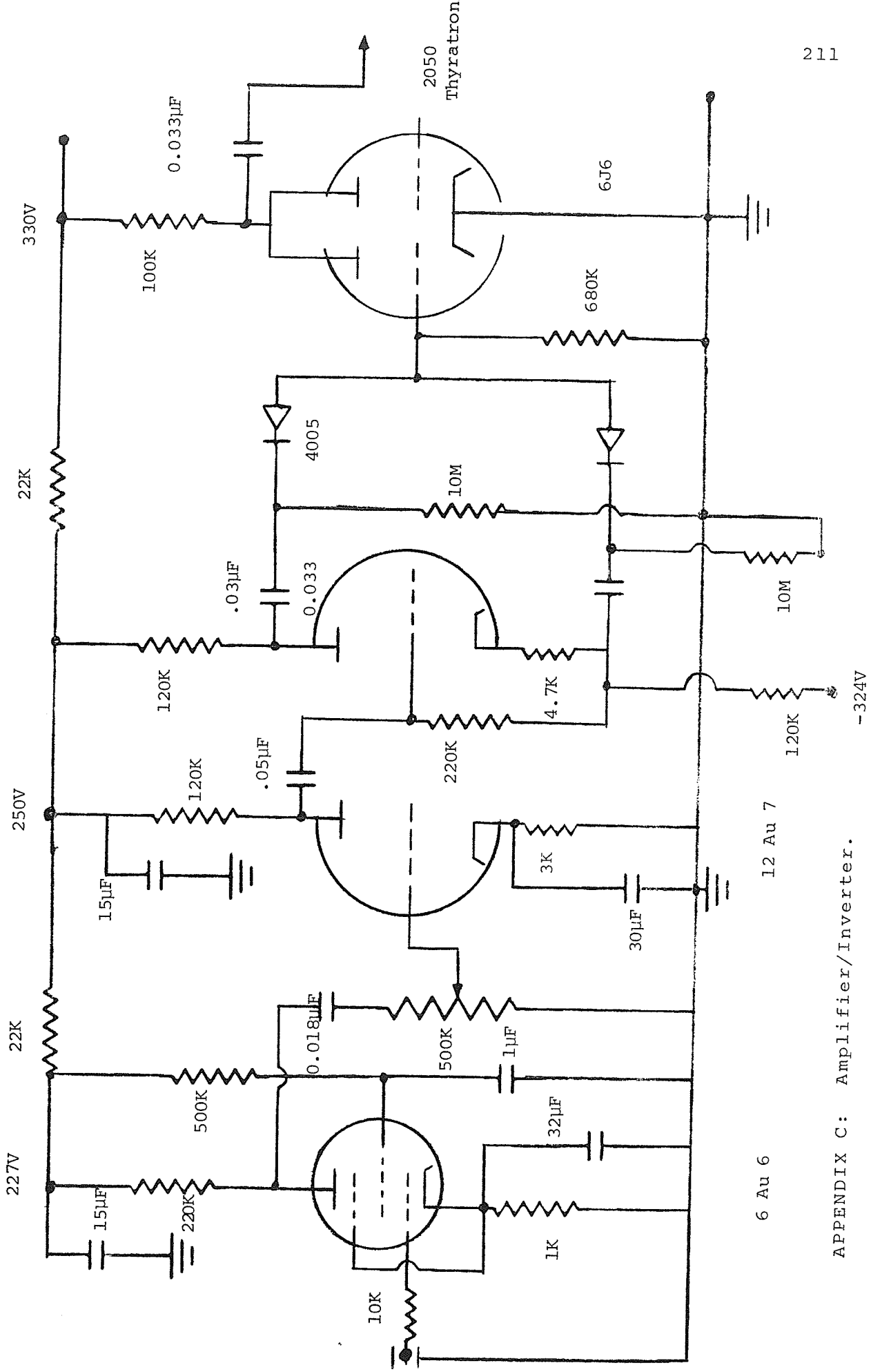

APPENDIX C: Amplifier/Inverter.

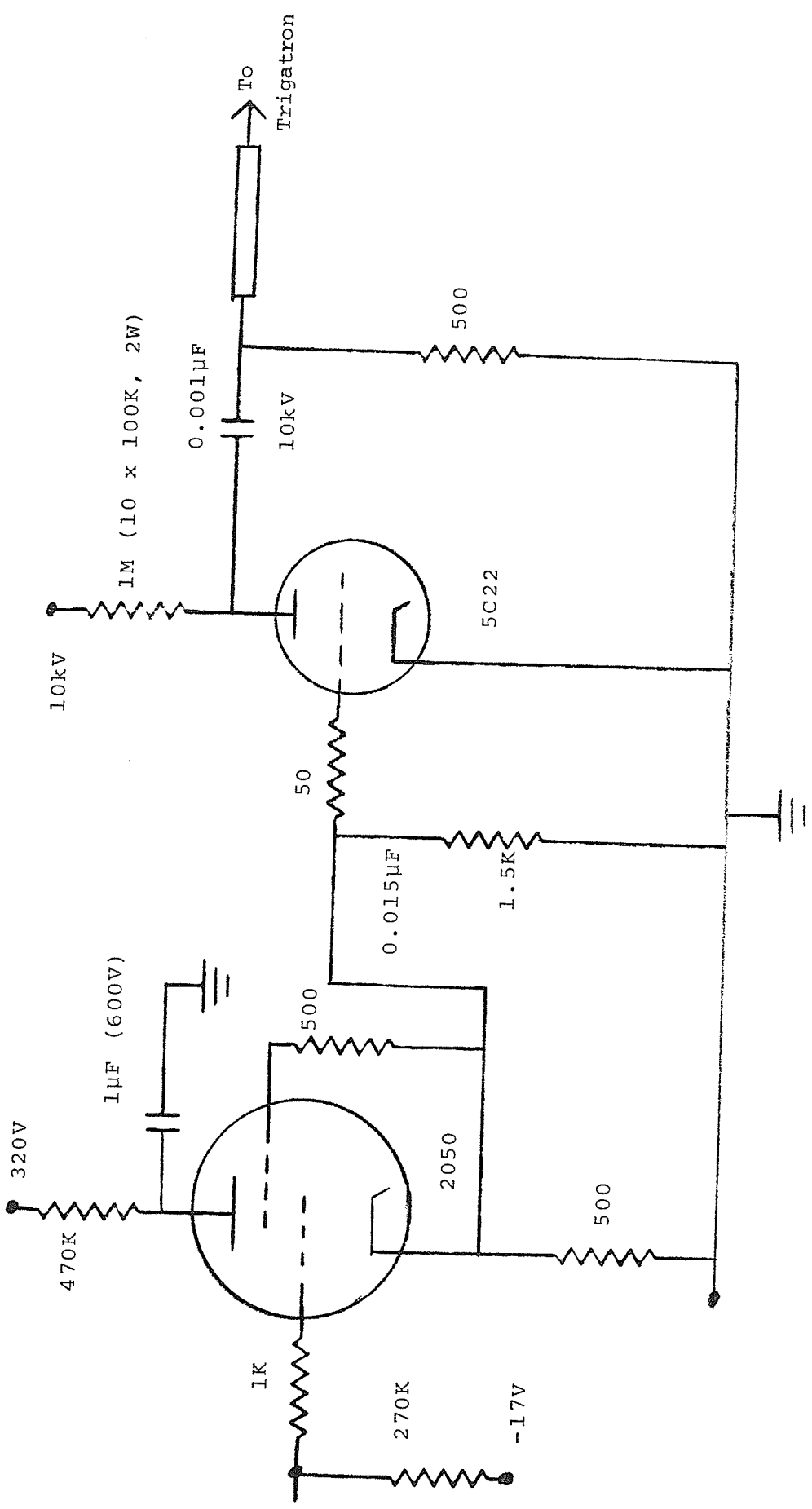

APPENDIX C: Thyratrons

APPENDIX D

EXPERIMENTAL DATA

Unless otherwise specified cup-plane electrodes were used

	PDMS Breakdown Voltage Level kV (peak)				
Gap (mm) / Test No.	1.05	2.1	2.5	3.15	4.2
1	40	65	70	85	110
2	38	65	68	80	120
3	38	73	70	80	115
4	40	70	68	85	120
5	42	65	68	80	120
6	42	70	76	90	120
7	40	73	70	80	120
8	42	67	75	90	120
9	40	70	74	95	115
10	38	72	78	85	120
11			80	95	110
12			80	90	110
13			78	85	110
14			70	82	
15			75	87	
16			79	90	
17			70	90	
18			70	90	
19			80	90	
20			80	90	
21				90	

APPENDIX D

PDM Breakdown Level kV (peak)

Test No. \ Gap (mm)	5.0	5.25	6.3	7.5
1	100	120	160	170
2	100	125	160	160
3	105	135	165	180
4	105	110	160	170
5	100	120	150	170
6	120	130	160	170
7	120	140	150	170
8	120	140	160	180
9	100	120	160	170
10	120	140	160	180
11	100	130		170
12	115	140		
13	120	120		
14	120	140		
15	120	140		
16	135			
17	135			
18	110			
19	120			
20	120			
21	130			

APPENDIX D

PDMS/XLPE Interface Breakdown Voltage kV (peak)

Test No. \ Gap (mm)	2.5	3.1	4.2	5.0	6.0	7.5
1	56	70	95	100	120	155
2	54	70	100	100	140	160
3	58	75	100	90	140	160
4	58	70	100	90	130	160
5	52	70	100	100	120	160
6	58	70	90	100	130	160
7	56	68	100	100	130	160
8	58	70	95	100	125	160
9	60	70	105	100	120	160
10	54	70	100	100	120	160
11	60		95	100		
12				100		
13				100		
14				110		
15				100		
16				100		
17				100		
18				110		
19				110		
20				100		

APPENDIX D

Effect of Other Electrode Geometries: PDMS 5mm Gap B/D kV (peak)

Test No.	Electrodes Type A	Electrodes Type B	Electrodes Type C	PDMS/XLPE Elect.Type A	PDMS/XLPE Elect. Type C
1	80	85	90	80	80
2	80	85	90	80	80
3	80	85	97	80	80
4	90	92	97	80	80
5	90	90	90	80	85
6	92	92	95	80	80
7	90	95	90	80	80
8	90	90	90	80	85
9	90	90	97	80	80
10	100	97	92	80	80
11	90	92	97		80
12	90	90	97		85
13	95	100	100		80
14	95	95	100		85
15	100	95	100		80
16	90	95	95		80
17	90	95	100		
18	100	95	100		
19	90	90	95		
20	95		100		
21	100		100		

Electrode Type A: plane-plane Brass

Electrode Type B: plane-plane Brass with 3 mm inset (sharp edges)

Electrode Type C: plane-plane Brass with 3 mm inset (rounded off edges)

APPENDIX D

Breakdown of PDMS/Other Solid Interfaces 5.1 Gap kV (peak)

Test No.	PDMS/ Rough XLPE	PDMS/Nylon	PDMS/PMMC 5.0 mm	TROIL/ XLPE
1	105	80	90	50
2	100	90	90	50
3	110	95	95	55
4	110	90	95	60
5	110	85	90	60
6	110	80	100	60
7	100	90	90	60
8	110	90	90	60
9	110	90	95	60
10	100	80	95	60
11		85		60
12		90		60
13		90		60
14		90		60
15		90		60
16		90		70
17		90		70
18				65
19				65
20				60

Rough XLPE → XLPE with a visibly rough surface

Nylon → Polyamide

PMMC → Polymethyl methacrylite

TROIL → Transformer oil (2.5 mm Gap used)

APPENDIX D

Standard Positive Impulse Breakdown Voltage Levels (kV).

Test No.	2.5 mm Gap PDMS	2.5 mm Gap PDMS/XLPE	5.0 mm Gap PDMS	5.0 mm Gap PDMS/XLPE	7.5 mm Gap PDMS	7.5 mm Gap PDMS/XLPE
1	140	120	220	210	300	260
2	140	120	220	215	285	270
3	130	120	225	225	280	270
4	125	128	225	240	300	260
5	130	120	240	210	280	260
6	140	128	230	225	270	270
7	140	125	245	260	270	260
8	120	120	240	260	280	255
9	125	120	220	230	285	260
10	148	125	260	230	280	270
11	140		230	260	290	
12	120		220	260		
13	135		265	220		
14	145		240	220		
15			240	225		
16			240	220		
17			250	200		
18			220			
19			220			
20			235			